AD-A076 559 ANALYSIS AND TECHNOLOGY INC NORTH STONINGTON CT F/G 17/7
TARGET TRACKING WITH MULTIPLE DATA SOURCES.(U)
AUG 79 H F JARVIS , N B NILL N00014-78-C-0707
UNCLASSIFIED P-515-1-79 NL

1 OF 2
AD A076559

OPERATIONS RESEARCH

LEVEL

SYSTEMS ENGINEERING

SYSTEMS ANALYSIS

OCEAN SCIENCES

SIMULATION

ANALYTICAL MODELING

COMPUTER SCIENCES

ANALYSIS & TECHNOLOGY INC.

ANALYSIS AT TECHNOLOGY

12

TARGET TRACKING WITH MULTIPLE DATA SOURCES

Analysis & Technology, Inc.
Report No. P-515-1-79

Contract N00014-78-C-0707
Task Number NR 274-302

15 August 1979

Prepared by:

H. F. Jarvis
N. B. Nill

Approved By: T. M. Downie
T. M. Downie, Manager
Systems Research Dept.

Prepared for:

Naval Analysis Program
Office of Naval Research
800 N. Quincy Street
Arlington, VA 22217

(Attn: Mr. James Smith, Code 431)

UNCLASSIFIED

SECURITY CLASSIFICATION OF THIS PAGE (When Data Entered)

REPORT DOCUMENTATION PAGE

READ INSTRUCTIONS BEFORE COMPLETING FORM

1. REPORT NUMBER	2. GOVT ACCESSION NO. / 3. RECIPIENT'S CATALOG NUMBER
4. TITLE (and Subtitle) (6) TARGET TRACKING WITH MULTIPLE DATA SOURCES •	5. TYPE OF REPORT & PERIOD COVERED (9) FINAL REPORT
	6. PERFORMING ORG. REPORT NUMBER (14) P-515-1-79
7. AUTHOR(s) (10) H. F. JARVIS, N. B. HILL	8. CONTRACT OR GRANT NUMBER(s) (15) N00014-78-C-0707
9. PERFORMING ORGANIZATION NAME AND ADDRESS ANALYSIS & TECHNOLOGY, INC. P.O. BOX 220 NORTH STONINGTON, CT 06359	10. PROGRAM ELEMENT, PROJECT, TASK AREA & WORK UNIT NUMBERS 65152N NR 274-302 (16) R0145-TW (17) R0145TW
11. CONTROLLING OFFICE NAME AND ADDRESS NAVAL ANALYSIS PROGRAMS (CODE 431) OFFICE OF NAVAL RESEARCH 800 N. QUINCY ST., ARLINGTON VA 22217	(11) 12. REPORT DATE 15 AUGUST 1979 13. NUMBER OF PAGES 130
14. MONITORING AGENCY NAME & ADDRESS(if different from Controlling Office) (12) 139	15. SECURITY CLASS. (of this report) UNCLASSIFIED 15a. DECLASSIFICATION/DOWNGRADING SCHEDULE N/A

16. DISTRIBUTION STATEMENT (of this Report)

APPROVED FOR PUBLIC RELEASE;
DISTRIBUTION UNLIMITED

17. DISTRIBUTION STATEMENT (of the abstract entered in Block 20, if different from Report)

18. SUPPLEMENTARY NOTES

19. KEY WORDS (Continue on reverse side if necessary and identify by block number)

20. ABSTRACT (Continue on reverse side if necessary and identify by block number)

This report presents the results of a study on the impact of a'priori estimates of range and/or target speed on the bearings-only TMA problem. The method selected for this evaluation was a computer simulation of Maximum A'posteriori Probability (MAP) estimate which incorporates the a'priori statistical information in an asymptotically optimum manner. The a'priori range information represents environmental predictions of likely range bands

DD FORM 1 JAN 73 1473 EDITION OF 1 NOV 65 IS OBSOLETE
S/N 0102-014-6601

AD A077677

UNCLASSIFIED

SECURITY CLASSIFICATION OF THIS PAGE (When Data Entered)

based on alternate propagation paths (direct, 1st CZ, 2nd CZ, etc.). An additional phase of the study evaluated the use of Depression/Elevation (D/E) estimates from environmental predictions for resolving horizontal bearing from conical angle measurements.

The results of the study indicate that the benefits achieved from the use of a'priori range information are algorithm dependent and primarily aid numerical convergence rather than solution accuracy. The use of a'priori range together with estimated D/E does provide solution improvement for conical angle measurements from line arrays. The use of speed estimates improves both numerical convergence and solution quality during the initial TMA legs.

EXECUTIVE SUMMARY

The value of incorporating a'priori range and/or target speed information into the bearings-only Target Motion Analysis (TMA) problem was studied through a series of computer simulations of an asymptotically optimum estimation algorithm. It was anticipated that use of a'priori estimates along with their estimated accuracy should provide a TMA solution which converges faster and is more accurate than a conventional bearings-only TMA algorithm. Two algorithms were selected for this evaluation and simultaneously compared. The algorithm which incorporates the full a'priori statistical information is a Maximum A'posteriori Probability (MAP) estimator. The other algorithm which incorporates a'priori information only for initialization is a Maximum Likelihood Estimator (MLE). Both algorithms are asymptotically optimum in the sense of minimizing solution error given sufficiently long observation sequences. These algorithms were chosen because of this property. Alternative TMA algorithms such as the Extended Kalman Filter (EKF) suffer from linearization errors and therefore may not accurately depict the value of the a'priori information.

The a'priori range information represents environmental predictions of likely range bands based on alternative propagation paths (direct, 1st CZ, 2nd CZ, etc). The a'priori estimates of target speed represents estimates obtained by turn count, classification information, or tactical considerations. The study also evaluated the use of Depression/Elevation (D/E) angle estimates for resolving horizontal bearing from conical angle measurements.

Comparison of the MAP solution to the MLE solution indicates that the MAP algorithm does not provide the expected solution improvement using a'priori range information. Although both MAP and MLE solution errors agree well (and with the theoretical lower bounds (Cramer-Rao)) at the end of the problem (i.e. for a fully converged solution), expected differences early in the problem were not observed.

The MAP algorithm using a'priori speed estimates provides substantially more improvement over the MLE algorithm then the case of the a'priori range estimates. In particular for closing target geometries (i.e. small target aspect), the MAP range, course, speed solutions converged during the early TMA legs. For targets with large aspect, the a'priori speed estimate does not

provide as much improvement because the bearing measurements resolve the solution due to the larger bearing change.

In the case of conical angle measurements from a line array, the major impact on the TMA solution is the bias error in the effective horizontal bearing due to D/E angle. If environmental predictions of propagation path are used to provide D/E angle estimates in addition to range estimates, then a substantial improvement in both MAP and MLE solution accuracy is achieved.

The major benefits derived from the a'priori information were associated with the numerical convergence properties of the algorithm tested. The algorithms, although asymptotically optimum, have two drawbacks. The solution procedure is iterative in nature and is computationally expensive if the number of iterations is large. In addition, the optimization problem posed is ill conditioned during the early stages. In the case of the MAP algorithm, incorporation of a'priori range information improves numerical convergence over the MLE algorithm because the iteration equations are further removed from singularity. The use of a'priori speed estimates in the MAP algorithm exhibited a remarkable improvement in the numerical convergence during the initial TMA legs (especially in the closing geometries).

The use of a'priori range information in the MAP algorithm is based on an assumed propagation path. The MAP solutions are biased under incorrect path hypotheses. Consequently, separate solutions should be pursued until the true path is resolved. All solutions converge to the true solution given sufficient measurements, however, to minimize the computational burden it is desirable to discard incorrect hypotheses quickly. The study indicates that it appears necessary to process nearly one half of the data (to solution convergence) to ensure retaining the correct path assumption.

In summary the results of the study indicate that the benefits achieved from the use of a'priori range information are algorithm dependent and primarily aid numerical convergence rather than solution accuracy. The use of a'priori range together with estimated D/E does provide solution improvement for conical angle measurements from line arrays. The use of speed estimates improves both numerical convergence and solution quality during the initial TMA legs.

CONTENTS

CONTENTS

LIST OF FIGURES

LIST OF TABLES

1.0 Introduction and Objectives

The classical bearings-only Target Motion Analysis (TMA) problem generally consists of fitting a solution to a time series of bearing measurements without (or with little) incorporation of external information, such as environmental predictions. The types of external information of concern here are acoustic propagation properties and foreknowledge of target ship parameters such as speed. Specifically, under the proper environmental conditions the acoustic signal can be received in various propagation modes: direct path, bottom bounce, and/or convergence zone paths. These propagation paths will limit the acoustic source to defined range bands which are predictable from ray trace propagation calculations. Incorporation of this information into the TMA solution process would reduce the initial range uncertainty. In a similar manner, if an estimate of target speed or a discrete number of possible speeds is available, perhaps from a target classification process, then a reduction in TMA solution time could result.

There are many approaches to solving the bearings-only TMA problem, some of which are adaptable to incorporation of external information. However, all techniques currently in use have some deficiencies resulting in solutions which are not optimal. This study is based on a TMA algorithm which is theoretically optimum in an asymptotic sense. The Maximum Likelihood Estimator (MLE) is generally considered when estimating parameters from nonlinear (or non-Gaussian) observations. The MLE solution is not optimum in a minimum estimation error sense, but is asymptotically optimum as the data base increases without bound. Although the MLE has been considered for the TMA application for many years, its computational burden has precluded its use in ship board computer systems. However, since this study is concerned with the potential advantage of incorporating external information it was decided to use a theoretically optimum algorithm which would best demonstrate this concept rather than choose one of the operational algorithms.

The external information can be considered in the context of a'priori statistical information on the TMA solution. The asymptotically optimum estimate when a'priori probability density functions are available is the

Maximum A'posteriori Probability (MAP) estimate. The approach taken in this study is a direct simulation of both the MAP algorithm and the MLE algorithm to determine the specific impact of the a'priori information on an "optimal" bearings-only TMA algorithm. The MLE algorithm uses the a'priori information for initialization (of range) to assist convergence of the iterative solution procedure. However, the MAP solution is always influenced by the a'priori information, whereas the MLE solution can "forget" its initial conditions almost immediately.

The a'priori information is represented by disjoint "bands" of likely target range. This information is therefore representative of a multimodal probability distribution. To obviate the numerical difficulties associated with multimodal optimization, the problem is treated by processing a separate solution for each potential range band, using the a'priori information for the appropriate band. The objectives for the study then become:

(1) Determination of the improvement obtained when correct a'priori information is used, and

(2) Determination of criteria to reject the incorrect a'priori hypotheses.

In addition, the study has two distinct phases corresponding to two different types of sensor measurements. The conventional problem is cast in the horizontal plane in a two dimensional geometry. Most sonar systems can resolve bearings in the horizontal plane. An important class of sonar arrays, which cannot directly resolve bearing, consists of a line of equally spaced hydrophones. This one dimensional array cannot separate the horizontal component of the vector representing the incident acoustic wave from the vertical component. This class of arrays therefore presents a different problem because another parameter, Depression/Elevation (D/E) angle, must be known to determine bearing. Furthermore, a line array cannot distinguish port from starboard. However, environmental predictions used to obtain a'priori range information can also be used to estimate a D/E angle appropriate for each range band. This type of estimate is included in the phase of the study

involving line array angles. For every range band two solutions must therefore be executed (port and starboard assumptions).

In most cases, the computer simulations were based on 30 Monte Carlo repetitions and the geometries simulated are typical submarine TMA maneuvering sequences. The magnitude of the bearing errors used are representative of many passive sonar systems.

2.0 Simulated Scenarios

Realistic operational scenarios were modeled by establishing own ship to target ship ranges from 10 kyds to 109 kyds for the horizontal bearing cases (Phase I) and covering direct, first and second convergence zone (CZ) acoustic propagation paths. For the line array angle cases (Phase II), ranges from 5 kyds to 54 kyds were established, covering direct, bottom bounce and first CZ paths. Two target ship courses were chosen for Phase I which substantially cover the gamut of expected course-related variations in results. Specifically, a course of 146° which presents an initial broadside aspect, and a course of 256° which closes the initial own-ship location with an angle on the bow of 20 degrees. In all cases the own-ship maneuver consisted of standard 60° lead/ 60° lag, maneuvering sequence with leg times of 5 minutes duration. In addition, both own ship and target were assumed to have a constant speed of 10 knots. Own ship turned at a constant rate of 2°/second during maneuvers.

The acoustic propagation properties assumed are realistic, yet general enough to represent many different geographic ocean area/season combinations. In order to establish the convergence zone locations and widths, nominal rules that have been established over the years were followed. Namely,

- Range to first CZ is between 20 kyds and 80 kyds.
- Width of a given CZ is 5% to 20% of its range.
- Higher order CZ's occur at ranges that are whole number multiples of the range to the first CZ.

In consideration of these rules, the first CZ was set at 45 to 55 kyds and the second CZ at 90 to 110 kyds. This combination can correspond to many mid-latitude ocean areas with a water depth of at least 1000 fathoms and a surface temperature around 52°F, for a shallow source and receiver.* As a specific example, the Levantine Basin area in the Mediterranean (32°30'N, 27°30'E)

*R. J. Urick, "Principles of Underwater Sound," 2nd ed., McGraw-Hill, 1975, Fig 6.13.

in summer exhibits first and second CZ's around 50 kyds, 100 kyds respectively, even though the surface temperature is considerably greater than 52°F (water depth = 1500 fathoms).*

2.1 Horizontal Bearing Measurements (Phase I)

For Phase I the direct path was assumed to extend out to 30 kyds and the locations of the CZ's were assumed to have an error of estimation of ±10 percent. Table 2-1 tabulates the propagation path data as well as the initial range estimates and standard deviations as used in the TMA computer simulation.

Table 2-1 Horizontal Bearing Acoustic Propagation Path and Range Data

TARGET COURSE (DEG)	PROPAGATION PATH	TRUE PATH RANGE (KYD)	TRUE TARGET RANGE (KYD)	CZ PATH WITH ±10% ERROR	EST. RANGE	RANGE STANDARD DEVIATION
256 (closing)	DIRECT	0-30	10, 20	---	15	7.5
256 (closing)	1st CZ	45-55	54	40.5-49.5	45	4.5
256 (closing	2nd CZ	90-110	109	81-99	90	9
146 (crossing)	DIRECT	0-30	10, 20	---	15	7.5
146 (crossing)	1st CZ	45-55	46	49.5-60.5	55	5.5
146 (crossing)	2nd CZ	90-110	91	91-121	110	11

In each case the estimated range is placed in the center of the assumed path, with a standard deviation of half the range estimate for direct path, and half the CZ width for CZ paths. The reason for placing the target in different locations within a CZ and making the CZ error minus or plus, for different target courses, is to ensure that the range remains within a given CZ, over a minimum 20-minute TMA track time. In most cases the target ship remains within a given CZ up to the maximum TMA track time allowed - 40 minutes.

---

*"Acoustic Environmental Scenarios and Predictions for ASW" - "Long Range Acoustic Propagation Project," Ocean Science Program, Maury Center for Ocean Science, Dept, of Navy, Washington, D.C., M. C. Report 011, Oct. 1972.

This approach was taken because the computer simulation does not account for loss of track which occurs when target leaves a CZ. Note a sudden loss of signal could provide confirmation of a suspected CZ target, but the study was directed to the effect of external information on the TMA solution.

Table 2-2 gives the cases that were run for Phase I. Each case was run with 30 Monte Carlo repetitions. This is adequate since the study concentrated on average properties of the solutions rather than anamolies. All cases in this study were run with an initial true bearing of 56° and a bearing measurement error standard deviation σ_β=0.2°, although a few cases were also run with σ_β=0.5°, σ_β=1.5°. A complete set of runs were made with an initial target speed estimate of 0 knots and standard deviation of 15 knots. A partial set of runs were made with an initial target speed estimate of 10 knots and associated standard deviation of 2 knots and 4 knots, as noted in Table 2-2. This reflects an external speed measurement based on classification information or turn count estimates. The actual initial speed used to initialize the iterations was zero since target course is not known a'priori. The 2 knot standard deviation represents external information while the 4 knot standard deviation encompasses typical transit speeds.

Table 2-2 Horizontal Bearing Cases Run

TRUE PATH	ASSUMED PATH
DIRECT (10 kyd)*	DIRECT
DIRECT (20)*	DIRECT
DIRECT (20)	1st CZ
DIRECT (20)	2nd CZ
1st CZ*+	1st CZ
1st CZ	DIRECT
1st CZ+	2nd CZ
2nd CZ*+	2nd CZ
2nd CZ	DIRECT
2nd CZ+	1st CZ

NOTES:
All cases were run with target courses of 146° and 256°. (90° and 20° AOB.)
+Speed σ=2, 4 knots in addition to σ=15 knots.
*Cases run at σ_β=0.5° and/or σ_β=1.5° in addition to σ_β=0.2°.

2.2 Line Array Angle (Phase II)

For the Phase II line array angle simulation, the D/E angle of arrival and a bottom bounce propagation path possibility become important considerations. As discussed in the introduction and shown mathematically in Appendix A, a line array cannot measure horizontal bearing directly. The angular measurement represents a conical surface which reduces to two horizontal bearing possibilities once D/E is specified.

Operationally, the D/E arrival angle of the major ray paths depends on depth, range, location, time of day, season, bottom characteristics, etc. The paths can be predicted from environmental models but the specific values are not important to this study. Therefore, simplifying assumptions about the D/E angle and bottom reflectance, are made for the calculations used in the simulation. The results are typical in spite of the simplistic models.

With the preceding in mind, a scenario was established with a direct path extending out to a range of 6 kyds, a bottom bounce range from 6 kyds to 25 kyds, and a first CZ at 45 to 55 kyds. For cases where the true or assumed propagation path is via bottom bounce, the incident and reflected rays are assumed to be straight and the bottom assumed to be a smooth, nonscattering horizontal plane. Own ship and target are assumed to be at shallow depths, relative to the bottom depth which is taken as 1500 fathoms. Under these conditions a simple triangle relates D/E to range. The true D/E is calculated from actual range while the estimated D/E is calculated from the a'priori range estimate. When the true acoustic propagation path is not via bottom bounce then the true D/E is set equal to -5°, which is a representative value for non-bottom bounce angle of arrival. When the assumed propagation path is not via bottom bounce, then the estimated D/E is set equal to 0 degree. In an operational situation, sophisticated environmental prediction algorithms, which are becoming an integral part of modern naval combat systems, could be used to supply the D/E estimates.

The propagation paths and range data for Phase II are given in Table 2-3, wherein all cases were run with $\sigma_\beta = 0.2°$ and a "crossing" target course of 146 degrees. Table 2-4 gives the actual cases run in Phase II.

Table 2-3 Line Array Angle Acoustic Propagation Path and Range Data

PATH	PATH RANGE (KYD)	TRUE TARGET RANGE (KYD)	EST. RANGE (KYD)	RANGE STANDARD DEVIATION (KYD)
DIRECT	0-6	5	3	1.5
BOTTOM BOUNCE	6-25	10	15.5	7.75
BOTTOM BOUNCE	6-25	20	15.5	7.75
1st CZ	45-55	46	55	5.5

Table 2-4 Line Array Angle Cases Run

TRUE PATH	ASSUMED PATH	TRUE D/E	EST. D/E
DIRECT	DIRECT	- 5°	0°
DIRECT	BOTTOM BOUNCE	- 5°	-21.05°
DIRECT	1st CZ	- 5°	0°
BOTTOM BOUNCE 10 KYD	BOTTOM BOUNCE	-30.82°	-21.05°
BOTTOM BOUNCE 10 KYD	DIRECT	-30.82°	0°
BOTTOM BOUNCE 10 KYD	1st CZ	-30.82°	0°
BOTTOM BOUNCE 20 KYD	BOTTOM BOUNCE	-16.61°	-21.05°
BOTTOM BOUNCE 20 KYD	DIRECT	-16.61°	0°
BOTTOM BOUNCE 20 KYD	1st CZ	-16.61°	0°
1st CZ	1st CZ	- 5°	0°
1st CZ	DIRECT	- 5°	0°
1st CZ	BOTTOM BOUNCE	- 5°	-21.05°
σ_β=0.2°			
Target Course = 146°			

3.0 Discussion of Simulation Results

The external information considered in this study is characterized by a discrete number of hypotheses representing different propagation paths. Each hypothesis can be separately incorporated into the a'posteriori density function resulting in the unimodal optimization problem described in Appendix A as the MAP estimate. The MAP estimate is an asymptotically optimum estimate as long as the correct path hypothesis is chosen. This study bypasses the difficult multimodal solution encountered with a true Baysian estimator by simply calculating a separate solution for each propagation path assumption. For this approach to operate efficiently in an operational system it is essential to minimize the impact of redundant solution computation by discarding incorrect hypotheses in a timely manner. The evaluation of the importance of external information to the bearings-only TMA solution is measured by the improved accuracy or reduced convergence time achieved using the statistical information based on the correct path assumption. As mentioned above, the MAP estimate provides the logical means for incorporating the correct path a'priori statistics. The improvement is measured by comparing the solution results to an MLE solution which uses the a'priori range estimate for initialization of the iterative numerical solution. From a practical viewpoint there are several other measures of improvement relative to use of MLE solutions to the TMA problem. For example, the use of external information can reduce the numerical problems associated with MLE iteration convergence. This results in potential reduction of computational burden represented by the number of iterations required for each solution. In addition, reduction of the numerical problem can also provide more "converged" solutions during the early TMA legs. Numerical convergence means satisfying the iteration stopping criteria within 21 iterations. Solution convergence on the other hand requires reducing the error bounds to meet an accuracy criteria. (Note that a solution that is not numerically converged is not counted in the solution accuracy statistics.) An integral part of the computational requirement for the approach under study is the amount of data required to dismiss incorrect propagation path assumptions.

An important factor for any operational TMA algorithm is its ability to determine the convergence status or quality of the solution. The MAP and MLE

solutions provide suitable measures based on the eigenvalues of the inverse of Fisher's information matrix. As discussed in Appendix A the MAP and MLE algorithms provide an estimate of this matrix which represents a lower bound on solution accuracy when evaluated at the exact solution.

The measures of solution accuracy are obtained by calculating mean errors and standard deviation of errors over the Monte Carlo repetitions. Computational requirements are calculated by counting the total number of solution iterations (Gauss Elimination iterations) over all solution times and Monte Carlo repetitions. Numerical convergence probability is determined by counting the number of Monte Carlo repetitions which satisfy the Gauss Elimination stopping criteria. The solution convergence criteria is evaluated by comparing the standard deviation of errors over the Monte Carlo repetitions at times "called" by the convergence criteria. A number of measures are considered for discarding incorrect path assumptions.

The results presented in this section are separated into two phases based on the bearing measurement model. The Phase I model assumes that the sensor can measure a horizontal plane bearing. For this phase the external information is based on three propagation paths; direct path at 20 kyds, 1st CZ at 50 kyds, and a 2nd CZ at 100 kyds. In addition, a limited number of simulations were made using a'priori target speed estimates with either a 2 kt or 4 kt uncertainty (standard deviation). For all Phase I simulations 30 Monte Carlo repetitions were executed.

The Phase II results presented in Section 3.2 represent bearings measured from a line array. For such an array the angular measurement cannot distinguish horizontal bearing unless the vertical arrival angle (D/E) is known. Each propagation path assumption therefore includes an estimated D/E angle to resolve horizontal bearing. The basic difference between Phase I and Phase II results is the solution bias error caused by use of an incorrect value of D/E in the latter case. Due to limited computer budget the Phase II results used only 5 Monte Carlo repetitions. Because of the domination of the bias error, the results are useful although statistical significence is limited. An additional feature of this phase is the necessity to decide whether the target lies on the port or starboard side of the array.

Figure 3-1a Range Error for Direct Path (True [20 kyds] and Assumed), Horizontal Bearing, Closing Target Course.

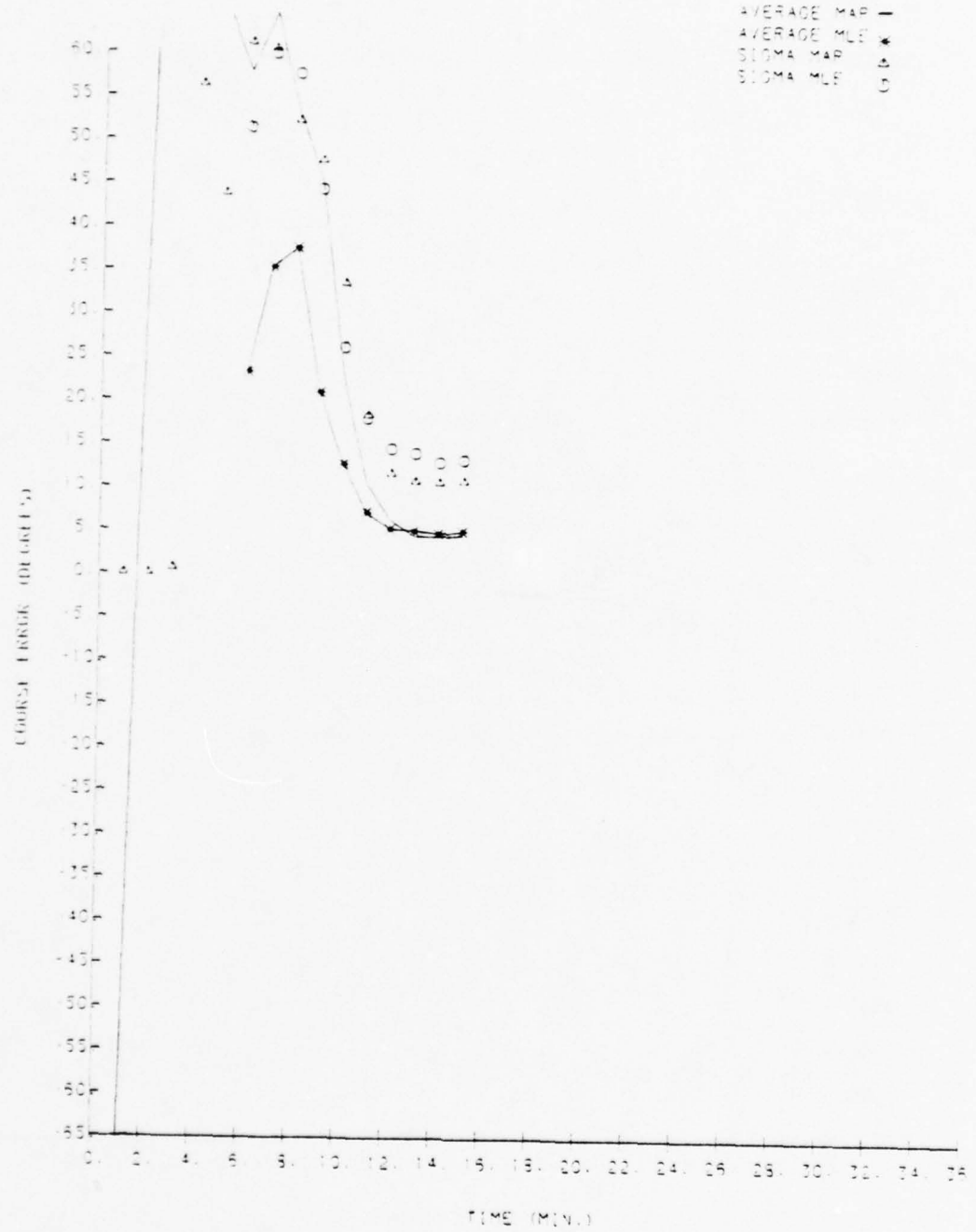

Figure 3-1b Course Error for Direct Path (True [20 kyds] and Assumed), Horizontal Bearing, Closing Target Course.

Figure 3-1c Speed Error for Direct Path (True [20 kyds] and Assumed), Horizontal Bearing, Closing Target Course.

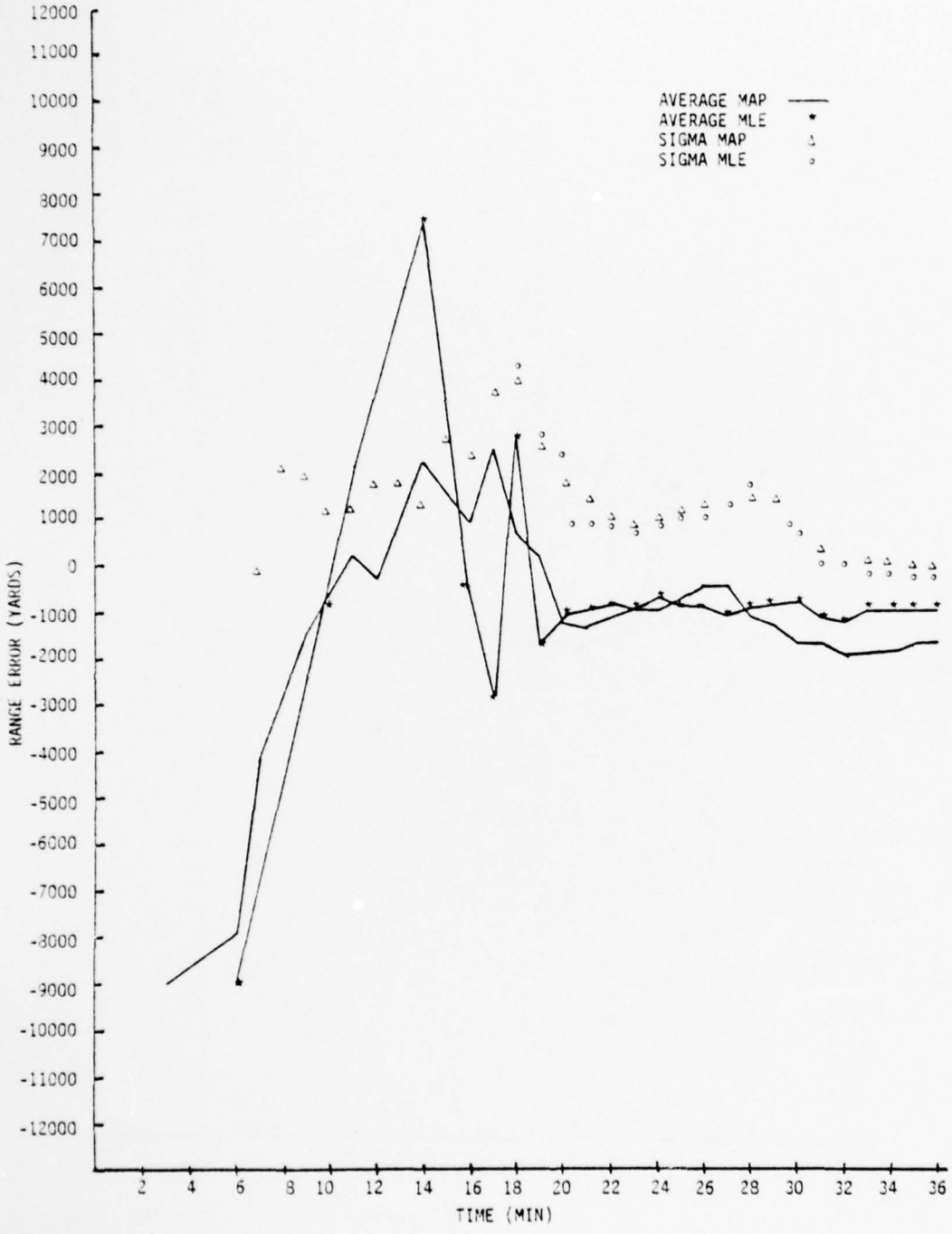

Figure 3-2a Range Error for 1st CZ Path (True and Assumed), Horizontal Bearing, Closing Target Course.

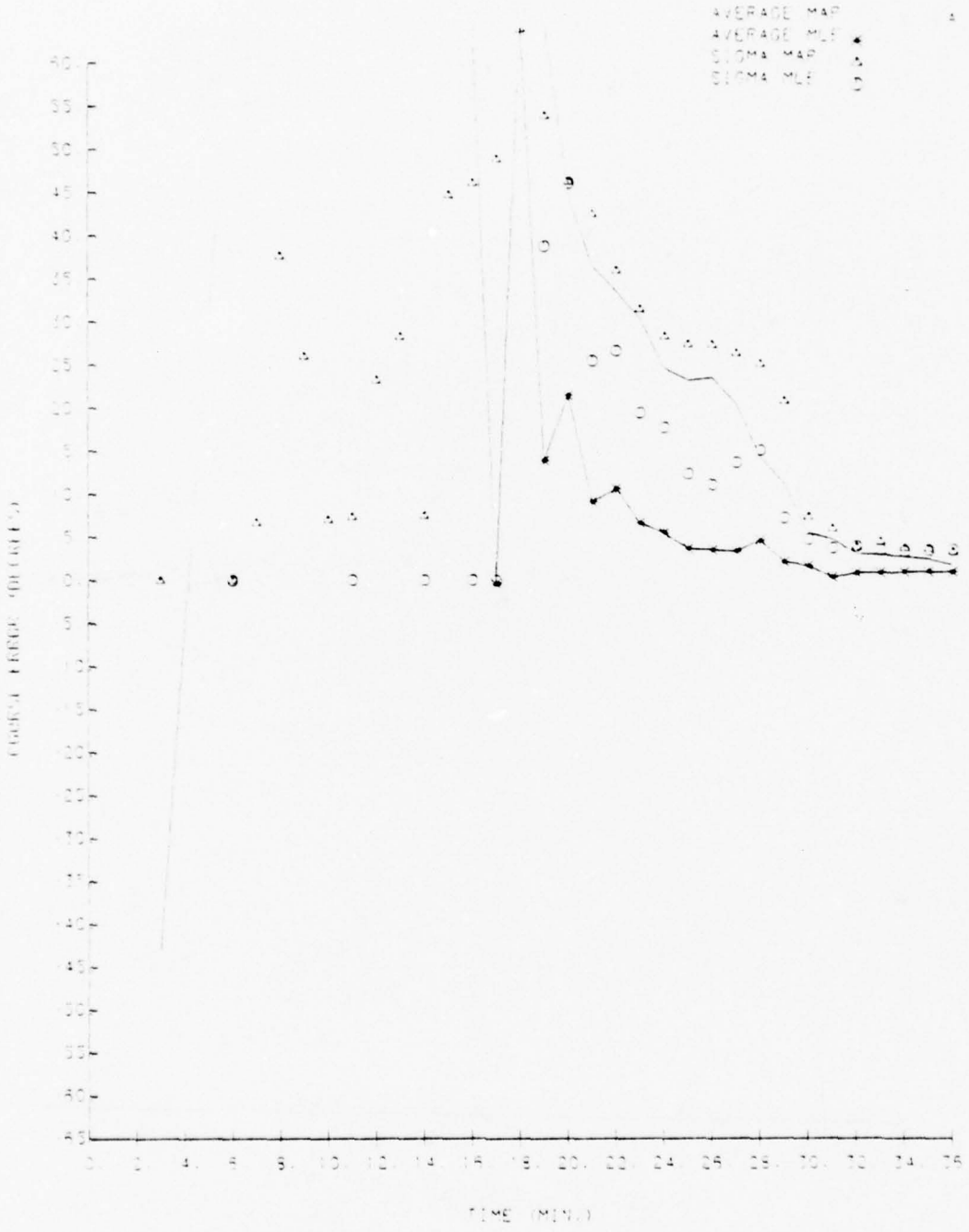

Figure 3-2b Course Error for 1st CZ Path (True and Assumed), Horizontal Bearing, Closing Target Course.

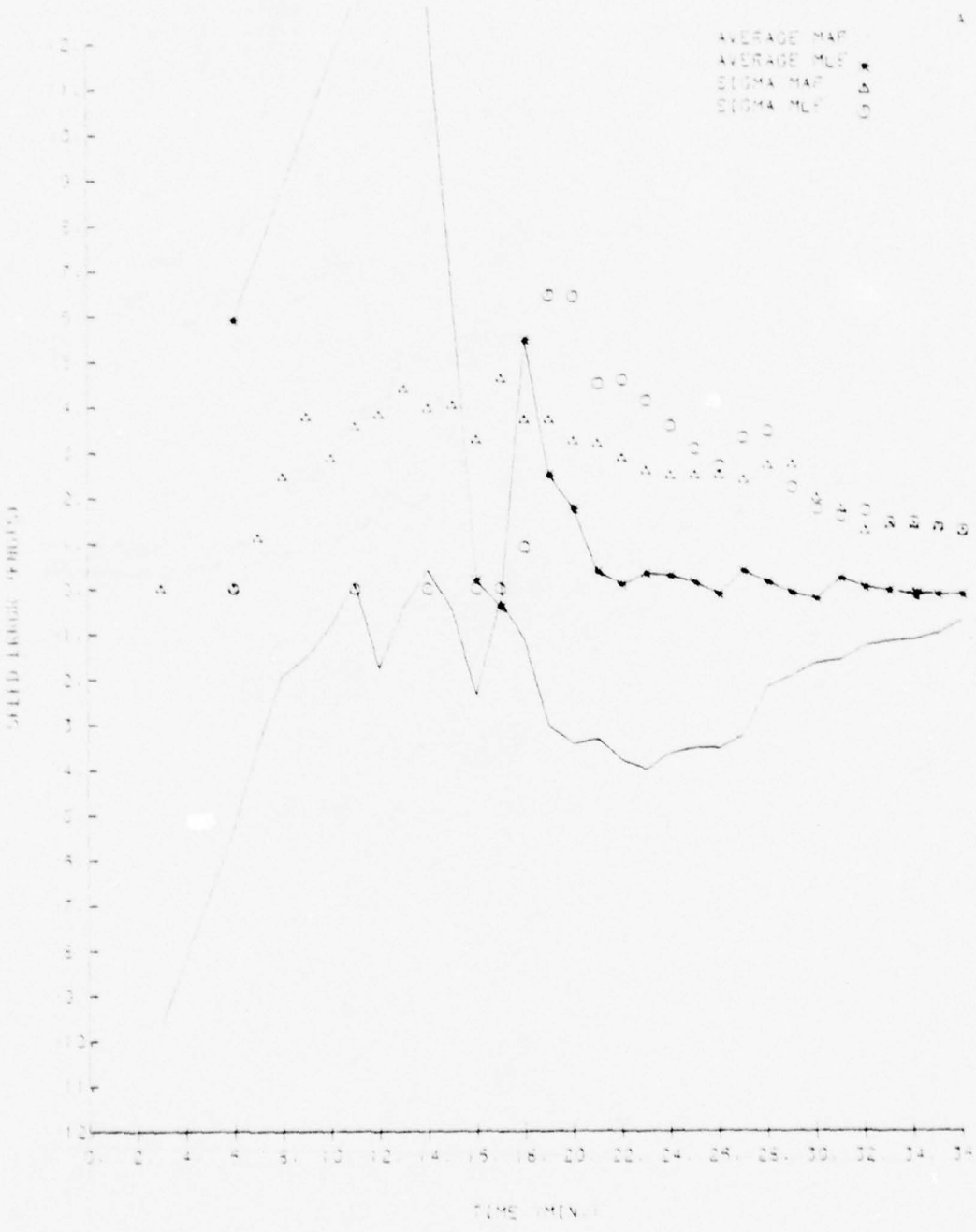

Figure 3-2c Speed Error for 1st CZ Path (True and Assumed), Horizontal Bearing, Closing Target Course.

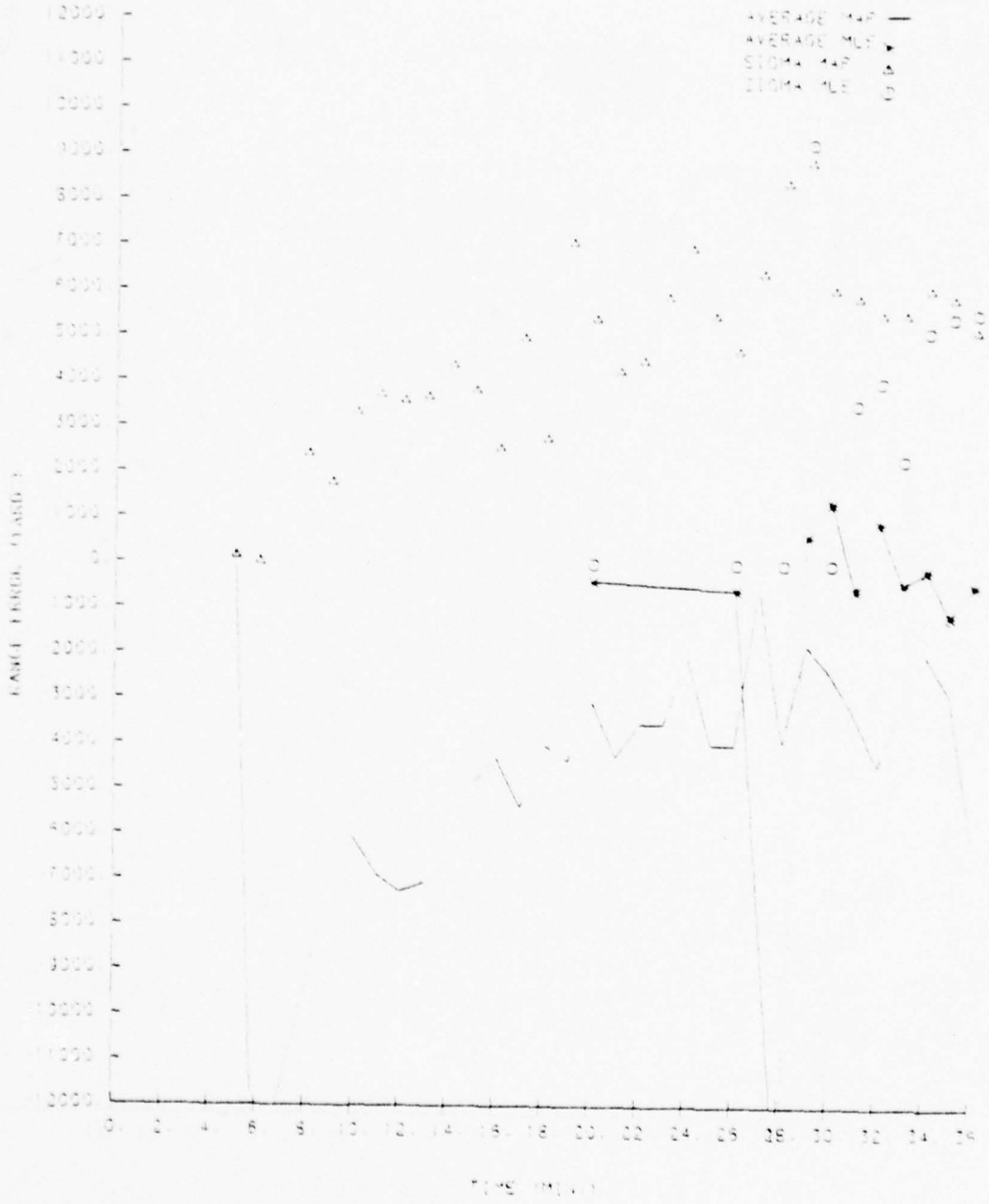

Figure 3-3a Range Error for 2nd CZ Path (True and Assumed), Horizontal Bearing, Closing Target Course.

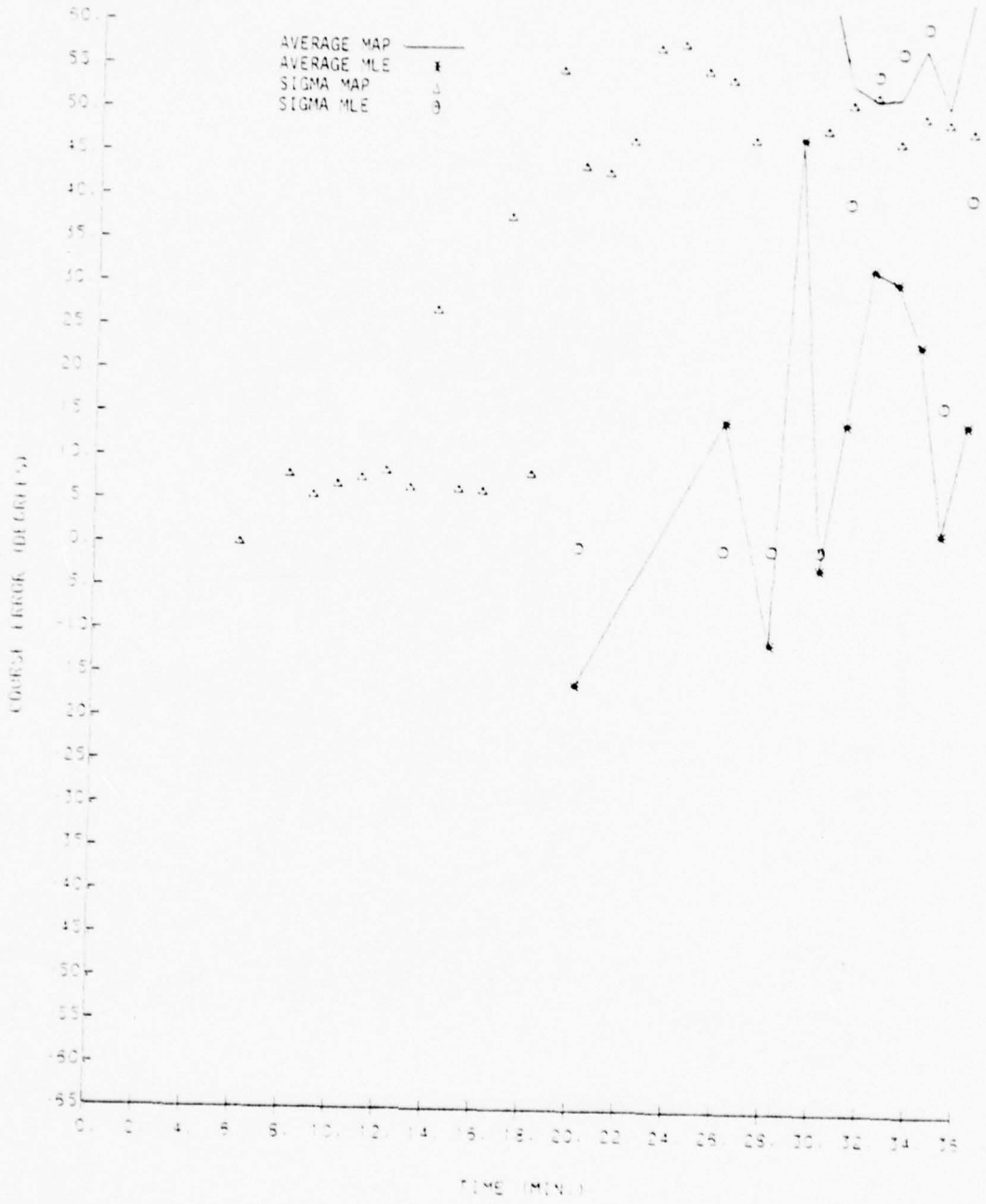

Figure 3-3b Course Error for 2nd CZ Path (True and Assumed), Horizontal Bearing, Closing Target Course.

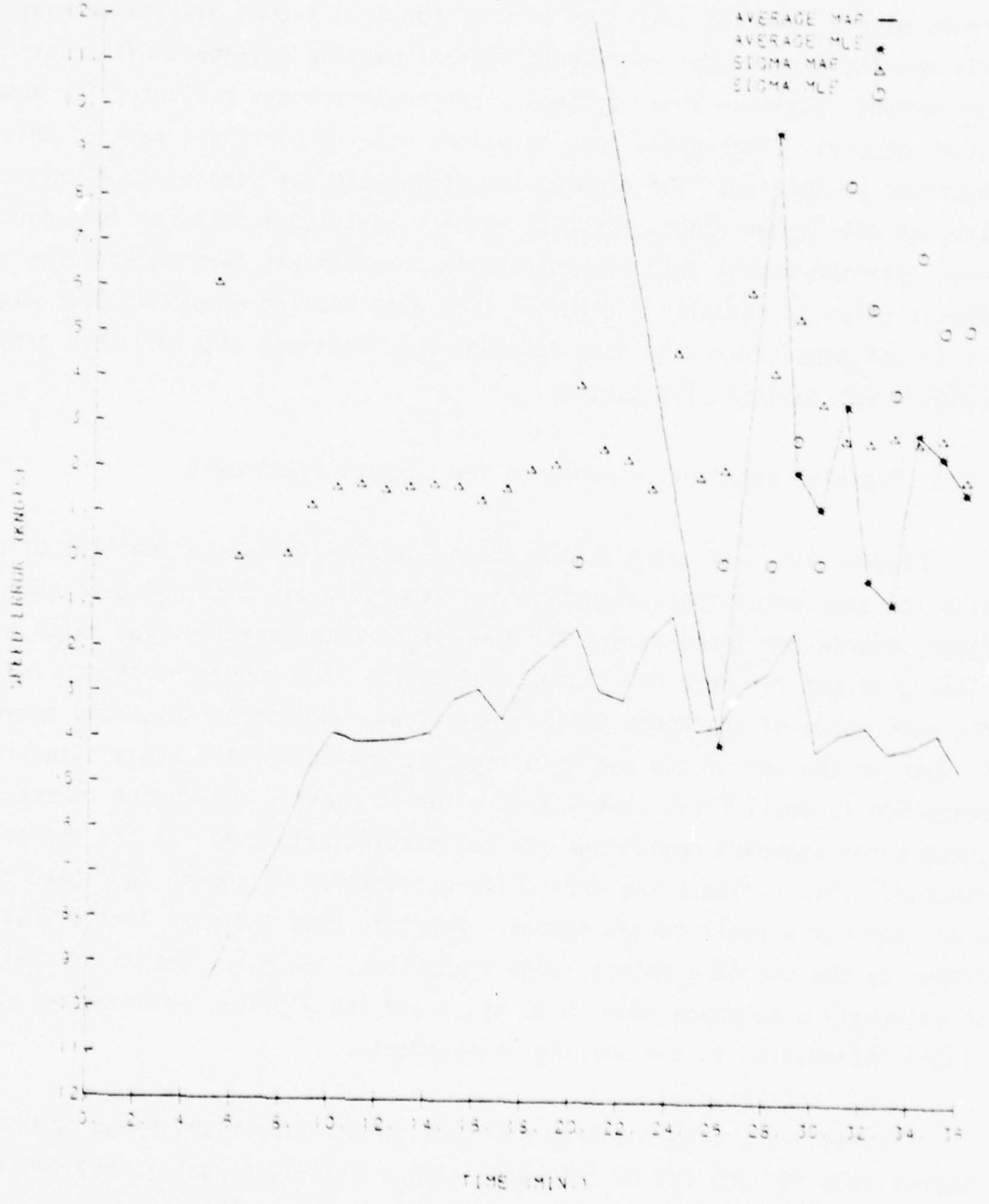

Figure 3-3c Speed Error for 2nd CZ Path (True and Assumed), Horizontal Bearing, Closing Target Course.

3.1 Phase I (Horizontal Bearing) Results

The majority of the simulations were based on unbiased random bearing errors with a standard deviation of 0.2° for a 20 second average bearing. This bearing error model represents typical passive broadband ATF tracking for current submarine sonar systems. Larger errors are evaluated for comparison, but in general, convergence zone solutions require bearing errors of this magnitude or smaller. The problem time simulated was limited to 40 minutes although the larger ranges (2nd CZ) require additional data for full convergence. For the direct path assumptions the problem was terminated after 15 minutes which is normally sufficient time with bearing errors of 0.2° magnitude. Two target aspects are analyzed (closing and crossing) with own ship executing 5 minute 60° lead/60° lag tactics.

3.1.1 Examples of Solution Behavior for Correct Hypotheses

Figures 3-1, 3-2 and 3-3 show the solution errors as a function of problem time for the correct path assumptions. Figures 3-1a, 3-1b and 3-1c show the range, course and speed errors for the direct path case (20 kyds) with a closing target for both MAP and MLE solutions. The connected points represent the mean value of the Monte Carlo repetitions. All three solutions converge in mean at the end of two own ship legs (11 minutes). The range standard deviation is small (less than 1 kyd) after 10 minutes, while the course and speed error standard deviations are not particularly small at the end of 15 minutes. This reflects the difficulty encountered in course and speed determinations for a small target aspect. For this case there is little advantage gained by the use of a'priori range statistics. However, the direct path is an extremely wide range zone (0-30 kyds) and the a'priori information adds little information to the bearing measurements.

Figures 3-2a, 3-2b and 3-2c show the range, course and speed errors respectively for the 1st CZ (54 kyds) with a closing target aspect and a measurement error standard deviation of 0.2 degrees. The convergence of the mean solution errors is somewhat better for the MLE solution while

The standard deviations are similar. Solution convergence for both MLE and MAP is essentially completed after 36 minutes. The bias error introduced by the a'priori range estimate in the MAP solution has more effect (for this geometry) on the course and speed mean errors than it does on the range error. Note that the MLE solution means are based on only one converged Monte Carlo repetition for the first 17 minutes. This is indicated by the omission of the standard deviation. With the MAP solution the standard deviation is initially too small because of a limited number of converged Monte Carlo repetitions.

Figures 3-3a, 3-3b and 3-3c show the results for a closing target at the 2nd CZ (109 kyds). The MLE solution converges in mean by the end of the problem while the MAP course and speed solutions are poor due to the closing target aspect. Notice however, that no MLE solutions converge numerically prior to 20 minutes into the problem. The principal advantage of the a'priori range information apparently is related to the numerical convergence of the solution procedure rather than an improvement in the ultimate solution, Basically, the a'priori range estimate does not improve until sufficient bearings and TMA legs are obtained to provide a range solution. The resolution of course and speed during the early legs are strongly geometry dependent. For the closing target of Figure 3-3 the solution takes on the flipped course (opening versus closing) for most of the run and never fully recovers. The standard deviation values shown on all three sets of curves must be viewed with caution since during the early legs the number of converged Monte Carlo repetitions may be small causing a poor estimate of the solution variation.

It is apparent from these sample plots that the value of the correct a'priori information to solution accuracy and convergence time is disappointingly small. However, the comparison is made to an MLE algorithm which benefits from good initialization using the a'priori range.

3.1.2 Comparison of MAP and MLE Solutions for Alternate Hypotheses

Using the criteria discussed in Section 3.1.5 a solution convergence time was established for each geometry/path hypothesis based on the major axis

of the velocity-ellipse-error bound, reaching a value of 1 knot. Table 3-1 shows the time; the corresponding rms range, course and speed errors and the average number of converged solutions for MAP and MLE solutions for all path assumptions. The rms errors are computed over the Monte Carlo repetitions as the root mean square combination of the mean and standard deviation. The number of converged Monte Carlo solutions are obtained by counting the total number of converged repetitions and dividing by the number of solutions attempted (problem time in minutes). If all attempted solutions converged, this number would be 30. As evident in the table, the solution convergence criteria was met within the problem time only for the direct path and 1st CZ cases with a crossing target aspect for the latter. The data presented in all other cases was taken at the end of the simulated problem (15 minutes for direct path and 40 minutes for 1st and 2nd CZ runs).

From Table 3-1 it can be seen that all path hypotheses eventually converge towards the correct solution with the smallest errors occurring with the correct assumption as expected. However, as suggested by the preceding solution error plots, the difference between the MAP and MLE solutions is small with a slight advantage in solution accuracy observable for the MLE solution. This conclusion is valid for all combinations of true and assumed hypotheses. Convergence time is also relatively independent of solution type (MAP and MLE) and path hypothesis. The convergence time is geometry dependent and the closing target requires larger convergence times at a given range and yields poorer course and speed solutions than those achieved with the crossing target. The best results would appear to occur with a MLE solution initialized at the correct a'priori path assumption. This is misleading because the rms errors are calculated based on the converged Monte Carlo repetitions. For many combinations of correct and assumed propagation path assumptions, the MLE algorithm experiences more difficulty in the numerical convergence of the iterations (Gauss Elimination). For example, for the 2nd CZ MLE solutions, the number of numerically converged Monte Carlo repetitions are much smaller than for the MAP solution. This reflects the fact that no MLE repetitions converged until the last TMA leg. In effect, the MLE algorithm generated no solutions for the majority of the problem time for this case. The MAP solution converges numerically more often in all cases. The MAP solutions for the incorrect hypotheses are biased so it is important to select the correct

Table 3-1 Summary of (Horizontal Bearing Input) TMA Solution Statistics at Solution Convergence Times.

	TRUE PATH/ ASSUMED PATH ***	PROBLEM TIME (MIN)	MAP					MLE				
			CONVERGED MONTE CARLO*	CONVERGENCE TIME** (MIN)	RMS ERROR			CONVERGED MONTE CARLO*	CONVERGENCE TIME** (MIN)	RMS ERROR		
					RANGE (YDS)	SPEED (KTS)	COURSE (DEG)			RANGE (YDS)	SPEED (KTS)	COURSE (DEG)
CLOSING TARGET COURSE	D/D	15	19.6	>15	826	3.42	11.9	17.9	>15	781	2.60	11.9
	D/1	15	19.3	>15	906	4.37	5.8	16.7	>15	802	3.18	10.8
	D/2	15	17.1	>15	869	3.85	9.0	16.1	>15	910	3.63	16.3
	1/1	40	22.1	>40	1055	.97	2.2	15.8	>40	933	.95	2.7
	1/D	40	22.1	>40	1208	1.45	3.8	16.1	>40	1228	.89	2.3
	1/2	40	23.9	>40	1419	1.32	2.6	9.9	>40	1272	.85	2.4
	2/2	40	12.8	>40	5641	4.52	42.6	2.8	>40	6016	3.83	43.9
	2/D	40	12.0	>40	13216	2.5	142.7	1.2	>40	8233	5.12	33.8
	2/1	40	21.0	>40	14159	2.64	142.7	1.6	>40	5216	4.50	57.3
CROSSING TARGET COURSE	D/D	15	23.7	15	516	.32	4.9	19.4	15	398	.27	4.3
	D/1	15	18.7	15	562	.36	4.8	18.7	15	566	.36	4.5
	D/2	15	16.9	15	652	.41	4.8	18.9	15	536	.31	4.6
	1/1	40	22.7	31	1264	.27	5.6	22.5	31	1110	.23	5.2
	1/D	40	23.9	30	2202	.50	8.5	23.0	30	2205	.50	7.2
	1/2	40	22.2	31	2192	.48	5.6	23.5	30	1265	.28	5.2
	2/2	40	16.2	>40	6687	1.02	13.8	14.7	>40	6512	.96	14.4
	2/D	40	20.6	>40	16791	1.72	13.6	13.9	>40	3917	.53	9.1
	2/1	40	21.7	>40	14162	1.53	9.0	6.7	>40	8529	.95	4.4

*"Converged Monte Carlo" is the average number of converged Monte Carlo iterations per solution time increment (maximum number = 30).

**Convergence Time is the time at which velocity error bound (major axis) drops to 1.0 knot.

***BB = Bottom Bounce, D = Direct Path, 1 = First Convergence Zone, 2 = Second Convergence Zone.

solution. This can be done at the end of the problem when all solutions converge toward the same solution, but it is important to discard incorrect solutions early to minimize computer burden in an operational system. Observing the 2nd CZ results it is obvious that a dismissal criteria should have a high confidence to minimize solution errors.

In summary, the incorporation of a'priori range uncertainty has little effect on solution accuracy and can in fact bias the solution. However, this information (incorporated in a MAP algorithm) improves numerical convergence during the early TMA legs. This improvement is expected since the coefficient matrix (ψ) used in the Gauss-Newton iteration procedure is normally ill conditioned during the early legs. The a'priori statistics ensure that this matrix is positive-definite and thus, improve the convergence of the iterations.

This incorporation of a'priori range estimates based on environmental predictions yields disappointing solution improvement. A limited study, involving a'priori speed estimates, yields results that are quite promising. This a'priori estimate may be based on turn count or classification information or simply a tactical guess. Figures 3-4a, 3-4b, 3-4c and 3-4d show the rms errors using the correct MAP hypotheses for the 1st CZ case with a crossing target. The rms solution errors are shown in these cases both without an a'priori speed estimate (σ_V = 15 kts) and with a speed estimate with an uncertainty (σ_V) of 2 knots. The actual error in the estimate was 1 knot. Note that the solutions with the a'priori speed estimate converge immediately whereas the normal MAP solutions iterations do not converge until the beginning of the second leg. The range solutions for that case are substantially improved over the first 22 minutes while the final solutions are identical. The course and speed solutions are much more accurate over the first 18 minutes. As shown in Figure 3-4d, the solution bearing error is independent of the a'priori speed information. Speed estimates are not always available, but these limited results show that it should be incorporated when available. As discussed in Section 3.1.3, the a'priori speed information can dramatically improve numerical convergence properties as well as improve solution convergence. Note, there is no equivalent MLE solution since the solutions are actually initialized at zero speed due to the absence of a'priori course estimates.

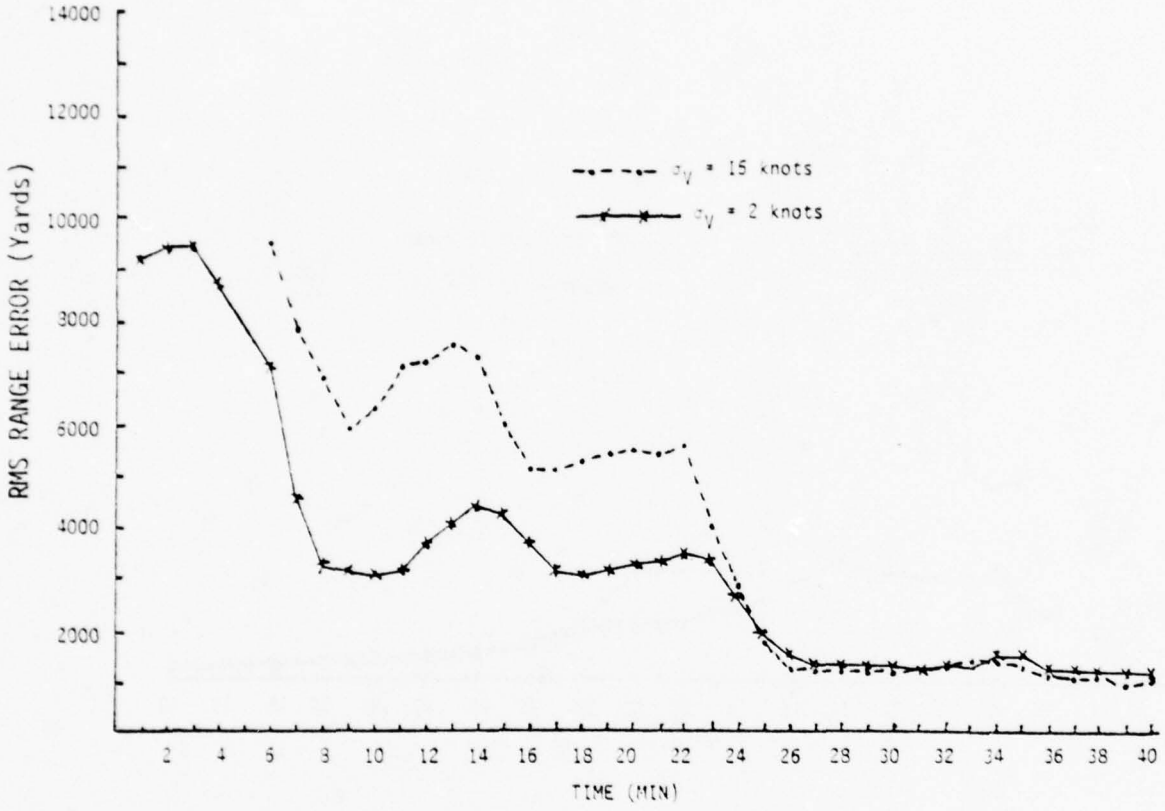

Figure 3-4a MAP rms Range Error for Two A'priori Speed Error Estimates (σ_V). [Horizontal bearing, crossing target course, 1st CZ (true and assumed path).]

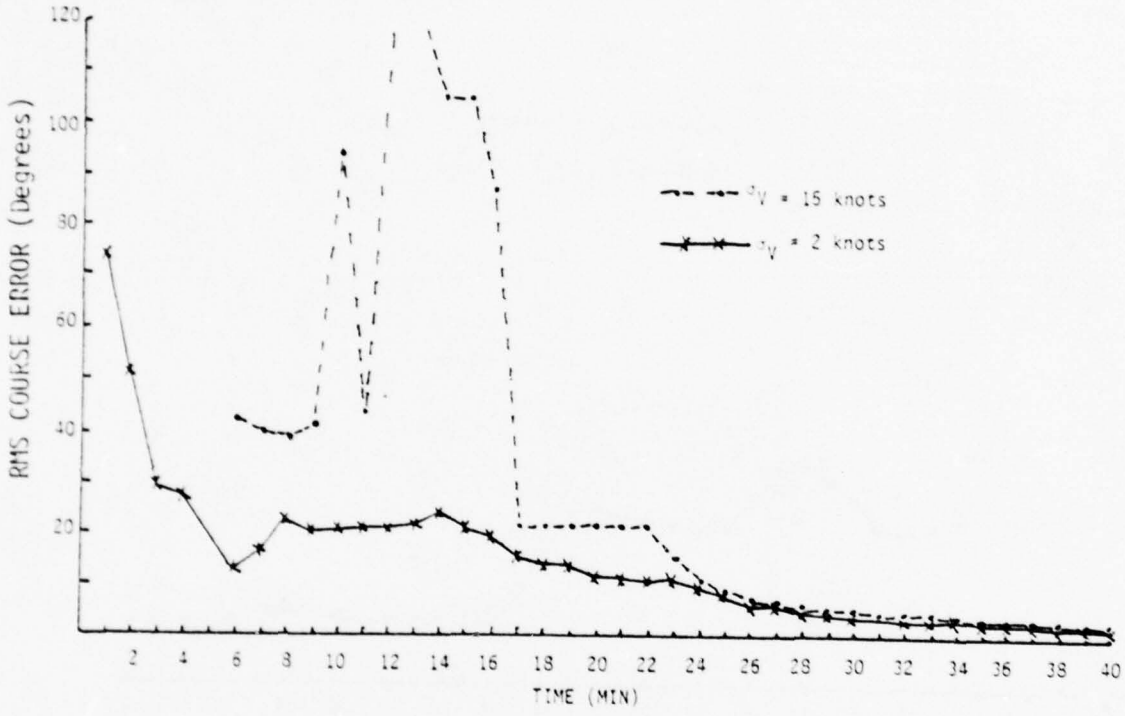

Figure 3-4b MAP rms Course Error for Two A'priori Speed Error Estimates (σ_V). [Horizontal bearing, crossing target course, 1st CZ (true and assumed path).]

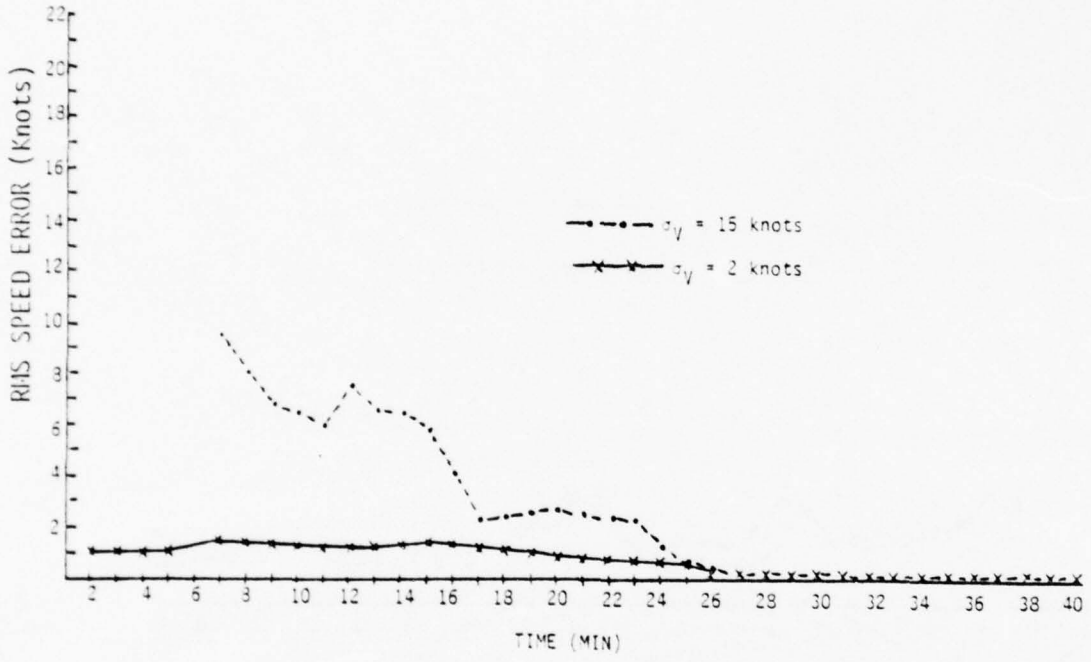

Figure 3-4c MAP rms Speed Error for Two A'priori Speed Error Estimates (σ_V). [Horizontal bearing, crossing target course, 1st CZ (true and assumed).]

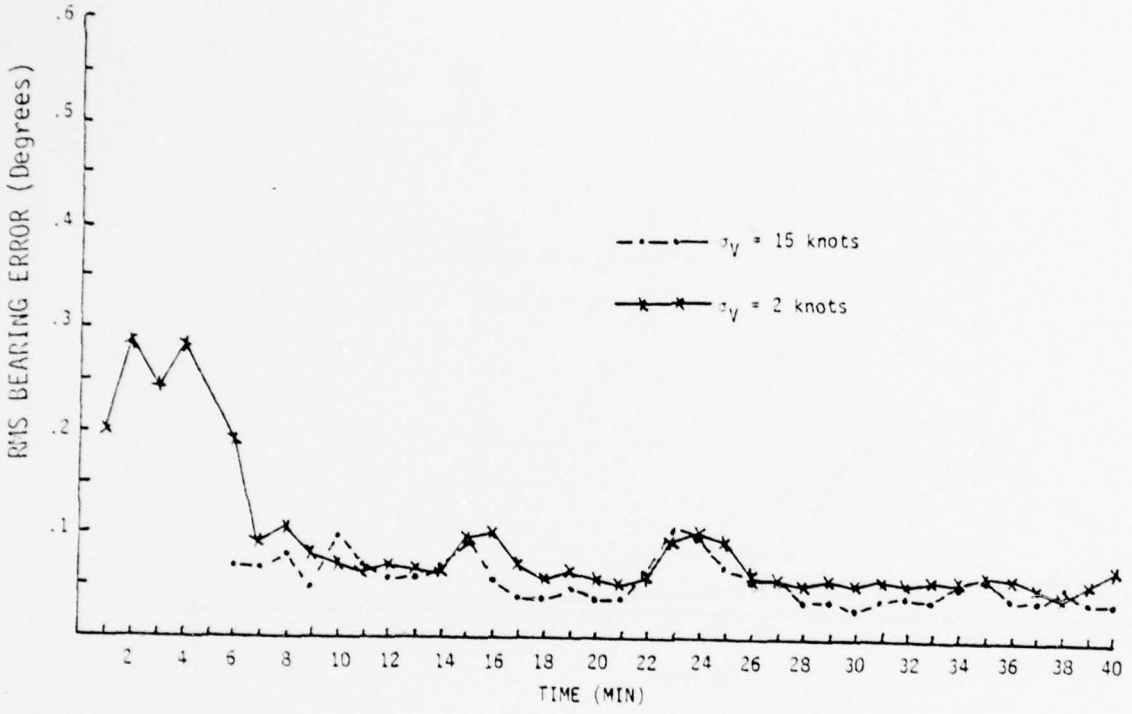

Figure 3-4d MAP rms Bearing Error for Two A'priori Speed Error Estimates (σ_V). [Horizontal bearing, crossing target course, 1st CZ (true and assumed).]

The only way of incorporating this information into a MLE solution would be to constrain speed which would bias the final solution by the a'priori speed error.

3.1.3 Numerical Convergence Properties for Horizontal Bearing Inputs

The number of Monte Carlo repetitions which meet the numerical convergence criteria at a particular problem time are shown in Figures 3-5 through 3-10 for all horizontal bearing geometries using a measurement bearing error standard deviation of 0.2 degrees. In all cases the MAP and MLE (correct path assumption) solution results are presented without a'priori speed estimates. For the 1st CZ and 2nd CZ cases the results are also presented for a MAP solution with a'priori speed estimates (2 kts standard deviation). For the direct path solutions at 20 kyds (Figure 3-5 and 3-6) the MAP solution generates more converged solutions on the second leg (6-11 minutes), but thereafter all Monte Carlo repetitions converge for both solutions. The 1st CZ results (Figure 3-7 and 3-8) show that the MAP solutions without a'priori speed estimates converge about 60 percent of the time after 9 minutes, while the MLE solutions do not meet the stopping criteria until 18 minutes into the solution for the closing target. With an a'priori speed estimate nearly all attempted solutions converged for the closing geometry. For the crossing geometry the comparison is much closer. This is expected because the higher bearing rates generated by that geometry simplify the numerical problems associated with the MLE techniques. The 2nd CZ results (Figures 3-9 and 3-10) exhibited the same properties. The closing geometry is very difficult for the MLE solution. A 50 percent probability of convergence is reached only at the end of the problem. The MAP solution without a'priori speed estimates converges 50 percent of the time after 10 minutes while the MAP solution with a'priori speed converges nearly all the time. With the crossing target the comparison is much closer.

These results demonstrate that the difficult geometries benefit from incorporation of a'priori range/speed inputs (and uncertainty) in the sense of increasing the probability of numerical convergence during the early parts of the problem. This is important because a closing CZ target geometry, which is the case that benefits the most, will result in loss of contact as the

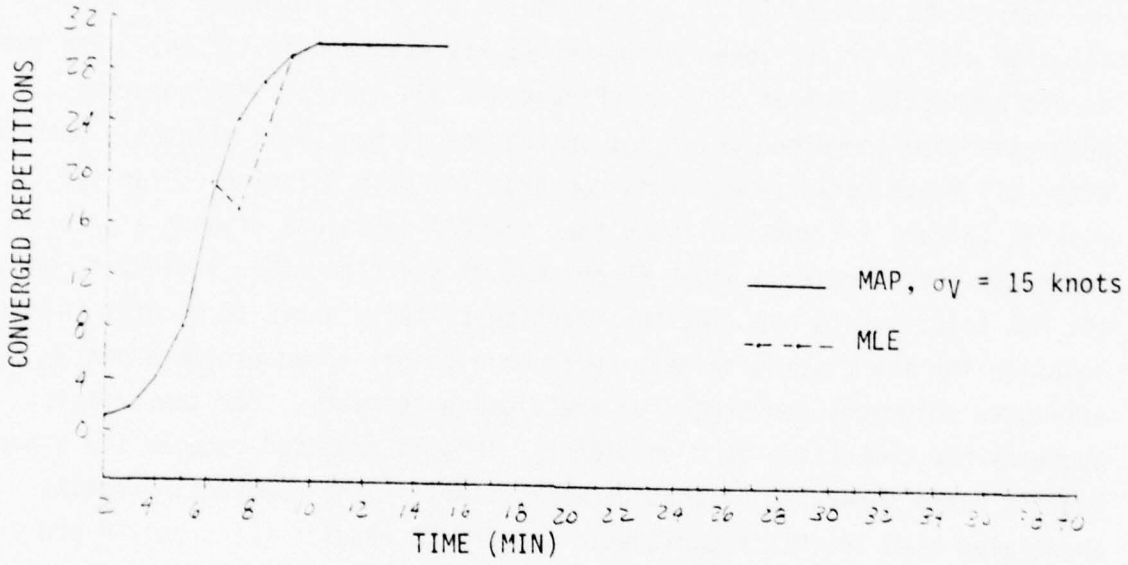

Figure 3-5 Converged Monte Carlo Repetitions, MAP Versus MLE, Horizontal Bearing, Direct Path (True [20 kyds] and Assumed), Closing Target Course.

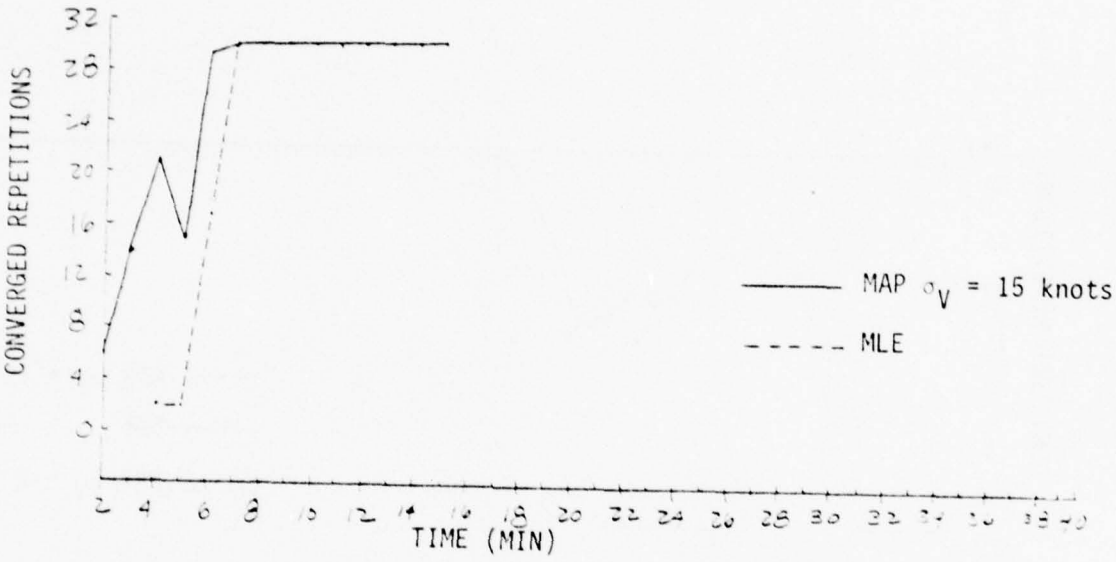

Figure 3-6 Converged Monte Carlo Repetitions, MAP Versus MLE, Horizontal Bearing, Direct Path (True [20 kyds] and Assumed), Crossing Target Course.

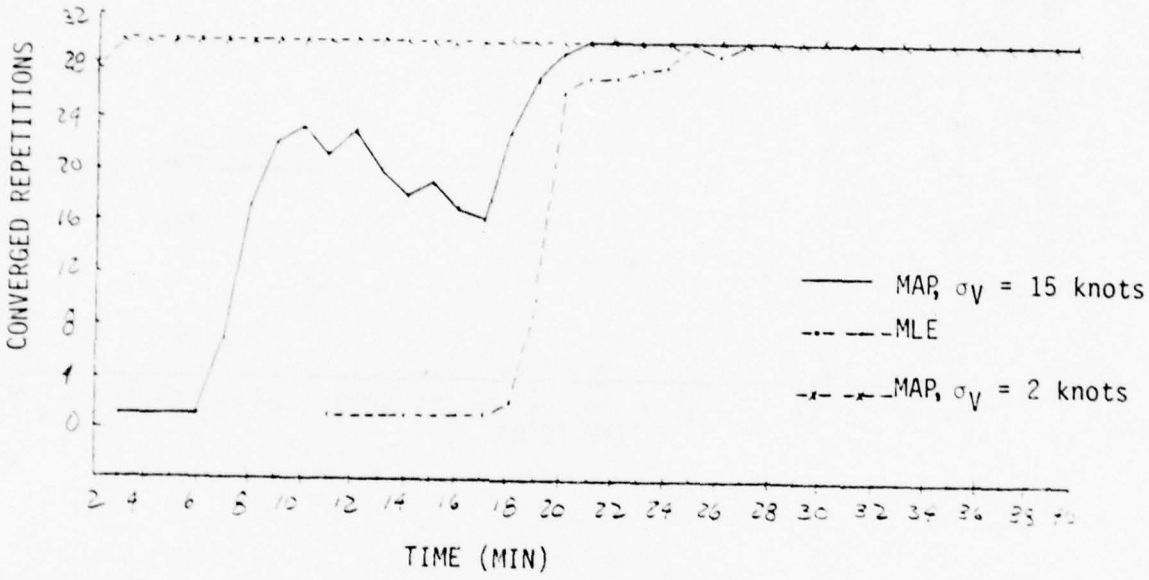

Figure 3-7 Converged Monte Carlo Repetitions, MAP Versus MLE, Horizontal Bearing, 1st CZ Path (True and Assumed), Closing Target Course.

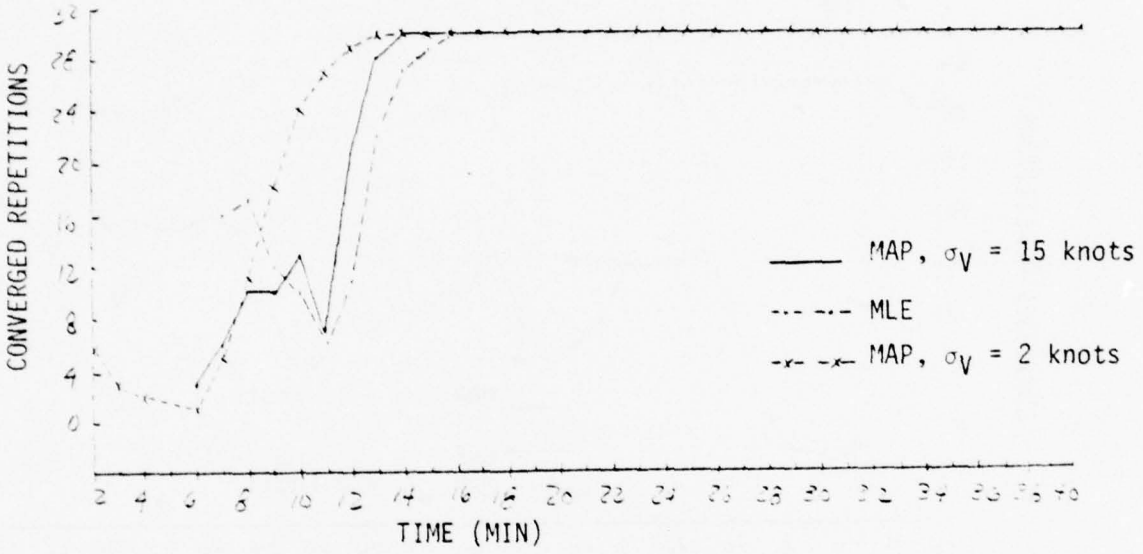

Figure 3-8 Converged Monte Carlo Repetitions, MAP Versus MLE, Horizontal Bearing, 1st CZ Path (True and Assumed), Crossing Target Course.

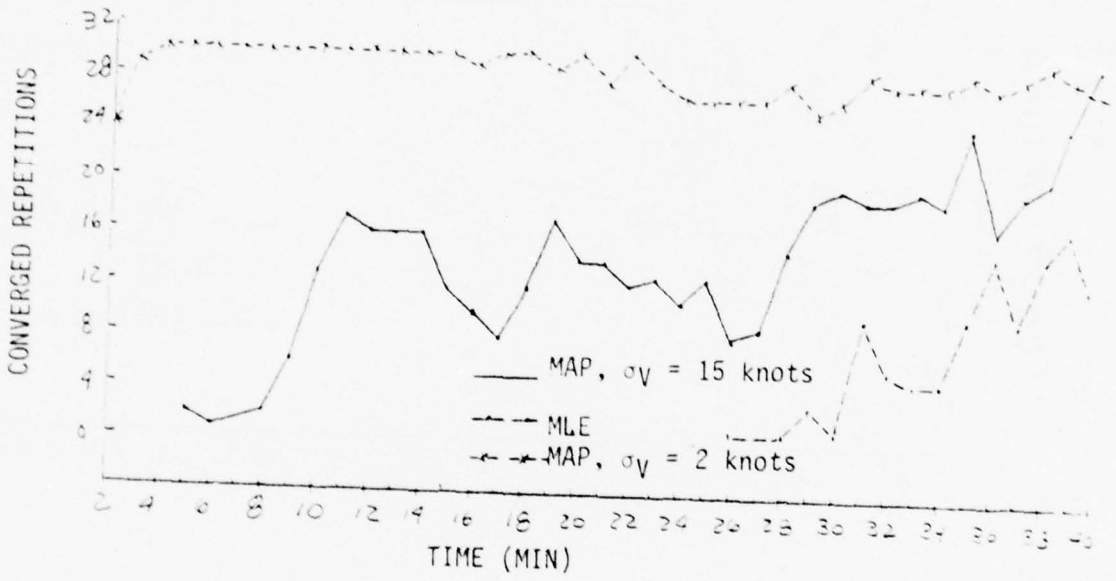

Figure 3-9 Converged Monte Carlo Repetitions, MAP Versus MLE, Horizontal Bearing, 2nd CZ Path (True and Assumed), Closing Target Course.

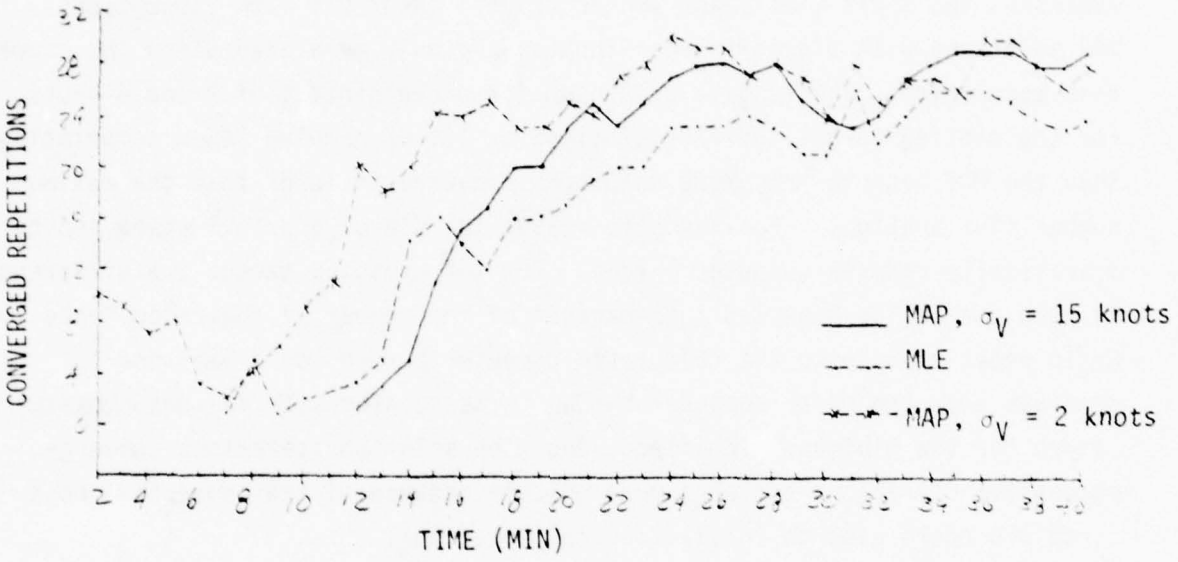

Figure 3-10 Converged Monte Carlo Repetitions, MAP Versus MLE, Horizontal Bearing, 2nd CZ Path (True and Assumed), Crossing Target Course.

target closes inside the convergence zone. The MLE technique will most likely generate no solutions before contact is lost.

The computational requirement for the three solution types is illustrated graphically in Figures 3-11 and 3-12. For MAP (no a'priori speed) and MLE solutions the center point for each range band shown is the total number of Gauss Elimination iterations for the correct hypotheses. The connected points represent the short (left) and longer (right) incorrect path assumptions. The MAP solutions with a'priori speed inputs were only generated using the correct path assumption. The results are shown for uncertainties of 2 and 4 knots. For the closing target the MAP solutions at 1st CZ require fewer computations than the MLE because many more solutions converge in fewer than the maximum number of iterations. For the same reason the use of a'priori speed inputs dramatically reduces computer burden. For the crossing target the difference is much smaller as expected. Comparison of the number of converged Monte Carlo repetitions with the calculated computer burden would lead one to conclude that the major computer burden is associated with the unsuccessful search for the minimum. In effect, once the solution iterations converge, successive iterations converge more quickly because of the sequential boot strap procedure used to initialize the iterations.

3.1.4 Dependence on Bearing Measurement Error

The simulation studies presented in this report are based on bearing measurement errors with a 0.2° standard deviation for the twenty second averages. A limited number of runs were executed using standard deviations of 0.5° and 1.5 degrees. For the convergence zone cases the 0.2° bearing errors are barely sufficient to obtain accurate solutions in a forty minute problem time. Therefore, results are not presented for those cases with larger bearing errors. In this section results are presented for direct path geometries to demonstrate the effect of increased bearing error. The 0.2° standard deviation is representative of broadband contact at relatively low signal-to-noise ratios for submarine sonar systems. At higher signal-to-noise ratios more accurate bearings can be obtained but smaller standard deviations were not simulated because the TMA problem would be simplified and the effect of external information obscured.

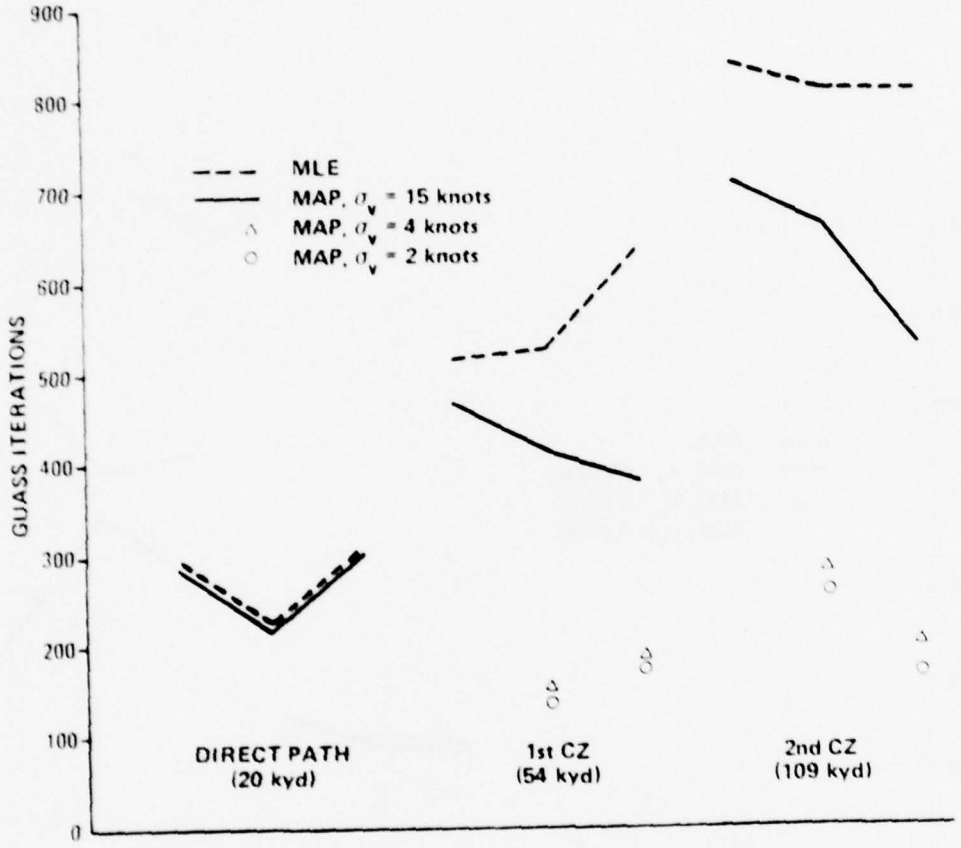

Figure 3-11 Total Gauss Iterations for MAP and MLE with Alternate Path Assumptions, Over 40 Minute Problem Time [Center point - correct path, horizontal bearing, closing target course].

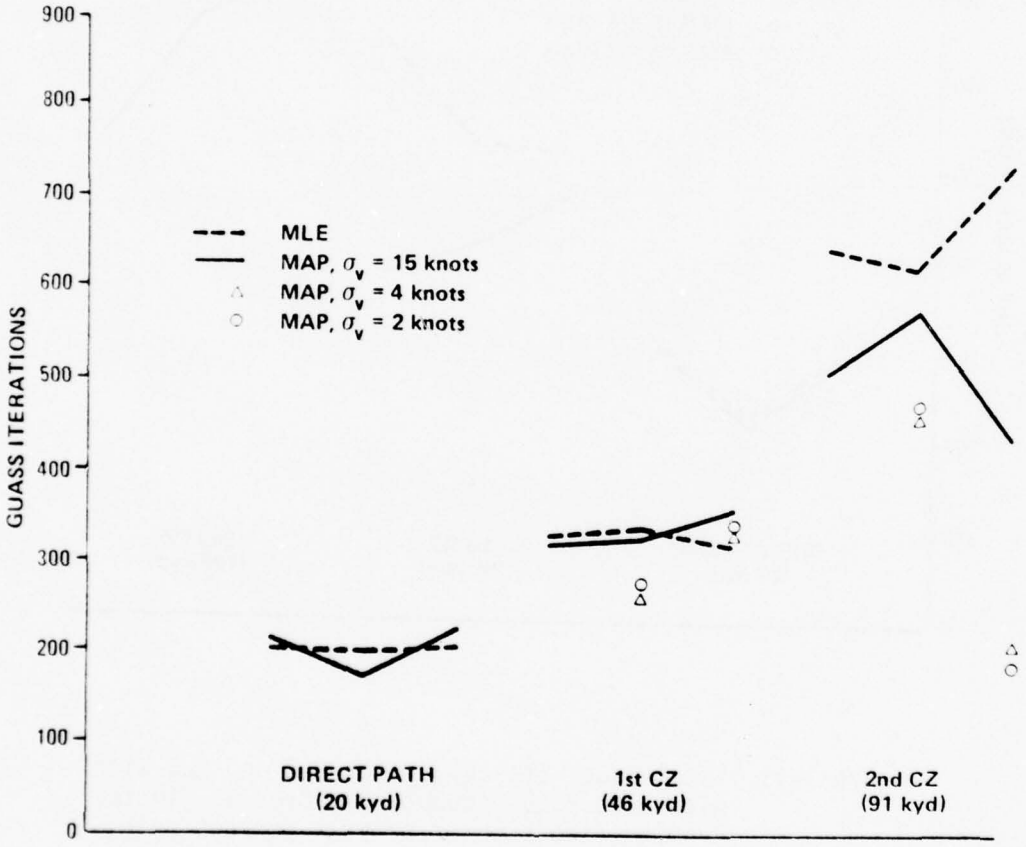

Figure 3-12 Total Gauss Iterations for MAP and MLE with Alternate Path Assumptions, Over 40 Minute Problem Time [Center point - correct path, horizontal bearing, crossing target course].

Figure 3-13 shows the mean and standard deviation of MAP solution range error versus time for bearing error standard deviations of 0.2° and 1.5 degrees. The geometry is a direct path at 20 kyds with a crossing target aspect. The principal effects of the increased measurement error is a delay in convergence of the mean error by about 6 minutes and an increase in standard deviation at the end of the problem. After 30 minutes the range error standard deviation is still larger than 1000 yards for the 1.5° bearing error standard deviation even though the crossing target aspect is a relatively easy TMA problem.

In Figure 3-14 the increase in convergence time with measurement error is shown for a 10 kyds and 20 kyds initial range. Two convergence times are indicated based on the range error standard deviation and speed error standard deviation over the Monte Carlo repetitions. At 20 kyds the two criteria yield equivalent convergence times while at 10 kyds it takes longer to converge speed than range. This discrepancy occurs because the speed convergence criteria is readily related to a given percent range error rather than an absolute range error (1000 yards in this case). The 0.5° bearing error standard deviation increases convergence time by 4 minutes (one leg) relative to the 0.2° bearing error. The 1.5° error causes a prohibitive increase in convergence time.

The effect on numerical convergence is shown in Figure 3-15. For the 10 kyds initial range numerical convergence is delayed by two minutes. For the 20 kyds initial range, consistent numerical convergence is delayed by eight minutes when the bearing error increases from 0.2° to 1.5 degrees.

3.1.5 Indicator of Solution Convergence Time

In an operational environment it is important to estimate the convergence status of the TMA solution in situ in order to determine when the solution can be applied to the tactical objective with reasonable confidence. The MAP and MLE solutions both calculate an estimate of Fisher's information matrix (ψ in Appendix A). If the true solution were used instead of the estimated solution, then ψ^{-1} would represent a lower bound on the solution error covariance matrix. In practice the actual solution error covariance matrix will exceed the bound because of unmodeled bearing bias errors. However, this lower bound

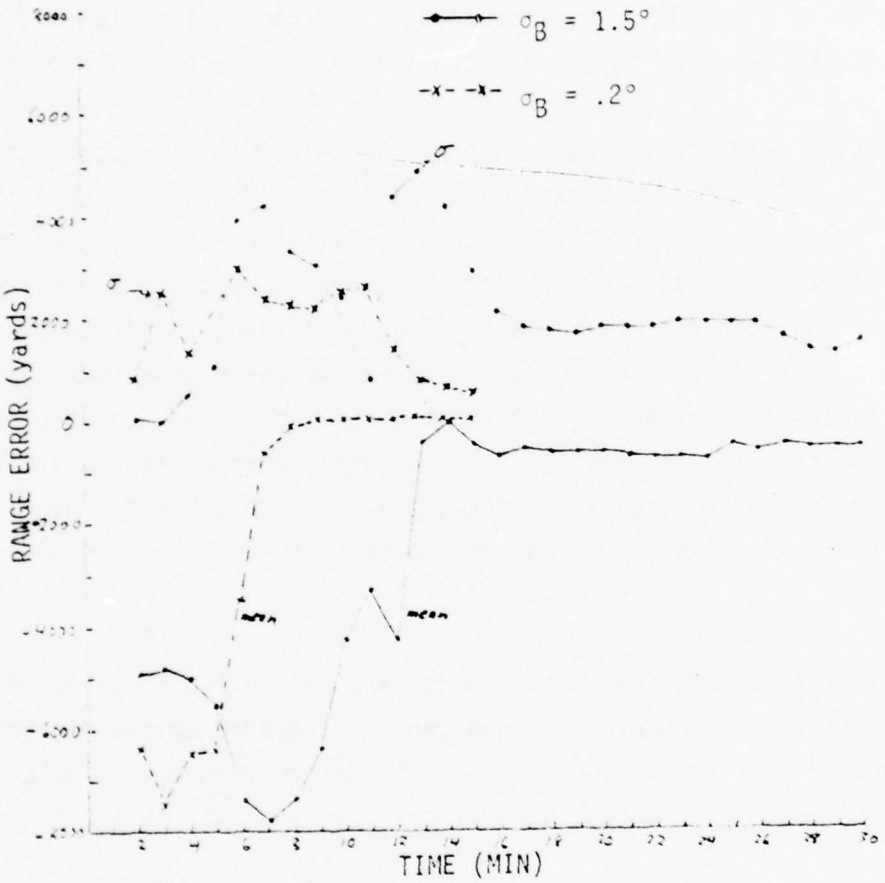

Figure 3-13 MAP Range Error for Two Bearing Measurement Errors. [Horizontal bearing, direct path (true and assumed), crossing target course.]

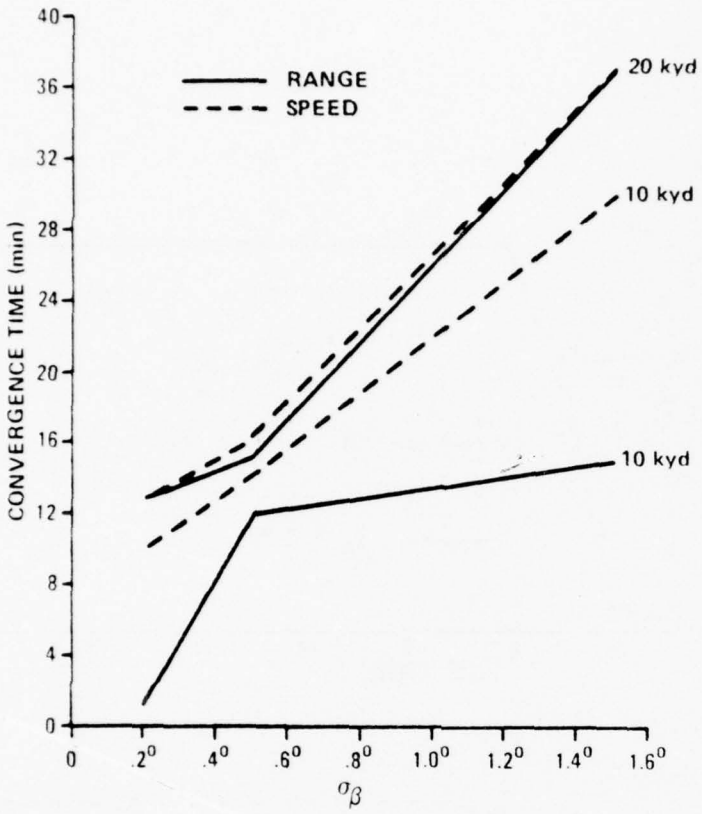

Figure 3-14 True Range and Speed MAP Convergence Time as a Function of Bearing Measurement Error (σ_B = .2°, .5°, 1.5°). [Horizontal bearing, direct path (true and assumed), crossing target course.]

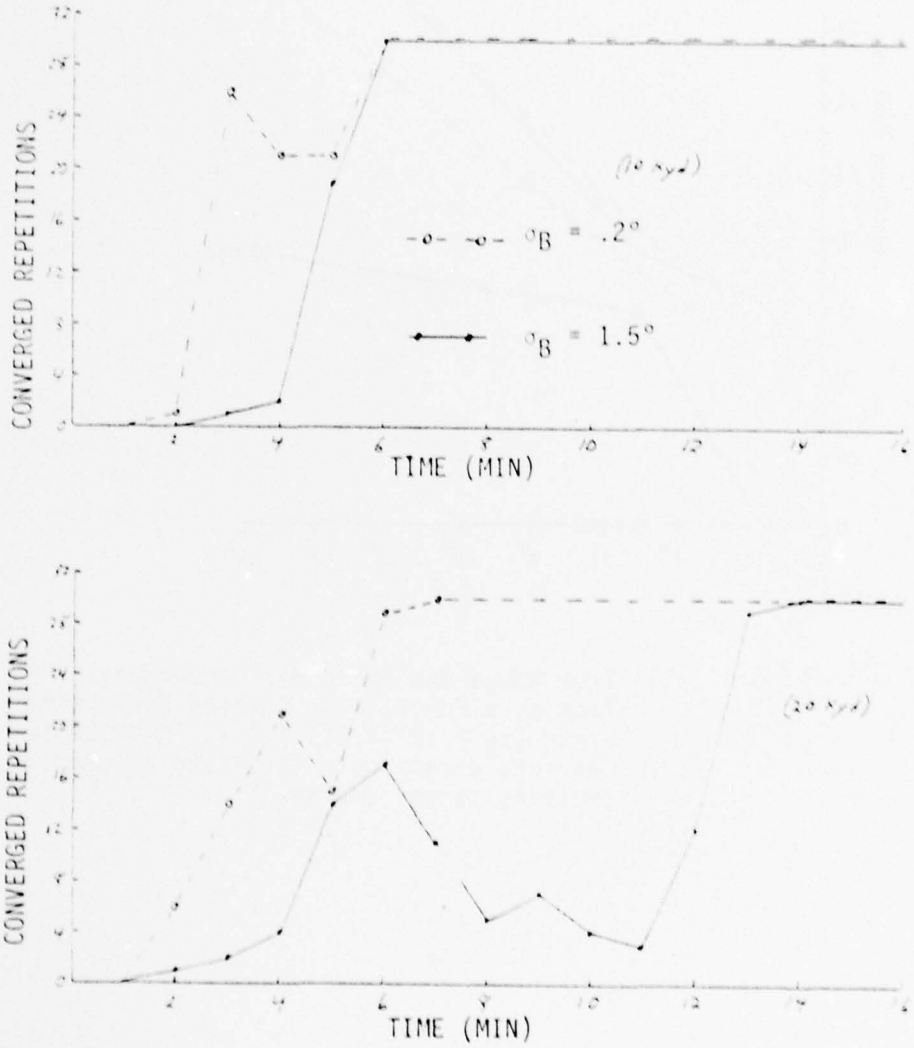

Figure 3-15 Converged Monte Carlo Repetitions (MAP) for Two Bearing Measurement Errors. [Horizontal bearing, direct path (true and assumed), crossing target course.]

does indicate the sensitivity of the solution to additional measurements and therefore can be used to ascertain if sufficient data has been processed. The validity of the converged solution can often be verified by examination of the "fit" to the measurements. To convert the lower bound matrix to simple scalar parameters, the inverse matrix (ψ^{-1}) is first partitioned into 2x2 position and velocity terms and the eigenvalues of the two submatrices computed. The square root of the larger eigenvalue for each case represents the major axis of the position error ellipse which represents a lower bound on range error, and the major axis of the total velocity error ellipse bounds the total velocity vector error. The major axis values computed from the solution are in error when the solution is in error, but they represent monotonic functions which converge to the lower bounds when the solution converges to the true solution.

In Figures 3-16, 3-17 and 3-18 the major axis for range and velocity are plotted for the direct path 1st CZ and 2nd CZ geometries respectively. (The target is closing for all three cases.) The MAP solution bounds and MLE bounds are presented for all cases along with Monte Carlo standard deviations of MAP solution range and speed errors. The error bounds for the MAP solutions are lower than those for the MLE solutions because of the a'priori information added to the former. The range error bounds indicate that the a'priori information represents a significant improvement in potential solution performance which was not actually realized by the algorithms studied. The discrepancy could be explained by the fact that the MAP estimate is only asymptotically optimum and does not necessarily provide an optimum solution for short or noisy measurement sequences.

The standard deviations of the Monte Carlo range error repetitions for the MAP solutions are in general smaller than the error bounds for the early parts of each problem, but tend to agree with the error bounds at the end of the problem. This is theoretically consistent with the asymptotically optimum nature of the solution and the initilization procedure. To compare true convergence with the lower bound during the early times it would be necessary to perform a Monte Carlo repetition sequence over the initial range estimate and include the mean error for each initial estimate into the standard deviation calculation. The speed error standard deviation is smaller than the error bound for the same reason. In addition, the speed error represents

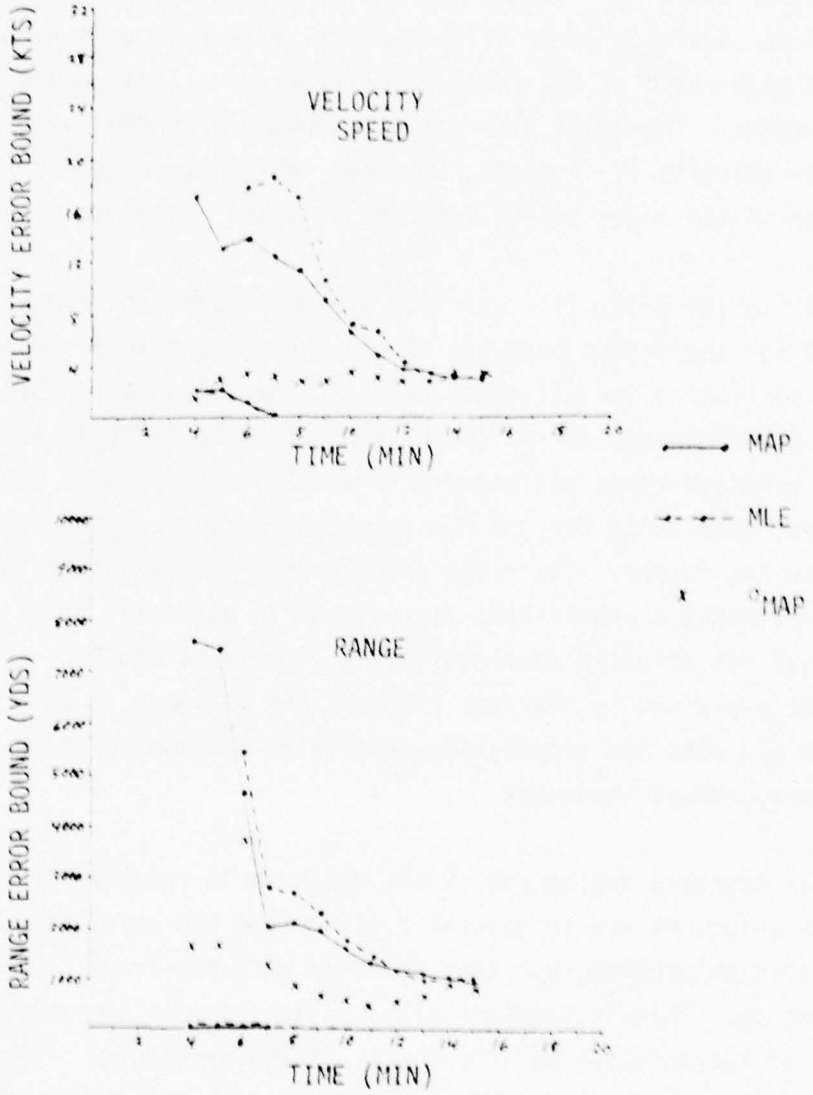

Figure 3-16 Theoretical Lower Bounds (Major and Minor Ellipse Axes) on Velocity and Range Errors [Direct path (true and assumed), horizontal bearing, closing target course].

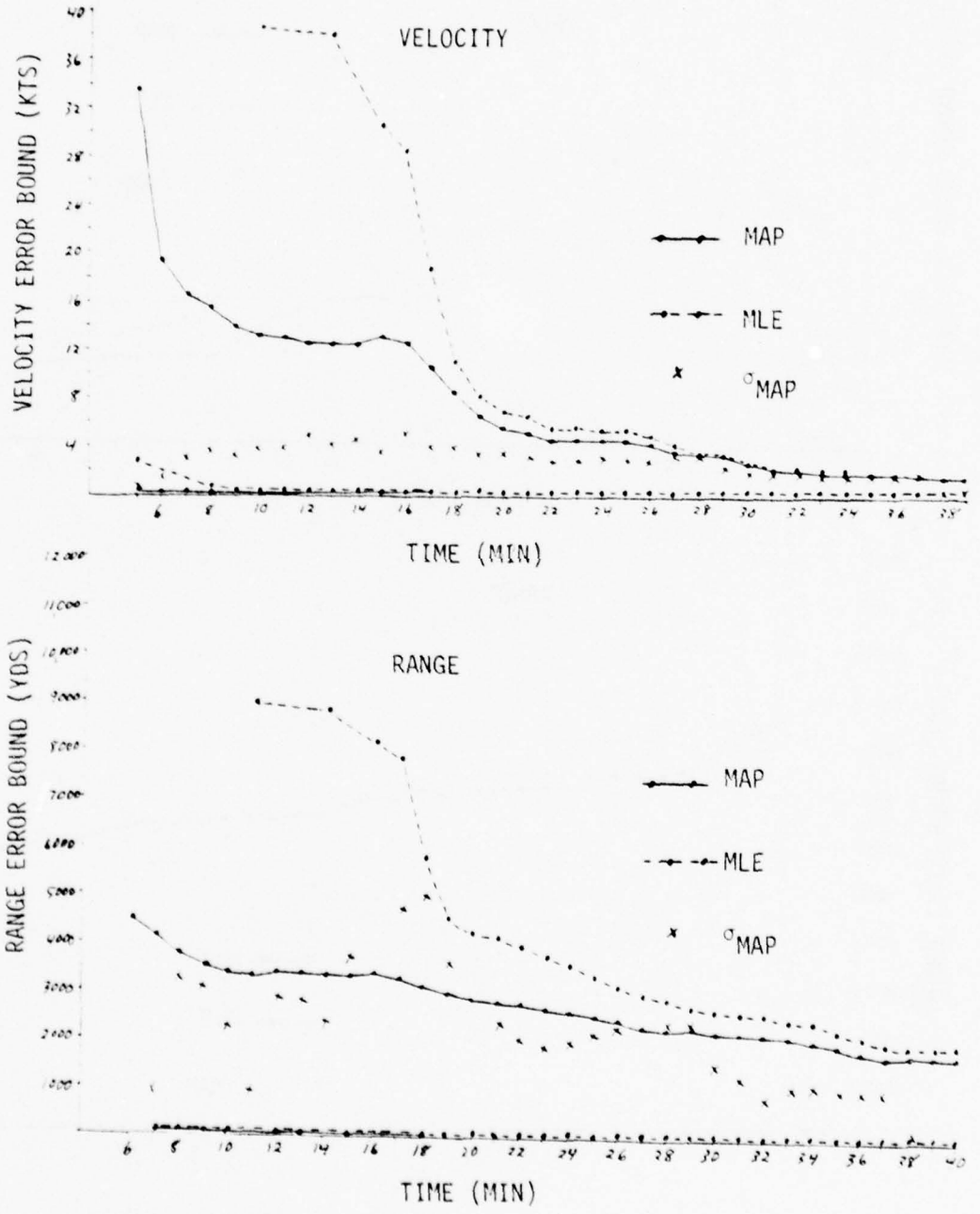

Figure 3-17 Theoretical Lower Bounds (Major and Minor Ellipse Axes) on Velocity and Range Errors [1st CZ (true and assumed), horizontal bearing, closing target course].

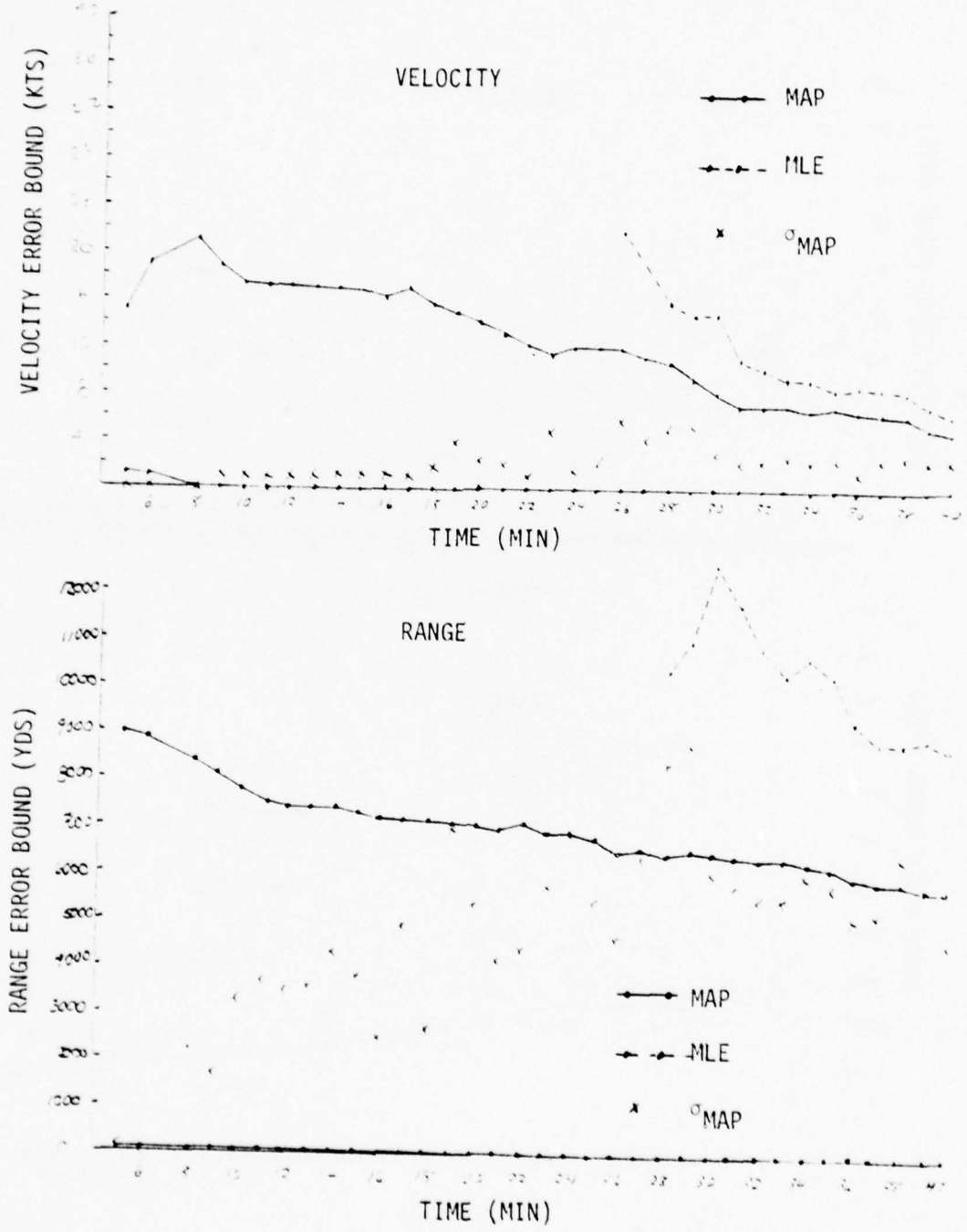

Figure 3-18 Theoretical Lower Bounds (Major and Minor Ellipse Axes) on Velocity and Range Errors [2nd CZ (true and assumed), horizontal bearing, closing target course].

only one component of total velocity error and therefore may have a smaller error standard deviation than the lower bound.

The effect on the range error bound of the incorrect path assumptions can be seen from Figure 3-19. This figure shows the range error bound for a 1st CZ crossing target geometry using all three path assumptions. The final convergence status is independent of path assumption. It does appear from these results that the major axes of the error bound ellipses can be used to predict solution convergence. Selection of a convergence time criteria is a somewhat arbitrary decision. Figures 3-20 and 3-21 show the major axis error bounds for range and velocity respectively for the MAP solution for the three path assumptions with a crossing target aspect. Examination of these figures in conjunction with the closing target cases in Figures 3-16 thru 3-18 leads to the obvious conclusion that convergence is a relative concept rather than an absolute one. The direct path cases show rapid initial convergence followed by a slow decline in the error bounds. Due to the incorporation of a'priori range statistics the convergence zone range error bounds decay extremely slowly from the a'priori standard deviation. The velocity error bounds in the convergence zone cases decrease rapidly at first before settling into a slower rate of convergence. Clearly a convergence criteria based on the range error bounds may lead to erratic convergence indications since the slope of the error bound curves is so small. Since the solution obtained is a complete TMA solution it makes sense to establish convergence based on convergence of the last component. In general, experience with bearings-only TMA indicates that course and speed solutions converge after the range solution. From these arguments it makes sense to use a convergence criteria based on the velocity error bounds while using the range error bound as a confirmation of convergence. A criteria, based on the velocity ellipse major axis reaching 1 knot, was selected for this report to establish a time for comparison of solution techniques.

3.2 Line Array Angle Simulation Results

The major impact on the TMA solution due to line array angle measurements is the bias error in the effective horizontal bearing due to errors in the D/E estimates. Since the effect on the solution of bearing bias error is to

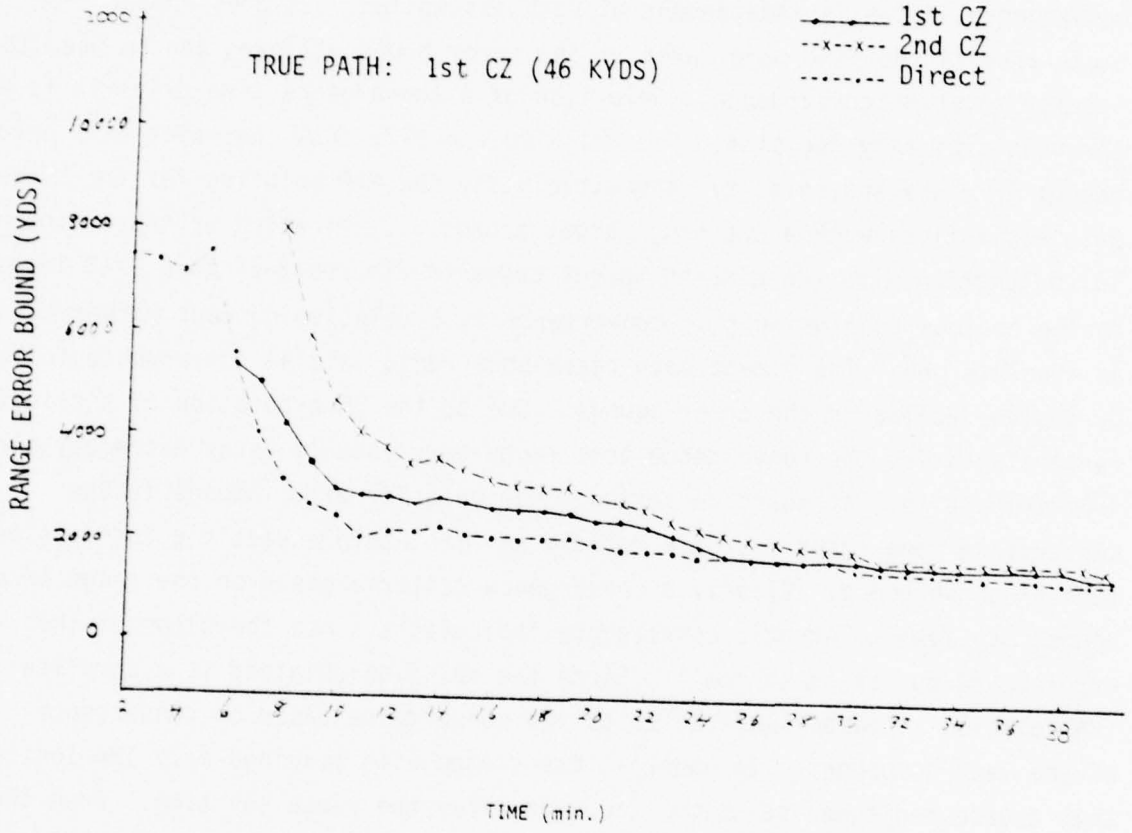

Figure 3-19 Theoretical Lower Bounds on MAP Range Error for Alternate Path Assumptions [Horizontal bearing, crossing target course].

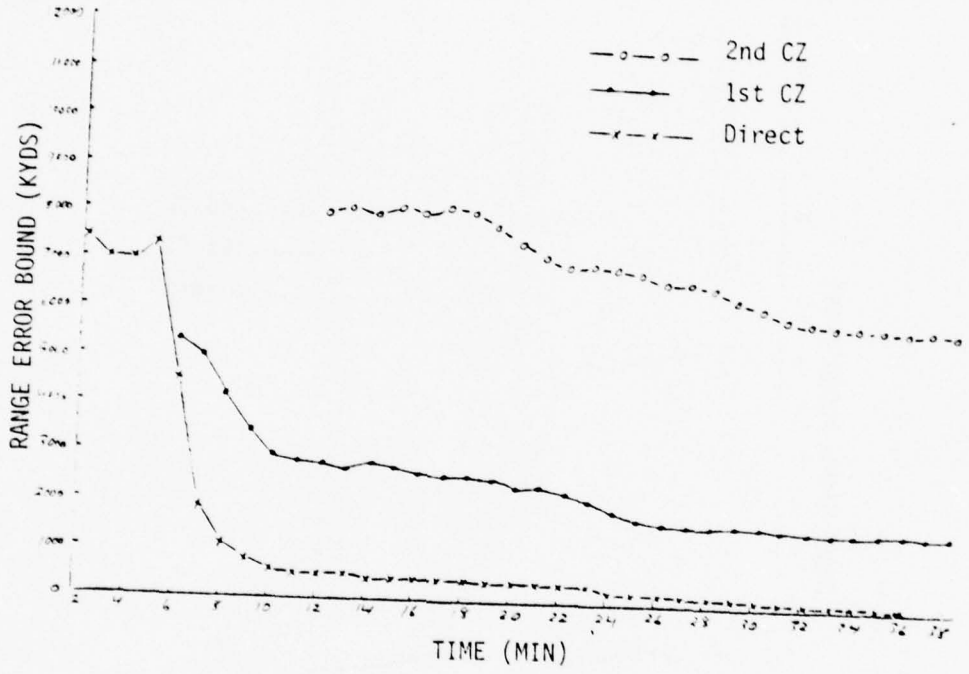

Figure 3-20 Theoretical Lower Bounds on MAP Range Error for 3 Correct Path Assumptions [Horizontal bearing, crossing target course].

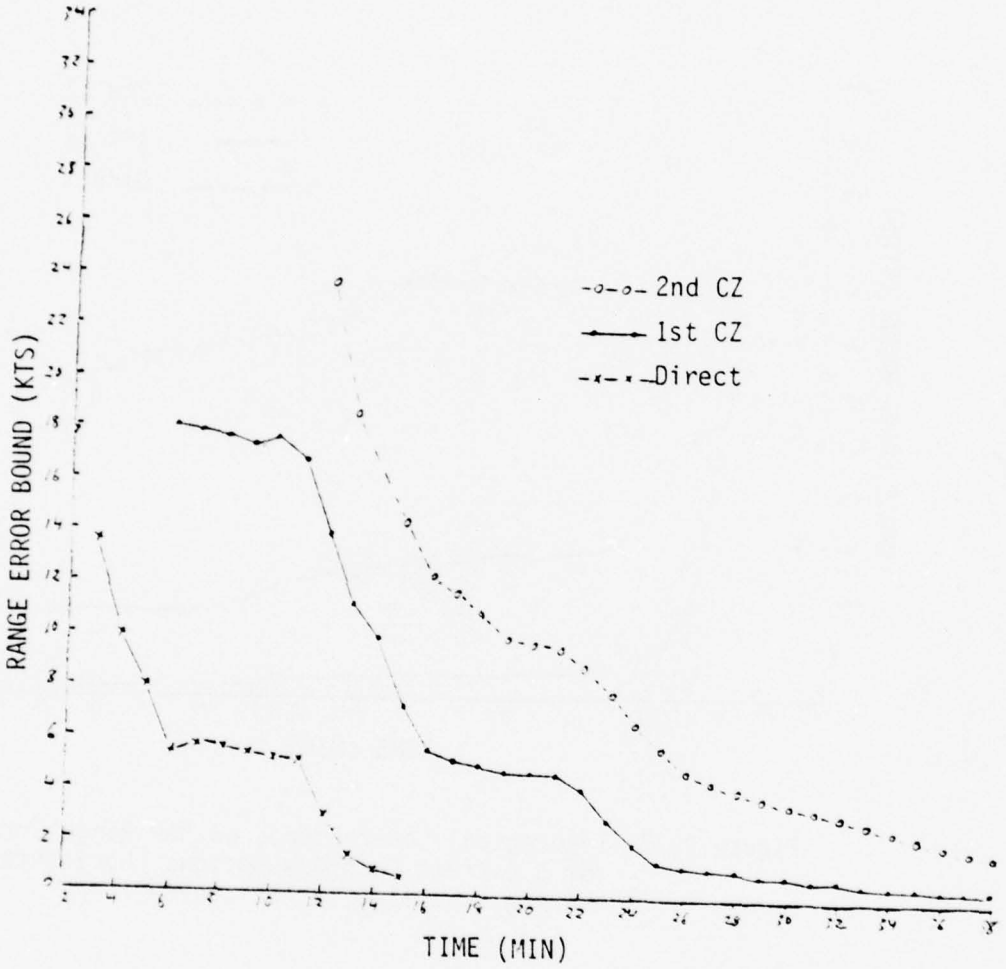

Figure 3-21 Theoretical Lower Bounds on MAP Velocity Error for 3 Correct Path Assumptions [Horizontal bearing, crossing target course].

bias the solution errors, it was decided to use only 5 Monte Carlo repetitions instead of 30, thereby significantly reducing computer costs. This is adequate for the description of the solution mean error, but does not provide accurate estimates of solution error standard deviation. Another important limitation of this study is the use of standard TMA maneuvering sequences without including uncertainty in array position and heading. A major class of line arrays is the towed array used on both submarine and surface ship combat systems. One of the major problems in towed array ranging is array position and heading uncertainty in response to own-ship course maneuvers. This aspect of the problem was ignored in order to concentrate on the second major towed array problem namely D/E bearing ambiguity. A more logical maneuvering sequence for towed arrays may be speed maneuvers rather than course maneuvers. It was decided to use course maneuvers in order to compare horizontal and line array bearing measurements.

All solutions were executed with a bearing error standard deviation of 0.2 degrees. Since the bias error due to D/E uncertainty is usually much larger than the random error, the solution mean error dominates the random error component. The geometries considered for this study include a direct path zone, a bottom bounce zone and the 1st CZ used for the horizontal bearing case. Two bottom bounce geometries were executed (10 kyds and 20 kyds). The direct path and 1st CZ propagation path use a 5° D/E angle in the measurements and an estimate of 0° D/E for the solutions. The bottom bounce solutions use the correct D/E for the actual range and an estimated D/E based on the a'priori range assumption (15 kyds). In all cases there is a D/E error between the measurements and the correctly assumed path, but a much larger error between bottom bounce assumptions and direct or CZ true paths.

Figures 3-22a, 3-22b, 3-22c and 3-22d show the mean and standard deviation of solution bearing, range, course and speed errors respectively for MAP and MLE solution for a 20 kyds bottom bounce correct path assumption. The standard deviations are not very meaningful since only 5 Monte Carlo repetitions are included. The solution bearing error exhibits a classical "delta bias" pattern due to the error in assumed D/E. This delta bias is reflected in the range, course and speed solutions as expected. The crossing target geometry

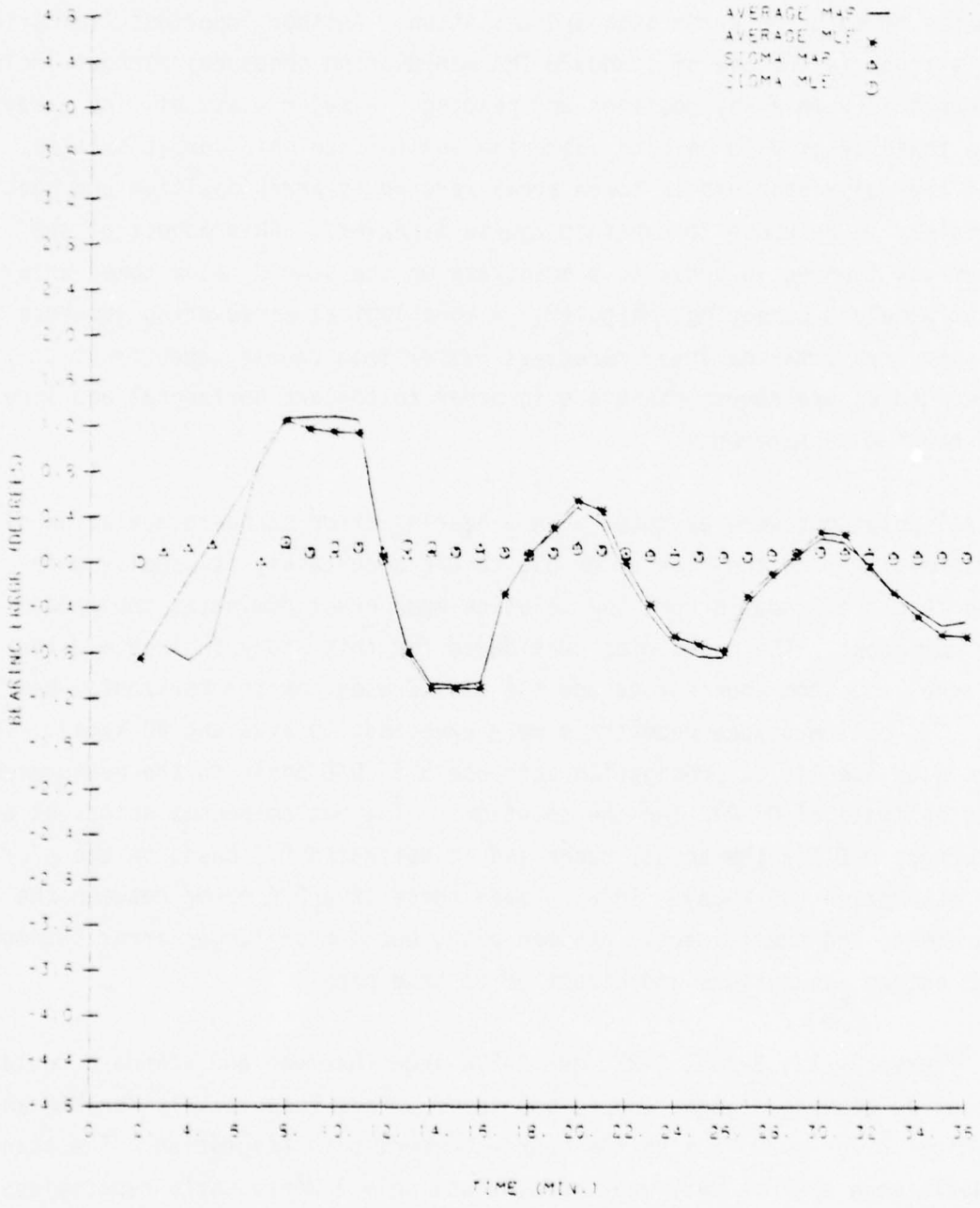

Figure 3-22a Bearing Error for Bottom Bounce Path (True [20 kyds] and Assumed), Line Array, Crossing Target Course.

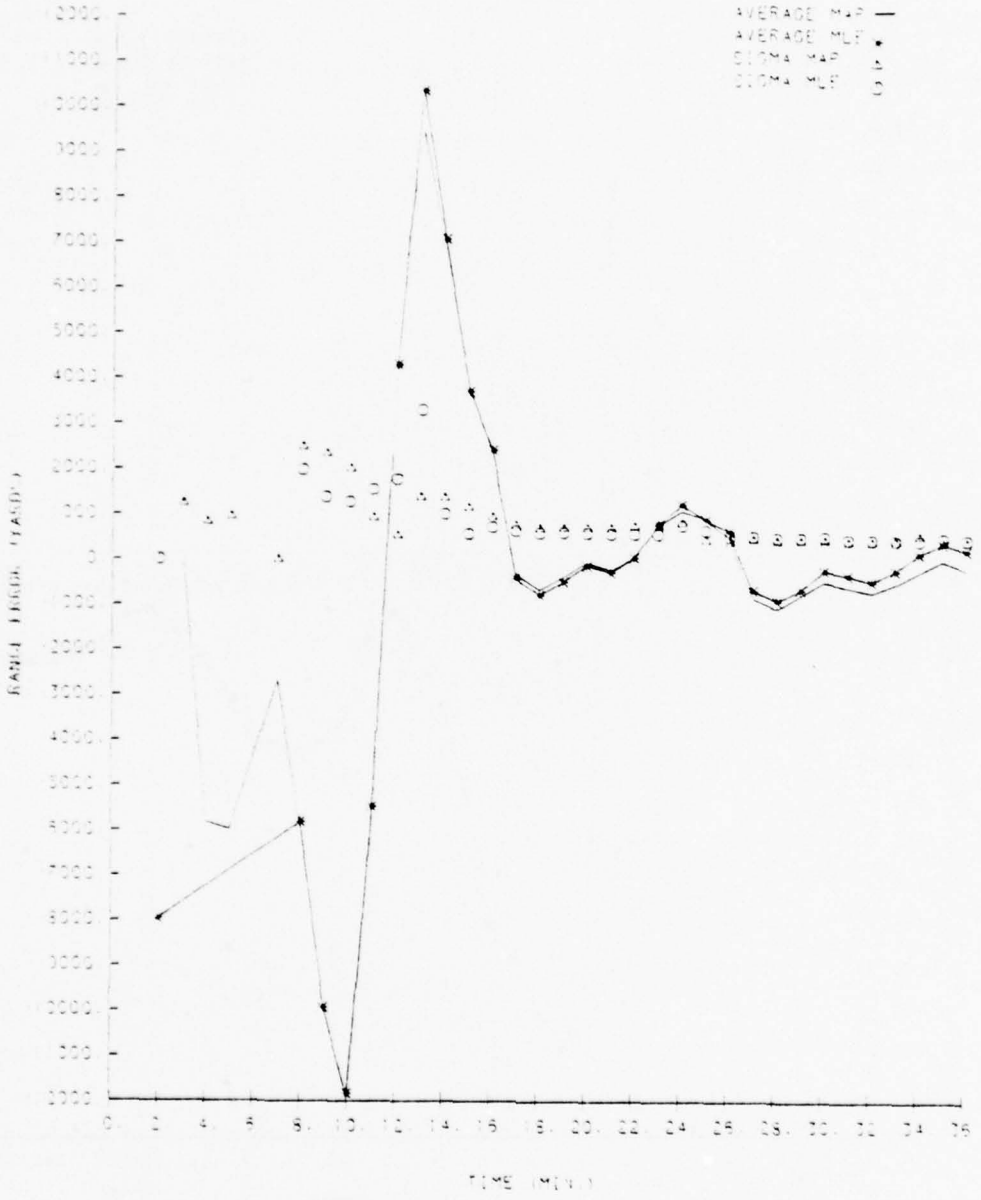

Figure 3-22b Range Error for Bottom Bounce Path (True [20 kyds] and Assumed), Line Array, Crossing Target Course.

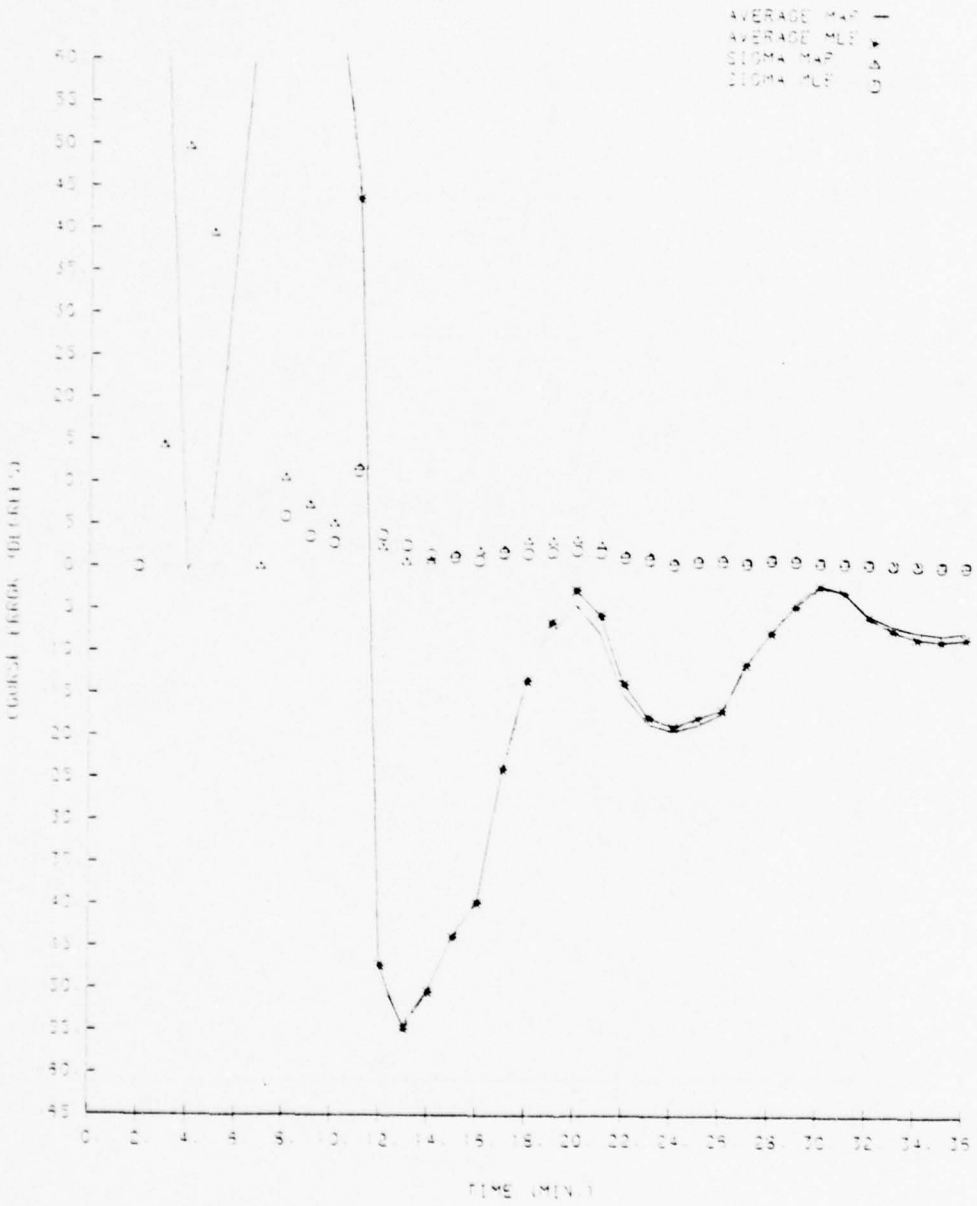

Figure 3-22c Course Error for Bottom Bounce Path (True [20 kyds] and Assumed), Line Array, Crossing Target Course.

Figure 3-22d Speed Error for Bottom Bounce Path (True [20 kyds] and Assumed), Line Array, Crossing Target Course.

would normally be fully converged within 15 minutes, but the bearing bias requires more TMA legs to "average" the bias out of the solution. This result is well known in bearings-only TMA. Standard doctrine now requires more than the minimum two legs in order to counter the effect of a bearing bias error which varies from leg to leg. Figures 3-23a, 3-23b, 3-23c and 3-23d show the results for a 1st CZ target. The delta bias is much less evident even though a 5° error in D/E is present. The bias in horizontal bearing is magnified when the nominal D/E angle is large as is typical in bottom bounce propagation. The effect of the bias error on the mean course solution is magnified by the long range geometry. In effect, the magnitude of the bearing bias is not the important quantity but rather the ratio of that quantity to the bearing change over the TMA problem time. The delta bias error at long ranges makes it very difficult to distinguish between opening and closing targets. There's little difference between the MLE solutions and MAP solutions since both use the same D/E estimate. Table 3-2 summarizes the rms errors for all geometries at the convergence time predicted by the velocity error bound. It can be readily observed that the correct path assumption (and therefore best D/E) yields substantially smaller errors (particularly course and speed), with the exception of the 20 kyds bottom bounce case. For that case the 1st CZ path assumtion yields smaller errors in range, course and speed for both MAP and MLE solutions although at a later time. The direct path and 1st CZ results are better than either bottom bounce case which suggests that further refinement of the D/E estimate is necessary for bottom bounce propagation. This could be done by adjusting the D/E estimate to minimize the bearing residuals once a converged solution is obtained. In practice the D/E is range dependent and will change over the TMA problem.

Another aspect of the line array angle measurements, is the ambiguity between port and starboard. If no a'priori information is available then two solutions must be executed for each path corresponding to each bearing quadrant. The bearing quadrant must be determined in addition to the correct path. Figure 3-24 shows the averaged residuals of the measurements (cos (line angle)), for both quadrant assumptions, for a bottom bounce geometry with a direct path assumption. Note that both quadrant assumptions converge on the 1st leg, but the incorrect quadrant does not converge on the second leg. In effect,

the maneuver resolves the ambiguity. On the third leg no solutions converge and after 17 minutes both solutions converge with the same residuals. The incorrect bearing quadrant assumption will not support solutions on adjacent TMA legs unless the solution corrects the bearing to the proper side of the array. The quadrant rejection may require additional legs if the correct quadrant does not converge on the second leg.

The relative computational burden between MAP and MLE was essentially equivalent for the cases run, but the numerical convergence comparison was not significant due to the limited number of Monte Carlo repetitions.

Figures 3-25a, 3-25b, 3-25c and 3-25d show a direct comparison of the rms range, course, speed and bearing errors respectively between the line array angle measurements and the horizontal bearing measurement for the 20 kyds crossing geometry. The effect of the error in the D/E estimate is quite obvious for the line array, bottom bounce case. The solution converges but at the expense of an additional TMA leg (5 minutes).

The results for the 1st CZ, crossing target geometry (Figure 3-26), show less differences in rms solution error between line array and horizontal bearing measurements. This is attributable again to the small D/E angle (5°) which causes the conversion between line array angle and horizontal bearing to be less sensitive to D/E error.

In conclusion, the use of line array angle measurements requires an estimate of D/E to resolve horizontal bearing. In non-bottom bounce modes the solutions are not very different from their horizontal bearing counterparts. In bottom bounce paths the error in D/E based on an a'priori range estimate at the center of the bottom bounce path may require multiple bands or an iterative search on the D/E estimate. The difference between MAP and MLE solutions for this phase was negligible.

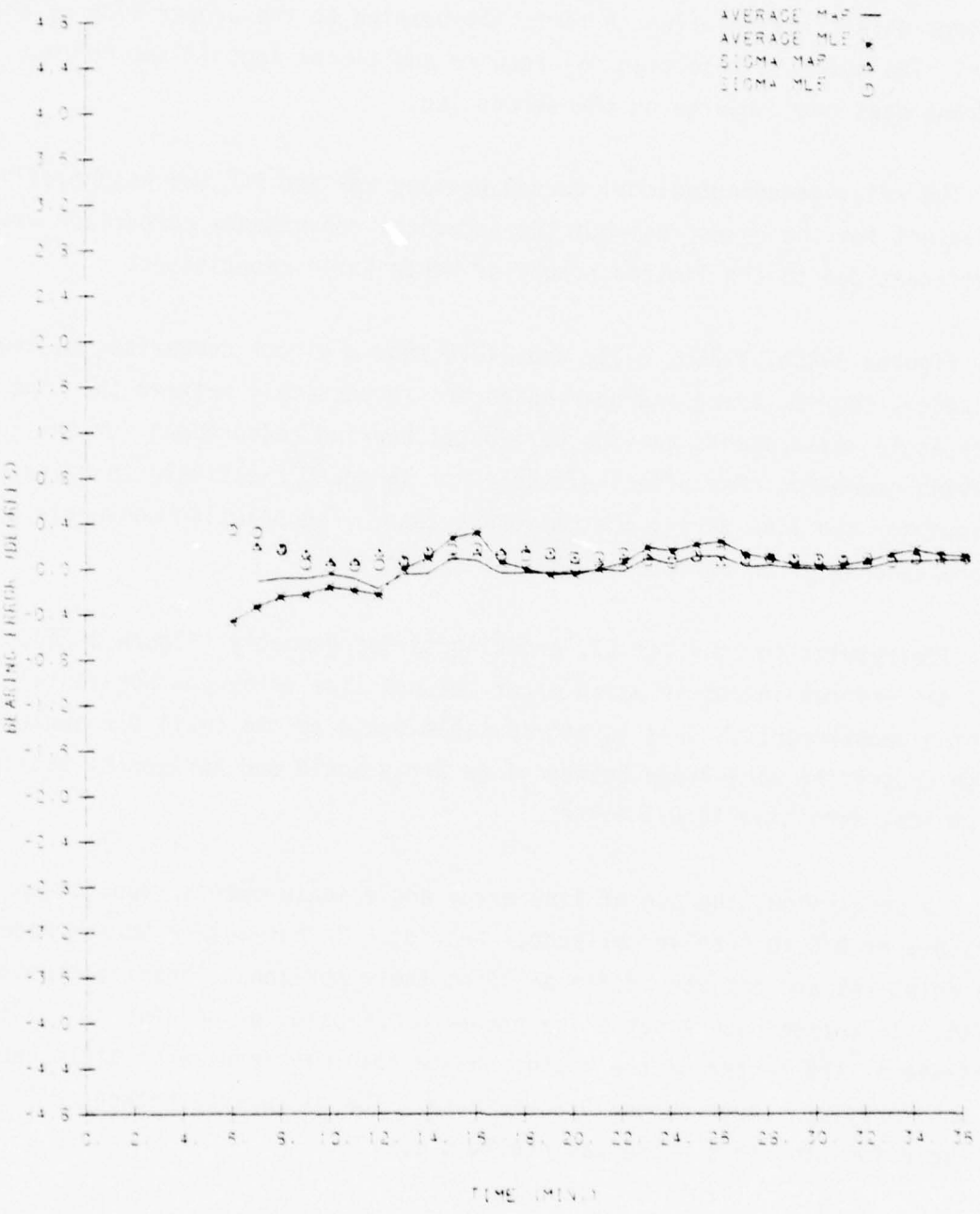

Figure 3-23a Bearing Error for 1st CZ Path (True and Assumed), Line Array, Crossing Target Course.

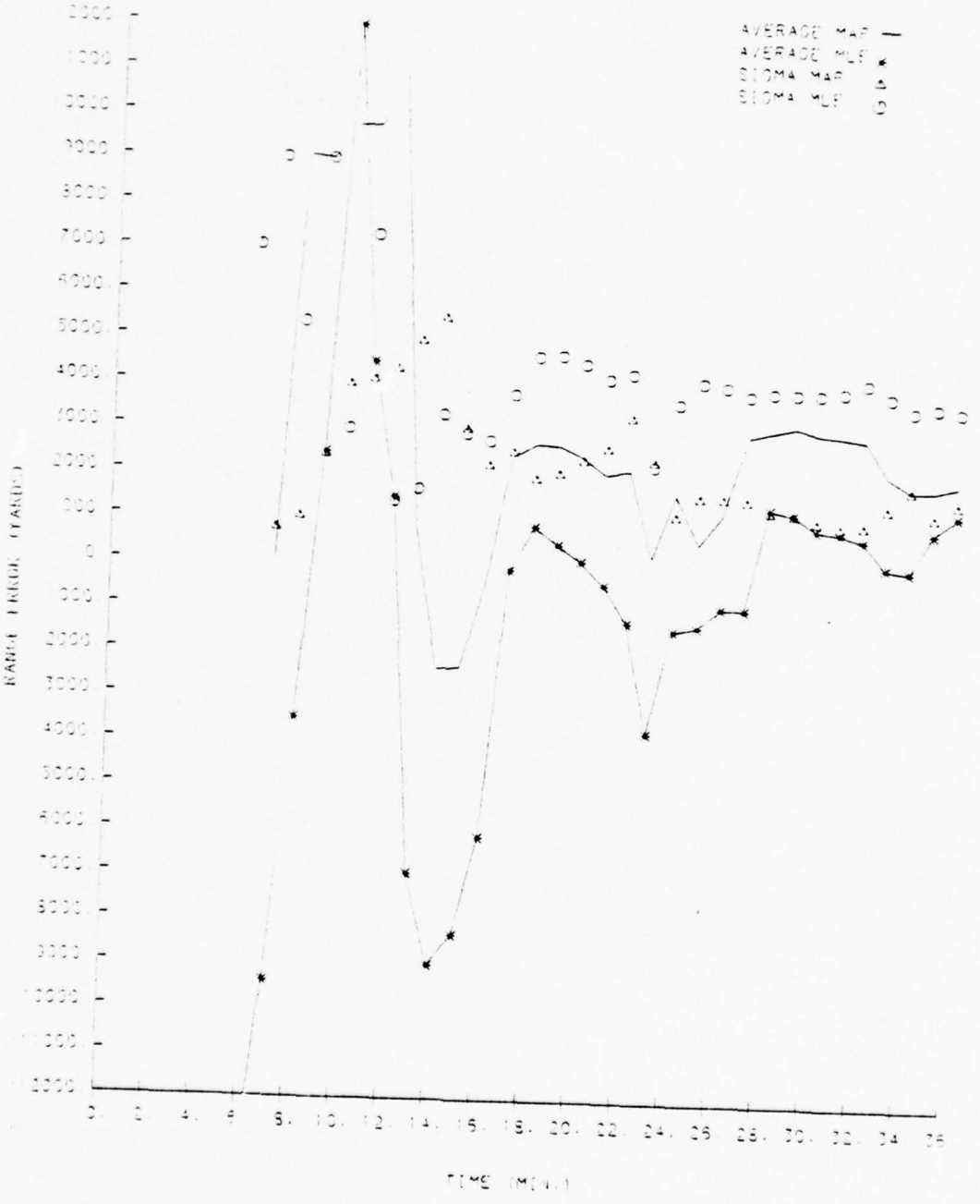

Figure 3-23b Range Error for 1st CZ Path (True and Assumed), Line Array, Crossing Target Course.

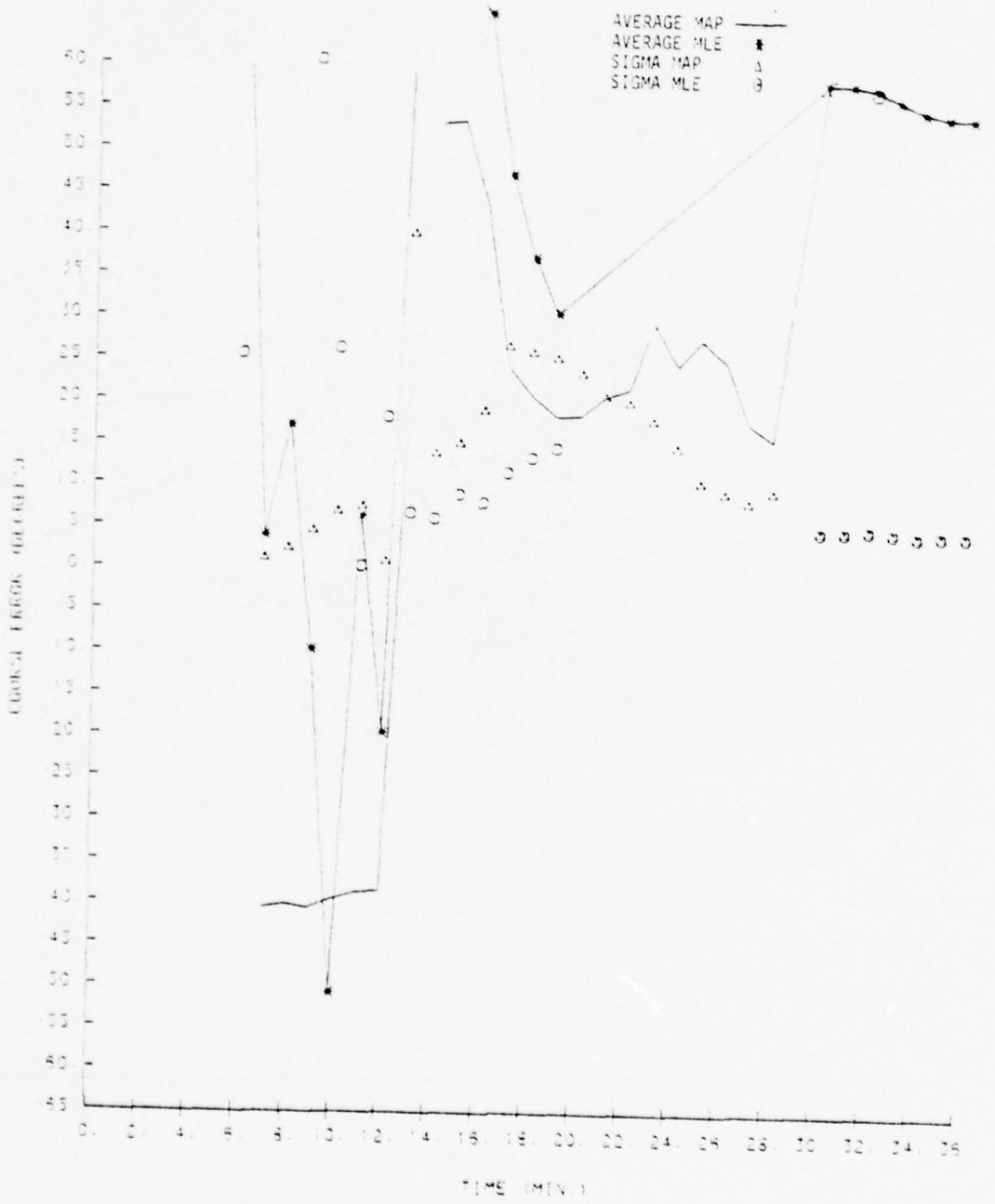

Figure 3-23c Course Error for 1st CZ Path (True and Assumed), Line Array, Crossing Target Course.

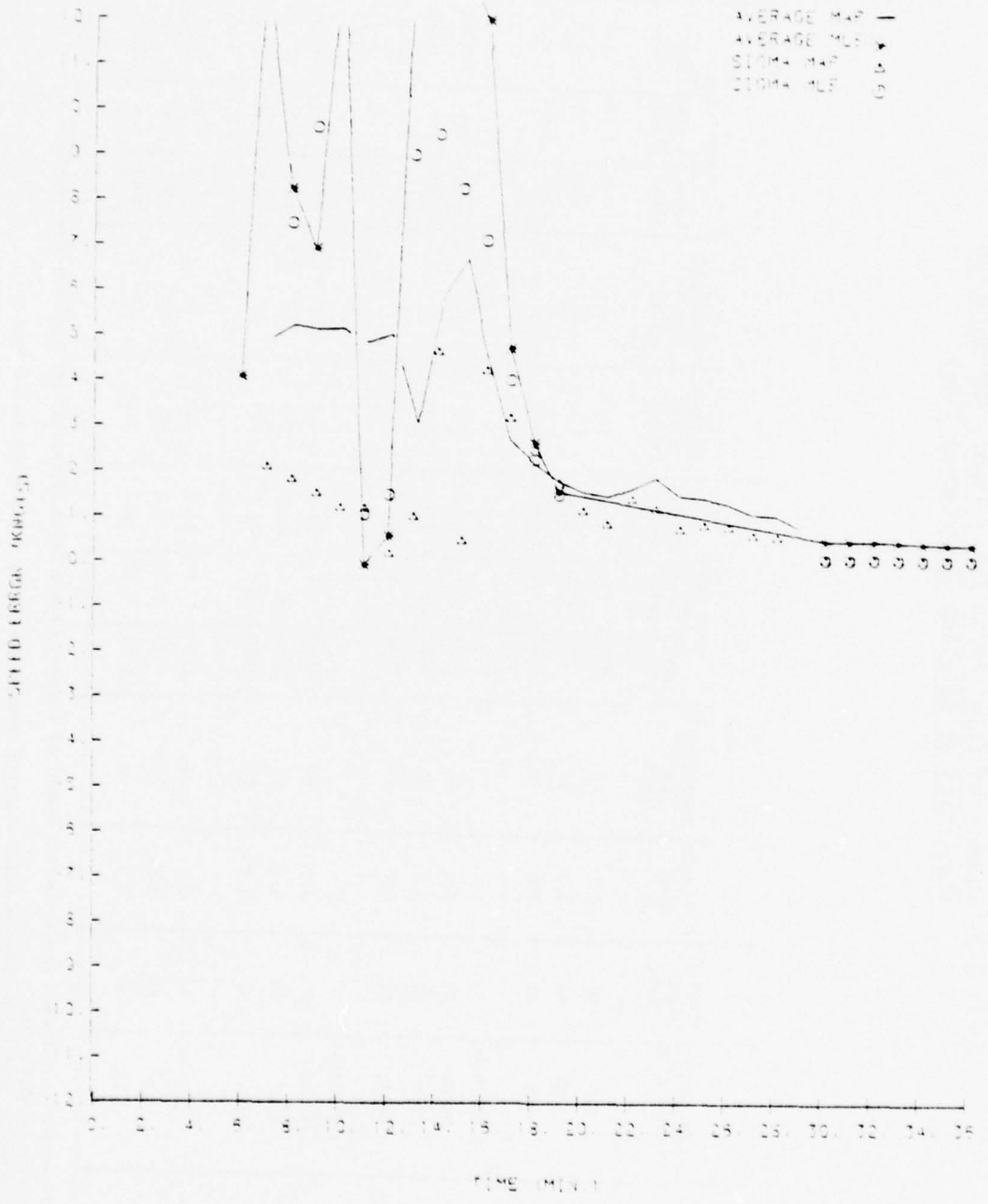

Figure 3-23d Speed Error for 1st CZ Path (True and Assumed), Line Array, Crossing Target Course.

Table 3-2 Summary of (Line Array Angle Input) TMA Solution Statistics at Solution Convergence Times.

	TRUE PATH/ ASSUMED PATH ***	PROBLEM TIME (MIN)	MAP					NLE				
			CONVERGED MONTE CARLO*	CONVERGENCE TIME** (MIN)	RMS ERROR			CONVERGED MONTE CARLO*	CONVERGENCE TIME** (MIN)	RMS ERROR		
					RANGE (YDS)	SPEED (KTS)	COURSE (DEG)			RANGE (YDS)	SPEED (KTS)	COURSE (DEG)
CROSSING TARGET COURSE	D/D	40	4.9	7	246	.79	2.0	4.3	7	374	1.20	1.8
	D/BB	40	3.3	12	795	2.50	9.5	3.4	10	544	.35	103.8
	D/1	40	7.6	8	206	.53	.75	4.3	7	507	1.60	2.2
	(10 KYDS)											
	BB/BB	40	4.3	14	1740	2.9	61.9	4.2	12	5020	8.5	84.6
	BB/D	40	3.9	14	1645	16.7	83.3	3.6	16	566	17.0	76.4
	BB/1	40	3.2	17	3500	6.3	98.9	3.1	7	5764	3.7	110.3
	(20 KYDS)											
	BB/BB	40	4.4	16	2504	5.4	39.2	4.1	16	2526	5.5	39.8
	BB/D	40	4.4	15	4337	6.7	67.8	4.0	18	1898	1.07	27.2
	BB/1	40	4.4	18	2018	1.2	26.1	3.9	18	1674	.69	23.7
	1/1	40	3.7	34	2609	.74	14.4	3.9	34	3630	.82	15.8
	1/D	40	2.5	26	147	2.04	25.6	NC	NC	NC	NC	NC
	1/BB	40	1.9	30	6357	9.10	57.3	1.6	37	5087	8.9	59.9

*"Converged Monte Carlo" is the average number of converged Monte Carlo iterations per solution time increment (maximum number = 5).
**Convergence Time is the time at which velocity error bound (major axis) drops to 1.0 knot.
***BB = Bottom Bounce, D = Direct Path, 1 = First Convergence Zone,

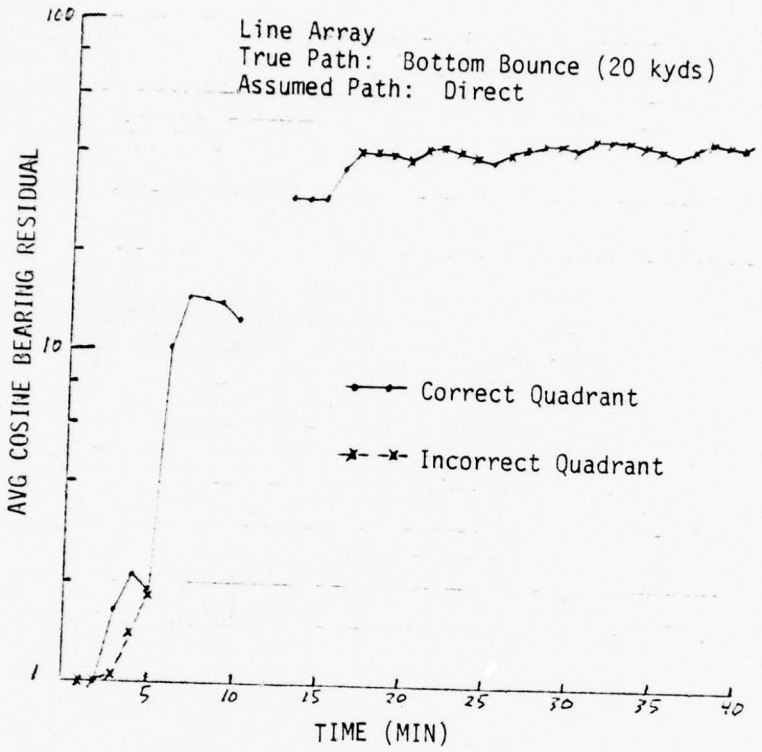

Figure 3-24 Average (Cosine Bearing) Residuals for Alternate Bearing Quadrant Assumptions.

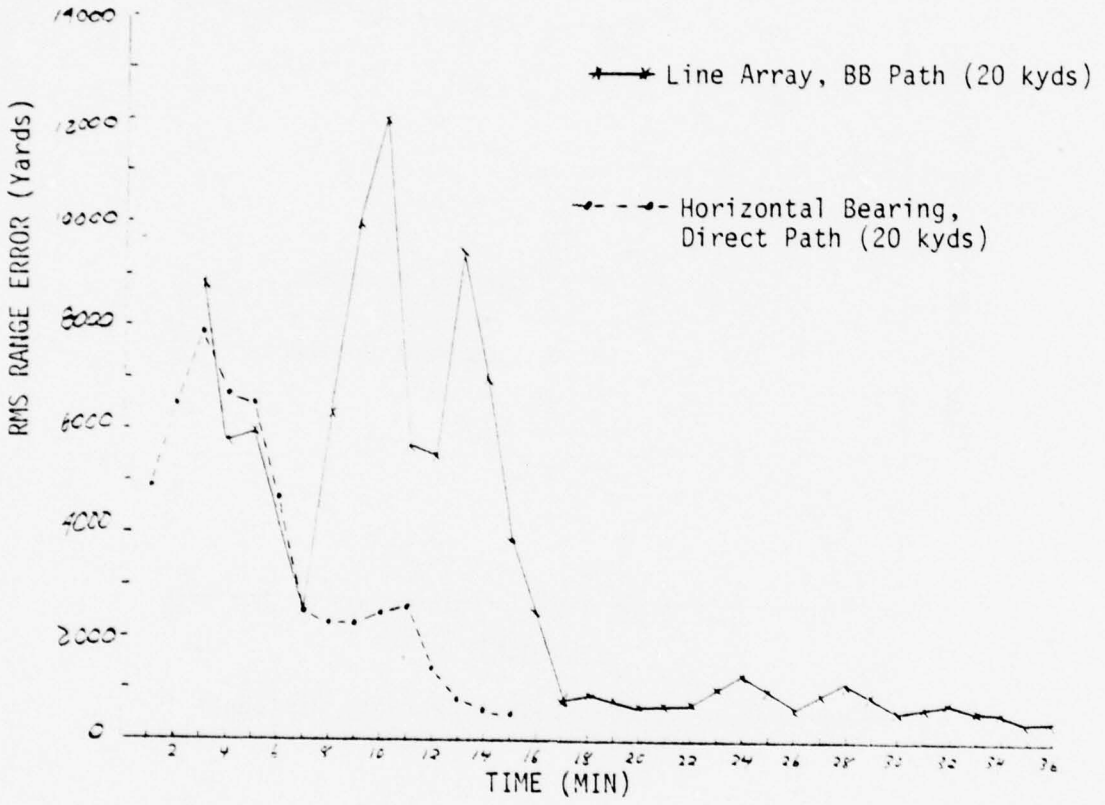

Figure 3-25a Horizontal Bearing and Line Array Comparison in Terms of MAP rms Range Error, for Crossing Target Course.

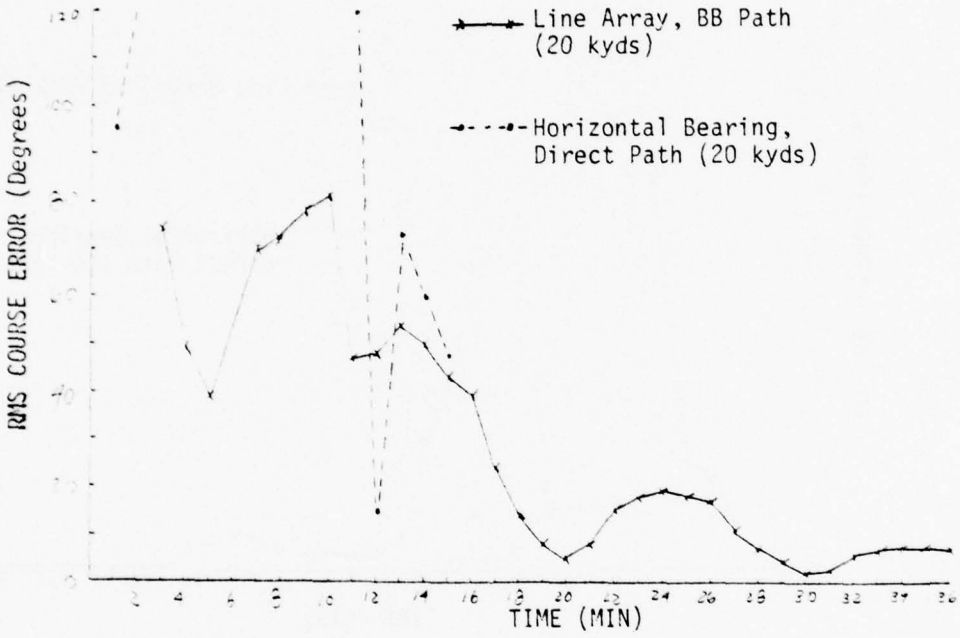

Figure 3-25b Horizontal Bearing and Line Array Comparison in Terms of MAP rms Course Error, for Crossing Target Course.

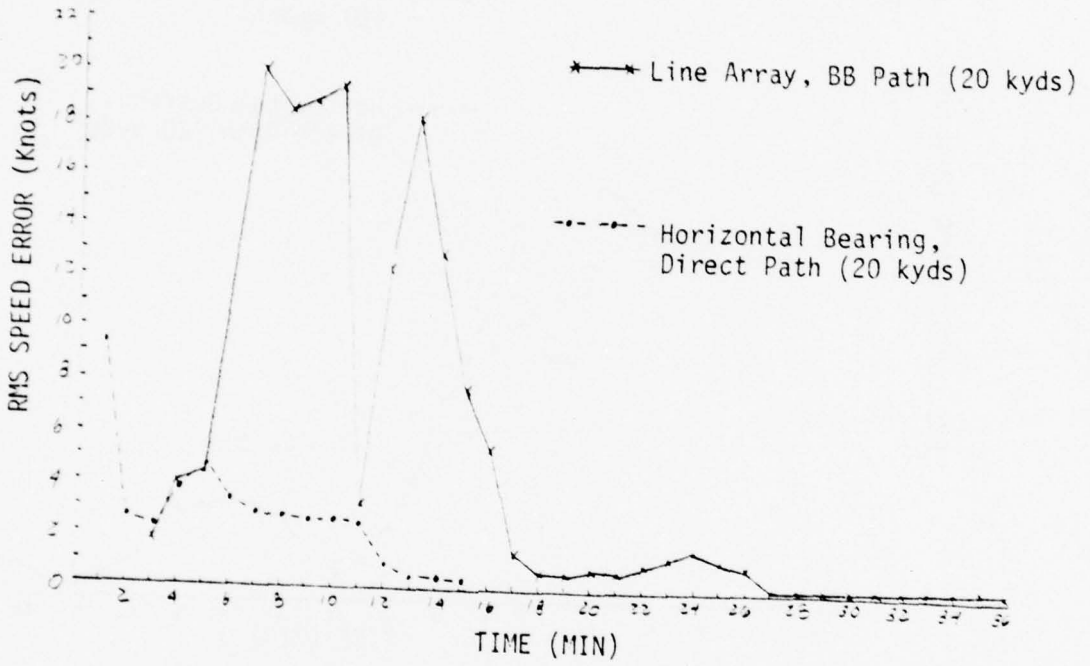

Figure 3-25c Horizontal Bearing and Line Array Comparison in Terms of MAP rms Speed Error, for Crossing Target Course.

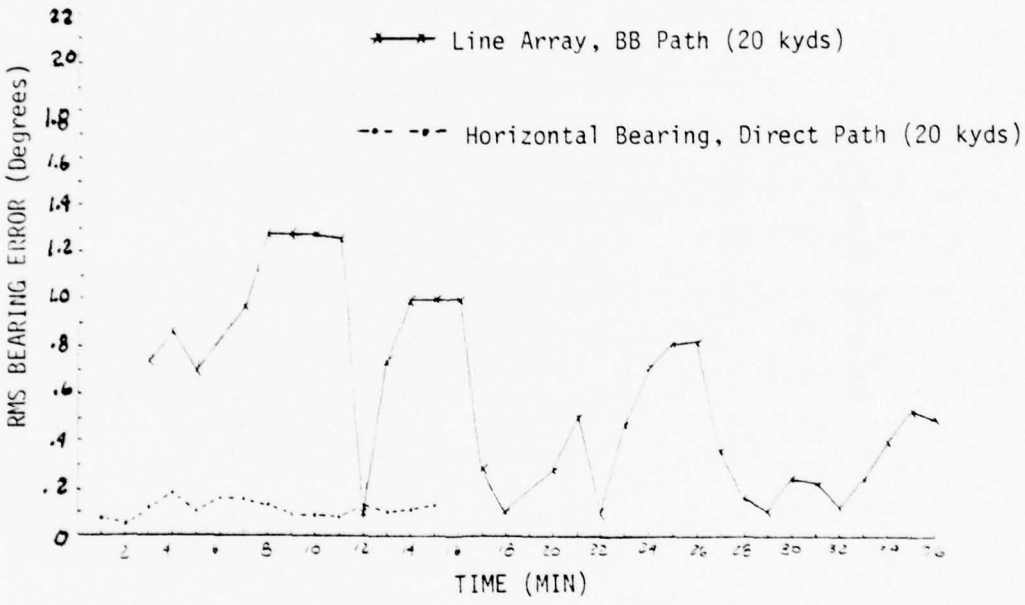

Figure 3-25d Horizontal Bearing and Line Array Comparison in Terms of MAP rms Bearing Error, for Crossing Target Course.

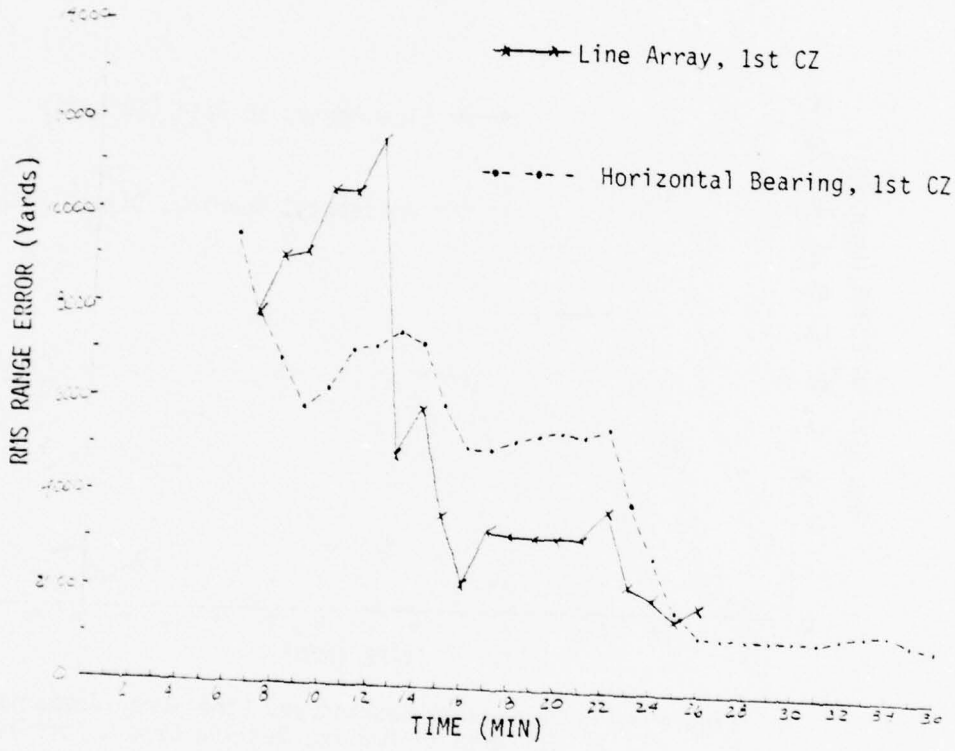

Figure 3-26a Horizontal Bearing and Line Array Comparison in Terms of MAP rms Range Error, for Crossing Target Course.

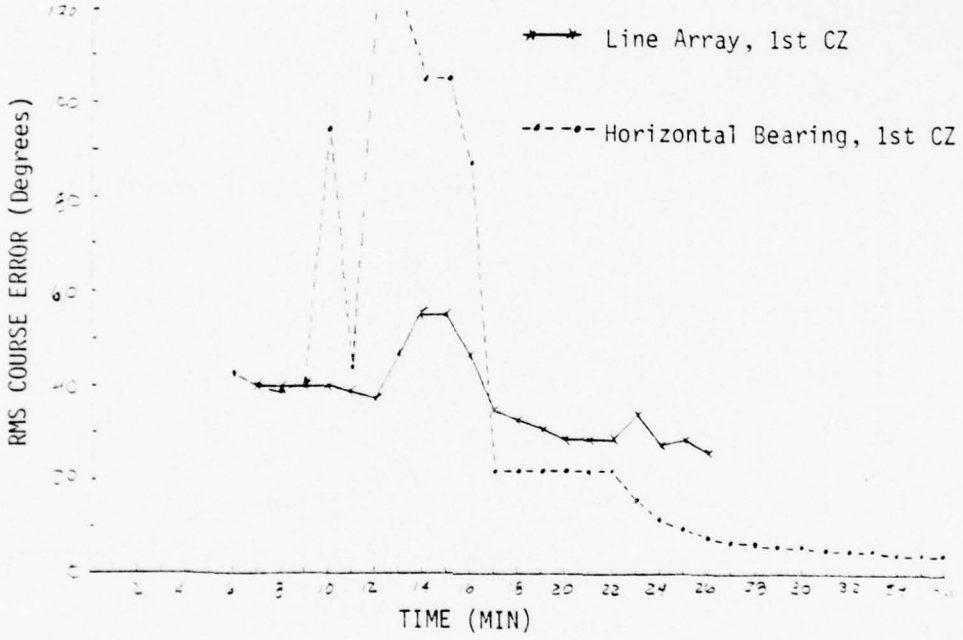

Figure 3-26b Horizontal Bearing and Line Array Comparison in Terms of MAP rms Course Error, for Crossing Target Course.

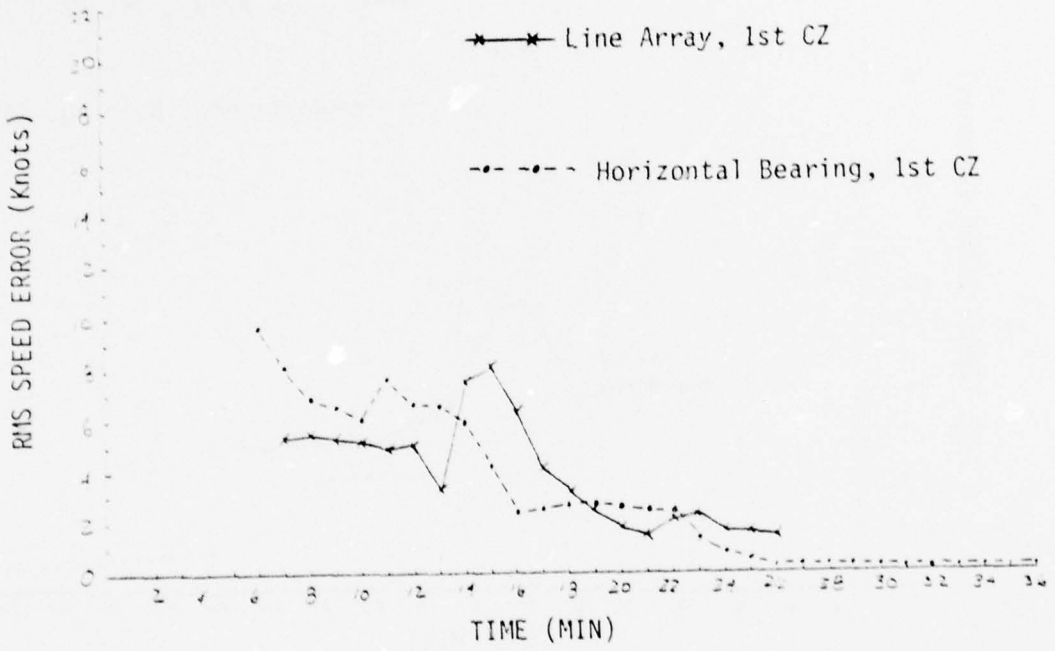

Figure 3-26c Horizontal Bearing and Line Array Comparison in Terms of MAP rms Speed Error, for Crossing Target Course.

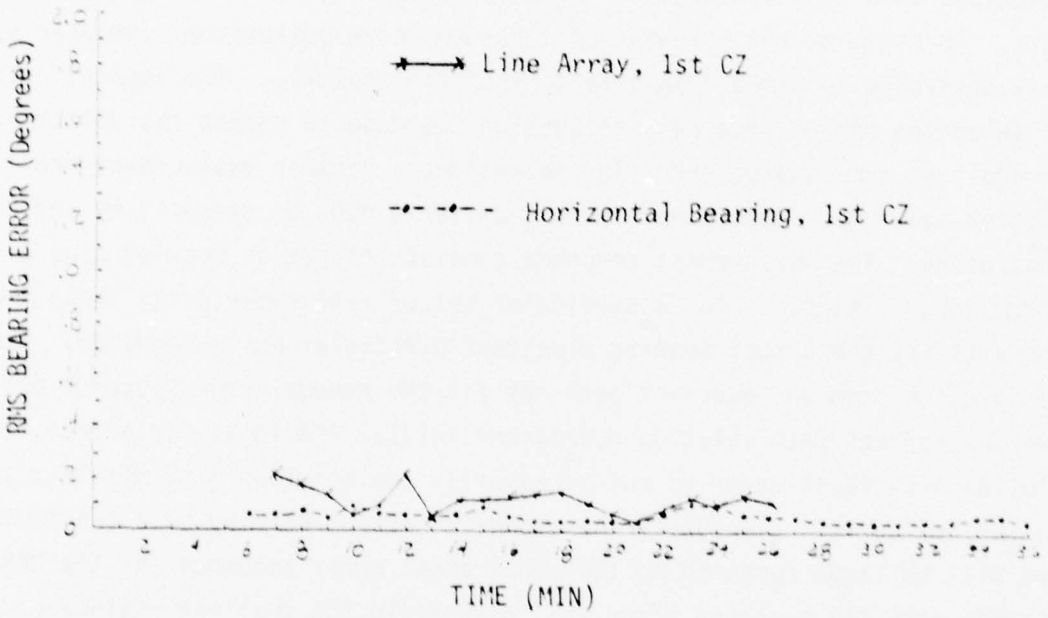

Figure 3-26d Horizontal Bearing and Line Array Comparison in Terms of MAP rms Bearing Error, for Crossing Target Course.

3.3 Rejection of Incorrect Path Hypotheses

3.3.1 Horizontal Bearing Measurements

The results presented in previous sections indicate that, while the use of a'priori range information based on assumed propagation paths improve the numerical solution convergence, the solutions are biased under incorrect path hypotheses. One should therefore evaluate each potential propagation path by a separate solution until the true path is resolved. Eventually all hypothesed solutions converge to the true solution given sufficient measurements. To minimize the computational burden on an operational computer system it is desirable to discard incorrect hypotheses quickly. The logical criteria for selecting the correct path assumption would be to choose the solution with the smallest sum squared error in the residuals between measurement and solution bearings. Unfortunately this criteria must be tempered by additional constraints. The measurement sequence consists of actual bearing plus a random error sequence. For a particular set of measurements the "best" solution will fit the actual bearing plus that particular noise sequence. Thus, the solution from an incorrect path may fit the random error sequence better than the correct path solution during the initial TMA legs. In effect, the solution with least error is not necessarily the solution with smallest sum squared residuals. Eventually the change in actual bearing as a function of time will be large compared to the measurement error sequence and the MAP solution with the smallest error will also yield the smallest residuals. Thus, some time must elapse before the bearing residuals can be used to dismiss incorrect propagation paths. After this time the bias in the incorrect path solutions will be resolved by the bearing residuals.

To illustrate the problem, Figures 3-27, 3-28 and 3-29 show the sum squared bearing residuals averaged over the Monte Carlo repetitions and normalized by the measurement error variance and number of points in the sum. The figures show the residuals for each path assumption and all geometries executed with horizontal bearing measurements. Since the results shown represent average values, one cannot assume that each Monte Carlo repetition exhibits the same relationship between alternate path hypotheses as shown in the figures. The

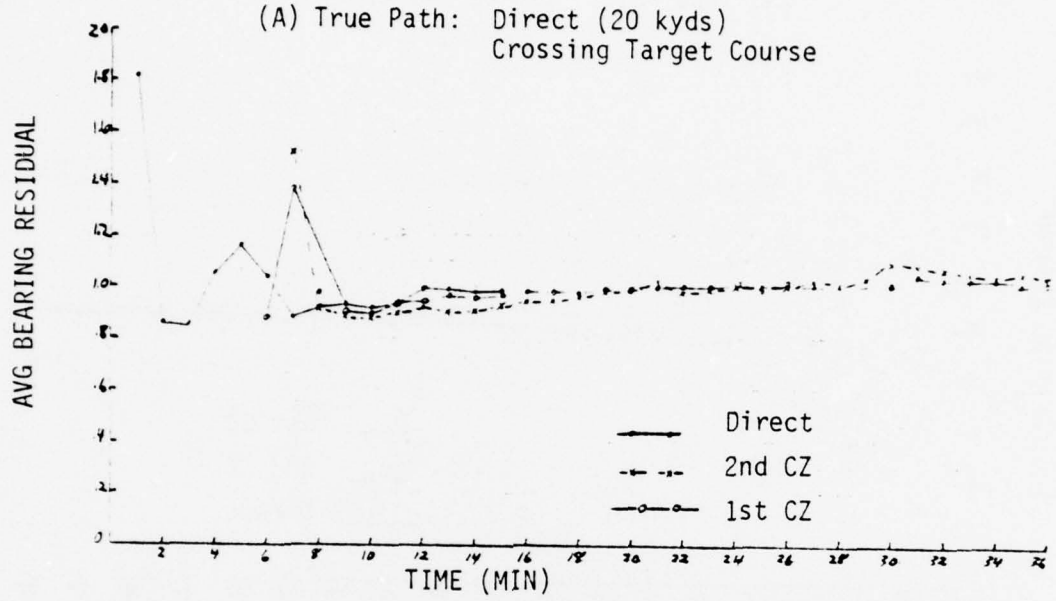

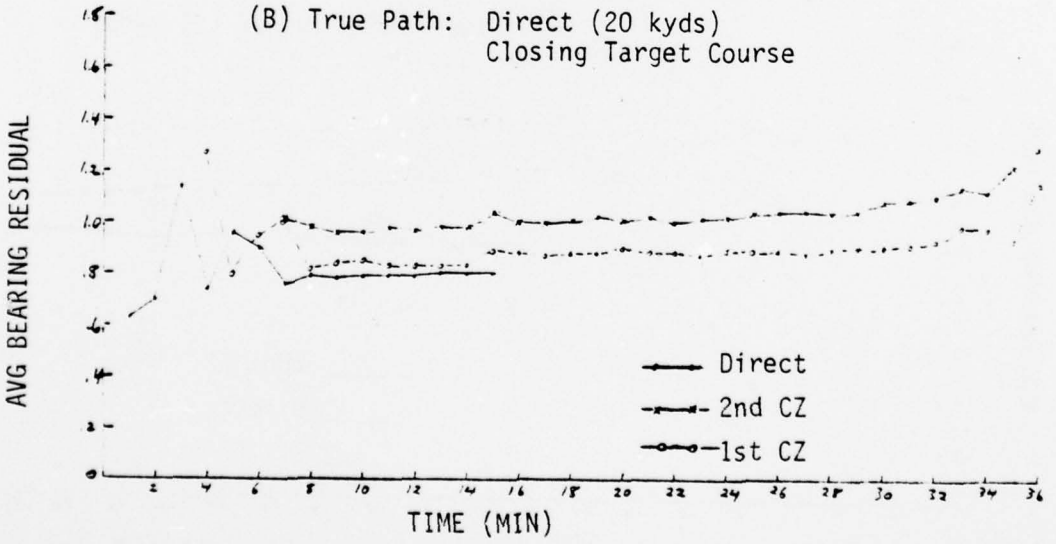

Figure 3-27 Average Horizontal Bearing Residuals for Alternate Path Assumptions (MAP).

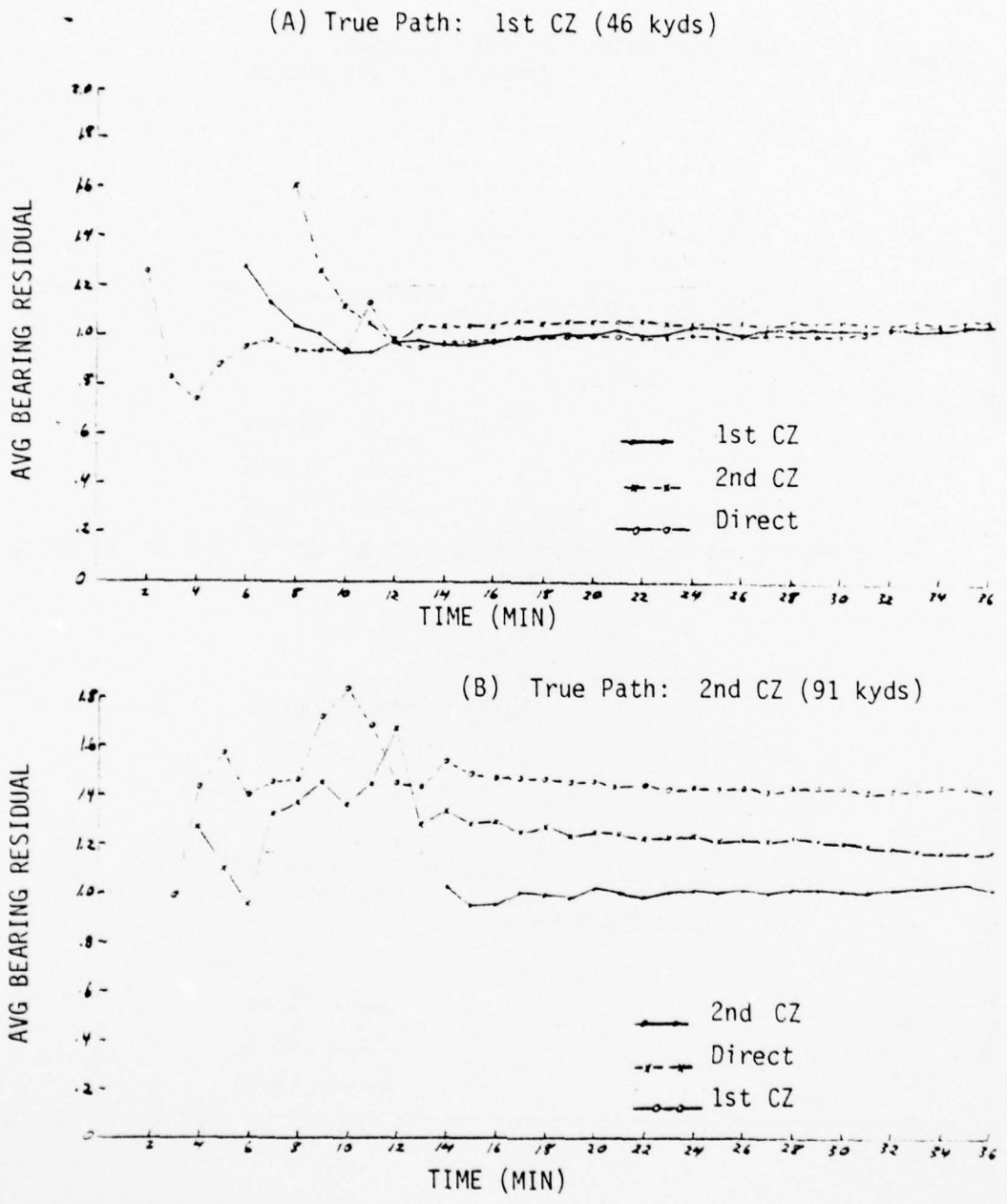

Figure 3-28 Average Horizontal Bearing Residuals for Alternate Path Assumptions (Crossing Target Course, MAP).

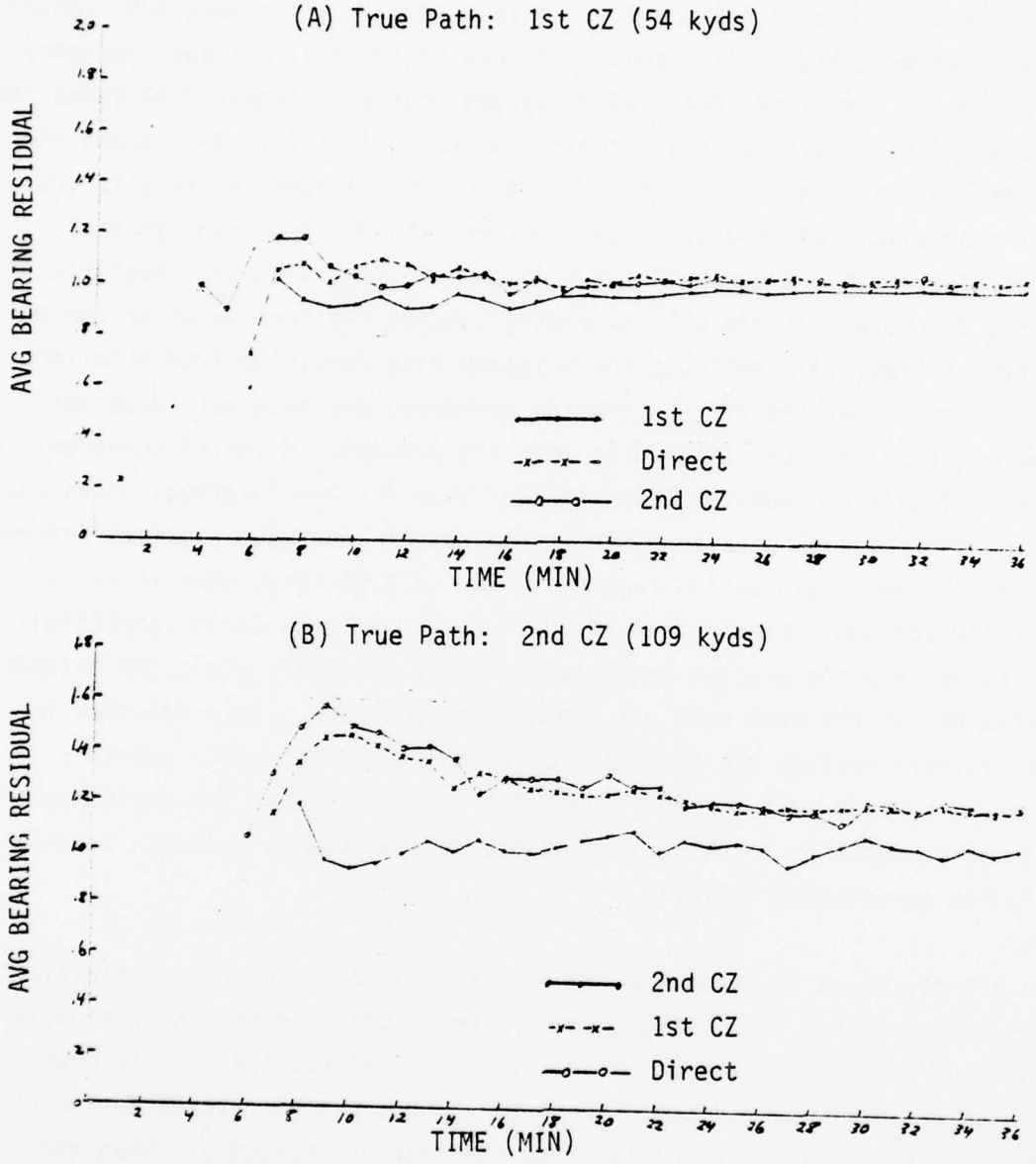

Figure 3-29 Average Horizontal Bearing Residuals for Alternate Path Assumptions (Closing Target Course, MAP).

theoretical average for a perfect solution is unity with an expected standard deviation of $\sqrt{\frac{2}{N}}$ · N represents the number of residuals included in the average. On all plots the averaged residuals are presented only after numerical convergence has occurred. Figure 3-27 shows the results for a direct path geometry (20 kyds) for both crossing and closing target courses. Figure 3-28 shows the 1st CZ and 2nd CZ results with a crossing target while Figure 3-29 shows the 1st CZ residuals for the closing target. Although the averaged results are smallest over almost all the solution times for the correct path hypothesis, it is not clear that one can pick the correct path from a single repetition. In effect, the solutions are all converging towards the true solution and the differences in residuals reflects the solution bias resulting from incorrect path hypothesis. For the 2nd CZ crossing geometry, the true path does not converge numerically until 14 minutes into the problem. After it converges the averaged residuals are substantially smaller than for the incorrect paths again reflecting the solution bias incurred by the use of incorrect a'priori information. Clearly one could easily reject the 2nd CZ hypotheses when it is in fact the correct one. Examination of the individual Monte Carlo repetitions at 15 minutes into the problem indicates that the residuals yield the correct hypothesis 80% of the time over all geometries simulated. This solution is not satisfactory because the best time of comparison is strongly geometry dependent. The best criteria for discarding incorrect paths for horizontal bearing measurements is a combination of bearing residuals, solution values and solution convergence criteria.

In effect, one must determine the sensitivity of the bearing residuals to solution errors before dismissing path hypotheses based on bearing residuals. The range and speed error bounds can be used for this purpose but one must not include the a'priori information. The error bounds can be calculated from the component of the ψ matrix calculated from the bearing residuals. When the range error bound reduces to a small fraction of the difference between alternate a'priori range estimates then two comparisons can be made. The solution ranges can be compared to each a'priori range. Presumably, the true hypothesis will be closer to all solutions than any incorrect hypothesis. The magnitude of the sum squared residuals should also be minimum for the solution based on the correct hypothesis. If both conditions are met, then one hypothesis can be

retained while the other solutions are discarded. If there is not sufficient separation to resolve two paths (normally 1st CZ versus 2nd CZ) then more than one solution should be retained. As the selected solution converges the comparison between solution range and the a'priori ranges should be continued in order to correct any decision error. The solution can always be reprocessed based on the correct a'priori hypothesis to improve the solution accuracy if necessary.

Based on the error bounds presented in Figures 3-16, 3-17 and 3-18 for the MLE solution, it appears that the dismissal of incorrect paths can be made at approximately 50% of final convergence time. For the direct path at 20 kyds with a closing target, the path decision can be made after 7 minutes. For the 1st CZ closing target 18 minutes is required to decide between 1st CZ and 2nd CZ hypothesis based on a range error bound of 20% of the difference between a'priori ranges. These specific results are geometry and measurement error dependent but the criteria can be evaluated in situ. The exact value of range error bound used to select the correct solution is arbitrary. A value of 20% of the difference between alternate hypotheses is conservative, but a conservative criteria may be necessary when the bearing measurements have substantial bias error.

3.3.2 Line Array Measurements

For the line array measurements the selection of correct bearing quadrant can be made on the second leg if the solution using the correct quadrant (port versus starboard) converges on both 1st and 2nd legs. As long as the 1st CZ and direct path results are separated by bottom bounce propagation, the path hypotheses can be separated much more readily than for the horizontal bearing cases because of the bias due to D/E mismatch.

Figures 3-30 and 3-31 show the average of the sum squared residuals in cosine bearing for direct path, two bottom bounce cases and the 1st CZ. In all cases the bottom bounce paths separate on the seond leg whether they are correct or incorrect. The D/E error encountered by an incorrect path assumption results in a much larger residual which is in fact presented on a logarithmic scale to allow comparison. The comparison between direct path and 1st CZ residuals show that the residuals do not by themselves distinguish

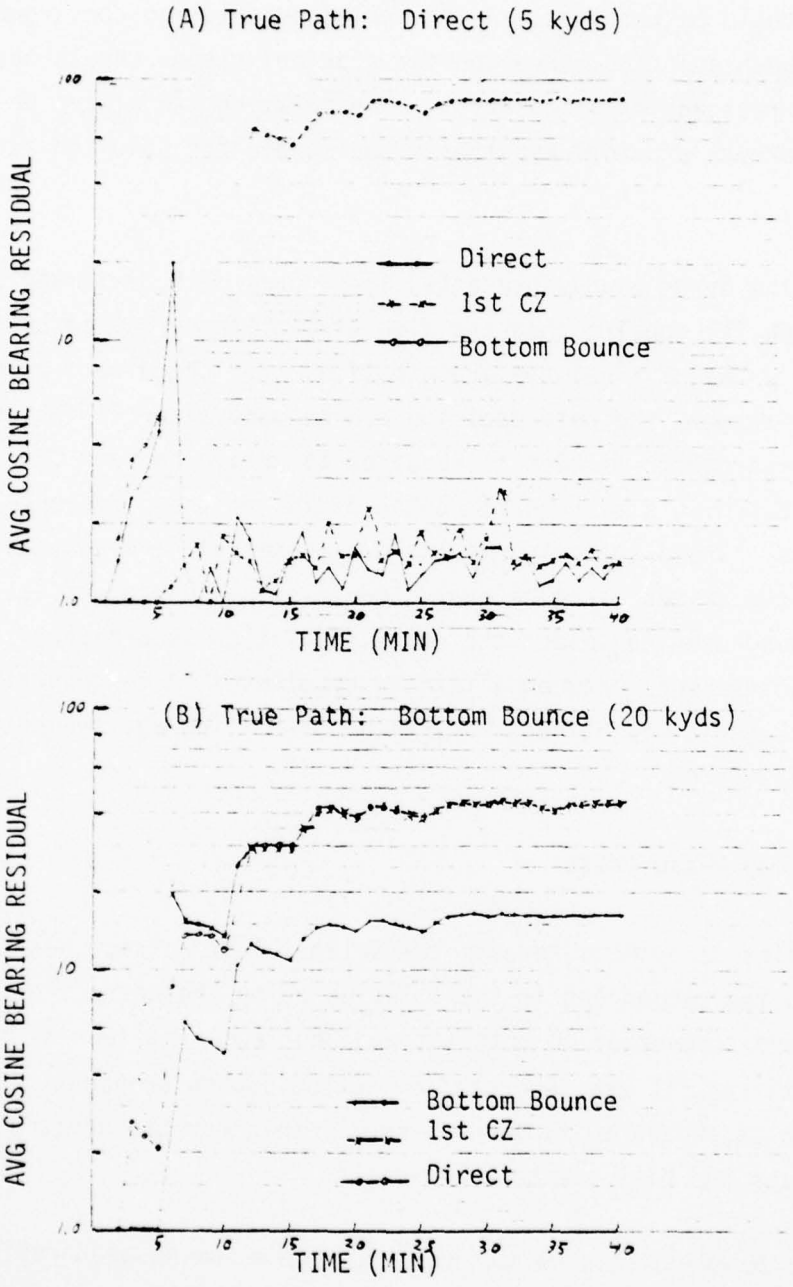

Figure 3-30 Average (Cosine Bearing) Residuals for Alternate Path Assumptions [Line array inputs, crossing target course, MAP].

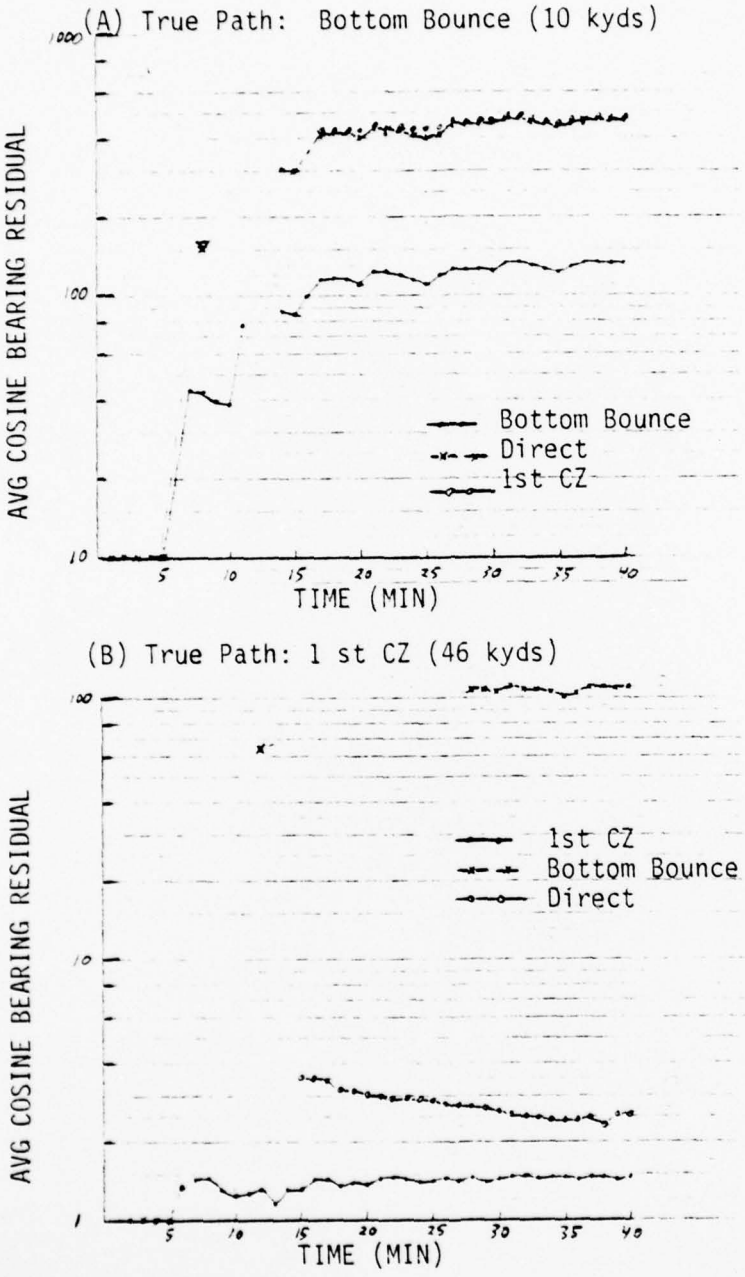

Figure 3-31 Average (Cosine Bearing) Residuals for Alternate Path Assumptions [Line array inputs, crossing target course, MAP].

the paths because the D/E errors are the same. However, the procedure outlined for horizontal bearings can be applied to resolving these two paths with similar confidence.

4.0 Conclusions

The value of incorporating a'priori range and speed information into the bearings-only TMA problem was studied through a series of computer simulations of an asymptotically optimum estimation algorithm. It was anticipated that use of a'priori range estimates along with estimated accuracy should provide a TMA solution which converges faster and is more accurate than a conventional bearings-only TMA algorithm. Two algorithms were selected for this evaluation and simultaneously compared. The algorithm which incorporates the full a'priori statistical information is a Maximum A'posteriori Probability (MAP) estimator. The other algorithm which incorporates a'priori information only for initialization is a Maximum Likelihood Estimator (MLE). Both algorithms are asymptotically optimum in the sense of minimizing solution error given sufficiently long observation sequences. These algorithms were chosen because of this property. Alternative TMA algorithms such as the Extended Kalman Filter (EKF) suffer from linearization errors and therefore may not accurately depict the value of the environmental predictions.

4.1 Results for Horizontal Bearing Measurements

The results of this study shows that the MAP algorithm does not provide the solution improvement expected using a'priori information. This conclusion is based on comparing the MAP solution to the MLE solutions. The MLE solutions uses the a'priori information during initialization but the impact of the information is lost once the solution converges numerically to its best estimate for a given data set. Good initialization reduces numerical iteration problems but not ultimate solution accuracy. The MAP solutions in general did not exhibit smaller errors during the initial TMA legs and were often biased by the a'priori range error.

Theoretical lower bounds (Cramer-Rao) are presented which predict a substantial improvement during the initial TMA legs attributable to use of a'priori range information. The improvement disappears by the end of the problem (i.e., for a fully converged solution). Although both MAP and MLE solution errors agree well with the lower bounds at the end of the problem, the

expected difference during early problem times did not materialize. There are several explanations for this discrepancy. There is no guarantee that the Cramer-Rao bounds can be achieved since they are lower bounds not predictions of attainable accuracy. In any event, the MAP algorithm is optimum only for long measurement sequences and may not provide the best solution with limited duration or poor measurements. The globally optimum solution is not known for this problem and the least mean squared error solution is not computationally feasible.

The use of a'priori target speed estimates with a standard deviation of 2 knots or less provides substantially more improvement (in certain geometries) than the a'priori range estimates. In particular the closing target geometries (at any range) with a small target aspect exhibit substantially improved range, course and speed convergence during the early TMA legs. For these geometries, bearing rates are small and the TMA problem is difficult. The a'priori speed estimate resolves target course and speed quickly which then converges range. Of course, if the speed is incorrect then the solution will be biased. For targets with a large aspect the a'priori speed does not provide as much improvement because the measurements resolve the solution quickly due to the larger bearing changes. A'priori estimates of target speed may be obtained by turn count measurement, classification information, or tactical estimates. This information is not always available, but clearly provision should be made for its inclusion when available.

4.2 Line Array Measurements

The above conclusions are based on horizontal bearing measurements. For measurements made from a one dimensional (line) array it is necessary to provide an estimate of D/E angle to resolve horizontal bearing. If environmental predictions of propagation path are used to provide D/E estimates in addition to range estimates, then a substantial improvement in solution accuracy can be achieved. If the D/E is large (e.g., bottom bounce propagation), then large bias errors in horizontal bearing are incurred if a poor estimate of D/E is included. In standard TMA geometries this bias varies from leg to

leg causing a classical delta bias, which may severly bias the TMA solution. Since the effect of D/E error is readily observable in the solution bearing residuals, it would appear to be possible to estimate D/E during the TMA solution estimation. Evaluation of this concept was beyond the scope of the study.

An important consideration using line array measurements is the potential ambiguity between port and starboard if the array is not baffled. The approach taken to this problem was to run simultaneous solutions for each case until the ambiguity is resolved. Resolution is not difficult since the incorrect bearing cannot be supported on two adjacent TMA legs.

The major limitation of this study is that the most important line array sonar systems are towed arrays for which problems in estimating array position and heading are compounded by course maneuvers.

4.3 Numerical Considerations

The major benefits derived from the a'priori information were associated with the numerical convergence properties of the algorithms tested. Unfortunately this improvement is related to the specific numerical approachs used and therefore does not provide the type of general results desired from this study. Although the MLE algorithm is asymptotically optimum it has two drawbacks. The solution procedure is iterative in nature and is computationally expensive if the number of iterations is large. In addition, the optimization problem posed is ill conditioned during early stages of convergence. The technique used in this study is a Gauss-Newton iteration procedure with a "stopping" criteria based on proximity of adjacent iterations. For long range (2nd CZ in particular) geometries the iterations for a normal MLE algorithm do not stabilize until well into the problem. Thus, for the majority of solution times the solution cannot be used. As an example of the importance of the specific numerical approach, it was found necessary to incorporate a step size limiting modification to improve numerical convergence. Prior to this modification it was found that the MAP algorithm using a'priori range

AD-A076 559 ANALYSIS AND TECHNOLOGY INC NORTH STONINGTON CT F/G 17/7
TARGET TRACKING WITH MULTIPLE DATA SOURCES.(U)
AUG 79 H F JARVIS , N B NILL N00014-78-C-0707
UNCLASSIFIED P-515-1-79 NL

2 OF 2
AD
A076559

END
DATE
FILMED
12-79
DDC

statistics exhibited far superior numerical convergence property when the initial estimate was poor. The difference between MAP and MLE was considerably reduced by incorporating the step size limiting feature. However, for longer range closing targets the MAP solution converges with fewer iterations than the MLE solution. For this ill conditioned problem the incorporation of a'priori information improves convergence because the iteration equations are further removed from singularity than for the MLE case. Thus, the probability of numerical convergence is improved by a'priori information at the expense of running simultaneous solutions for each propagation path. It appears necessary to process nearly one half of the data (to solution convergence) to ensure retaining the correct path assumption. This is similar to an initial grid search on the MLE algorithm except the number of trial solutions is reduced, but they are retained longer. The advantage of this approach is assurance of generating early solutions which may require tactical decisions.

The use of a'priori speed estimates exhibits a remarkable increase in probability of convergence during initial legs (especially in the closing geometries). This improvement was not expected since the speed estimate is not used in initializing the solution.

4.4 Recommendations for Future Studies

Since the principal benefits derived from the use of a'priori range estimates were found to be related to numerical convergence properties of the algorithm it would be appropriate to study this aspect in more detail. In particular, the use of step size limiting reduced the advantage attributable to the a'priori information. It would be desirable to test an optimum step size calculation to determine if the convergence probability and/or execution time can be improved without use of a'priori information. The improvement was observable only during initial TMA legs where numerical convergence was difficult. To obtain useful information during initial legs it could be beneficial to constrain range or speed and solve the observable three state problem until the full solution can converge.

The effect on EKF algorithms of a'priori range should be investigated. Normally EKF solutions are not highly sensitive to initial range but for the extreme differences considered in this study, improvement in convergence properties would be expected. Since the computational burden is small it would not be prohibitive to run parallel solutions.

The use of environmental predictions in a multisensor algorithm should be investigated (bearing/frequency, multiple array bearings, etc.). It is likely that a'priori information can significently improve solution convergence for multisensor TMA particularly when own ship maneuvers are not included.

The use of D/E predictions for line array angles appears promising, but additional studies are required. Estimation of D/E may be possible since its effect on bearing residuals is quite observable. One might optimize D/E for the initial solution followed by regeneration of the solution based on the improved D/E estimate. Since towed arrays are an important class of line arrays it would be appropriate to investigate TMA maneuver tactics which reduce the uncertainty in towed array position and heading. For example sprint and drift tactics may be better than 60° lead/lag tactics.

The incorporation of bearing bias error into the measurement model should be considered and a tactically useful solution convergence criteria developed. In effect, for typical random error/bias error combinations, one should determine the values of range and velocity error bounds which provide timely solutions with an accuracy that matches tactical requirements.

APPENDIX A

Formulation of the MAP and MLE TMA Algorithms

This appendix develops the mathematical algorithms for the application of Maximum A'Posteriori (MAP) and Maximum Likelihood (MLE) statistical estimation principles in solving the bearings-only Target Motion Analysis (TMA) problem. There are two distinct MAP and MLE algorithms developed in this appendix, corresponding to two typical bearing sources.

One normally considers the target localization problem in the horizontal plane and ignores differences between target and own-ship depth. This is a reasonable approximation when depth differences are small compared to range and the acoustic wave arrives at the receiver with a small Depression/Elevation (D/E) angle. In any event if the sonar receiver has vertical extent and is baffled from behind, the receiver can measure a bearing in the horizontal plane. This type of receiver corresponds to most ship mounted passive sonar arrays and represents the first type of bearing source. If the receiver can track in the vertical plane, the D/E measurements obtained could be used to estimate target depth but this is beyond the scope of the study.

In addition to the sonar arrays discussed above, both submarine and surface ship combat systems include towed arrays which consist of a line of equally spaced transducers. A linear array can measure the angle of arrival of an acoustic wave relative to the array axis. The locus of wave directions corresponding to a given line array angle is a conical surface whose axis is the array. Thus, determination of horizontal bearing from a line array angle requires knowledge of D/E and specification of which side of the array the target is actually located on. A line array angle represents the second type of bearing source considered in this study.

A.1 Description of the Geometry

The bearings-only TMA problem requires maneuvers by own ship to resolve range. In addition, it assumes that the target maintains constant course and speed over the duration of the problem. Figure A-1 shows the conventional cartesian coordinate system formulated on a North-East frame of reference. As discussed previously the problem is treated as a two dimensional problem in the horizontal plane even though the true geometry is three dimensional. The TMA solution is defined as the range (R), target course (C_T), target speed (V_T) and target bearing (B) at some instant in time. These four parameters define the target location at all times because of the assumption that the target does not maneuver. The TMA solution is most easily solved in the cartesian coordinate frame because the position keeping (PK) equations are linear in that coordinate frame. Let $\underline{x}$ denote the solution vector in cartesian coordinates. $\underline{x}(t_k)$ is a four dimensional vector with components ($x_1(t_k)$, $x_2(t_k)$, $x_3(t_k)$, $x_4(t_k)$) which describes the TMA solution at time t_k. From Figure A-1 the relationships between TMA parameters can be readily obtained.

$x_1(t_k)$, $x_2(t_k)$ - Target distance East and North respectively from the origin at time t_k (1)

$x_{OS_1}(t_k)$, $x_{OS_2}(t_k)$ - Own ship distance East and North respectively from the origin at time t_k (2)

$x_3 = V_T \sin C_T$ - East component of target velocity (3)

$x_4 = V_T \cos C_T$ - North component of target velocity (4)

$V_T = \sqrt{x_3^2 + x_4^2}$ - Target Speed (5)

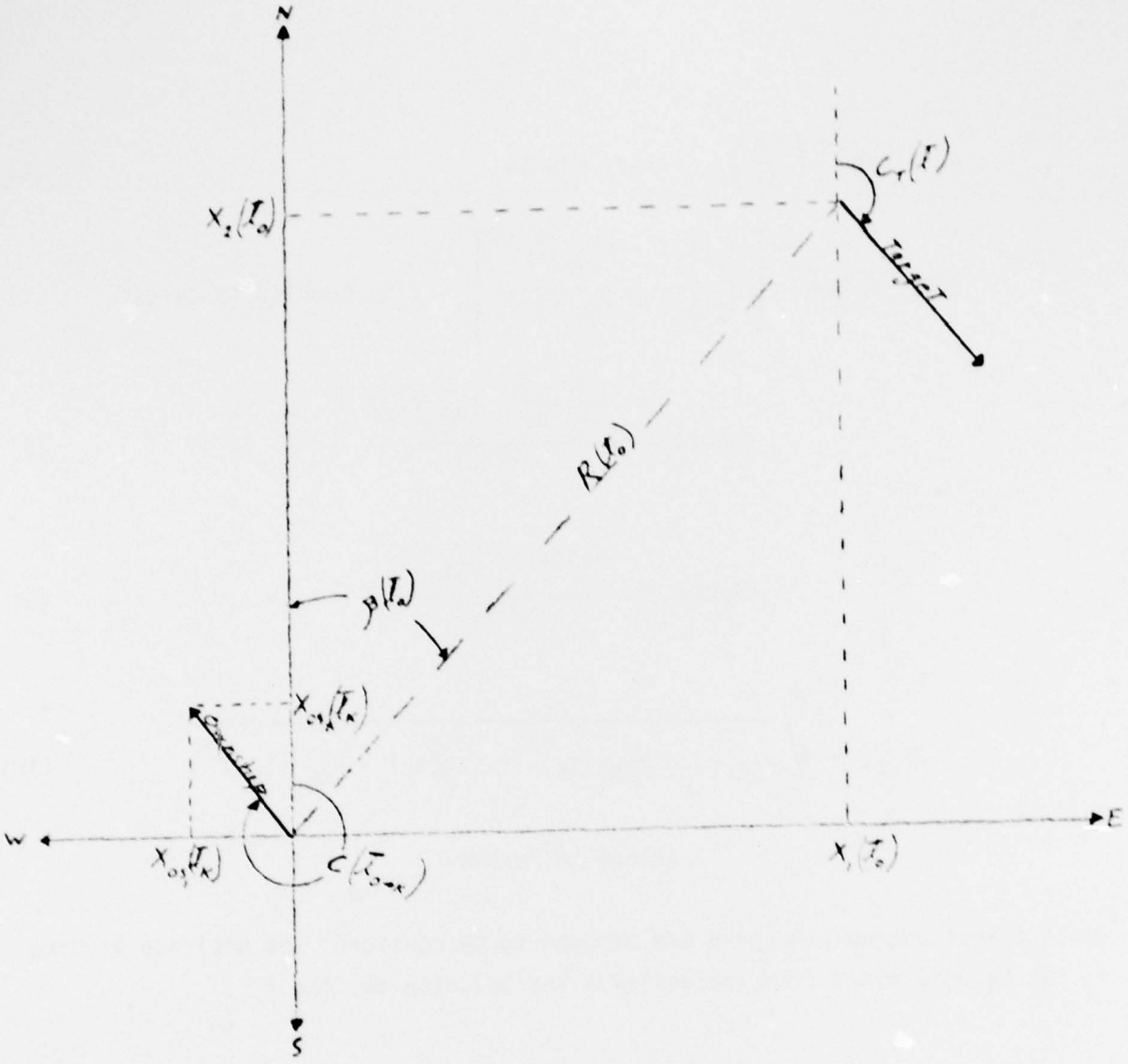

Figure A-1 Own ship and Target Ship Geometry for TMA (Cartesian Coordinates).

$$C_T = \tan^{-1}\left(\frac{x_3}{x_4}\right) \text{ - Target Course} \tag{6}$$

$$B(t_k) = \tan^{-1}\left[\frac{x_1(t_k) - x_{OS_1}(t_k)}{x_2(t_k) - x_{OS_2}(t_k)}\right] \text{ - true bearing to target} \tag{7}$$

$$\cos B(t_k) = \frac{x_2(t_k) - x_{OS_2}(t_k)}{R(t_k)} \tag{8}$$

$$\sin B(t_k) = \frac{x_1(t_k) - x_{os_1}(t_k)}{R(t_k)} \tag{9}$$

$$R(t_k) = \sqrt{(x_1(t_k) - x_{OS_1}(t_k)^2 + (x_2(t_k) - x_{OS_2}(t_k))^2} \tag{10}$$

(Range to Target)

Since target course and speed are assumed to be constant, the position at time t_j can be determined from the position and velocity at time t_k.

$$x_1(t_j) = x_1(t_k) + (t_j - t_k)x_3(t_k) \tag{11}$$

$$x_2(t_j) = x_2(t_k) + (t_j - t_k)x_4(t_k) \tag{12}$$

From these position keeping (PK) equations the solution can be PK'd to match each time a bearing measurement is obtained. In particular, the solution can be referred to the initial time t_0.

$$x_1(t_k) = x_1(t_0) + (t_k - t_0)x_3(t_0) \tag{13}$$

$$x_2(t_k) = x_2(t_0) + (t_k - t_0)x_4(t_0) \tag{14}$$

since $x_3(t_k) = x_3(t_0)$ and $x_4(t_k) = x_4(t_0)$,

$$\underline{x}(t_k) = \Phi_k \, \underline{x}(t_0); \; \Phi_k = \begin{bmatrix} 1 & 0 & t_k - t_0 & 0 \\ 0 & 1 & 0 & t_k - t_0 \\ 0 & 0 & 1 & 0 \\ 0 & 0 & 0 & 1 \end{bmatrix} \tag{15}$$

Note the $R(t_k)$ and $B(t_k)$ are explicit functions of $\underline{x}(t_k)$ and therefore (through Equation 15) explicit functions of $\underline{x}(t_0)$.

In the remaining discussions in this appendix $\underline{x}(t_k)$ is used to denote the true solution while $\hat{\underline{x}}(t_k)$ denotes the solution estimate at time t_k. The notation $\hat{B}$ and $\hat{R}$ denote the bearing and range estimates respectively, based on $\hat{\underline{x}}$ and the bearing measurements are denoted $B_m(t_k)$.

A.2 MAP and MLE Estimates for Horizontal Bearing Measurements

The assumption is made that the bearing measurements contain a zero mean Gaussian random error which is independent from sample to sample. This error can then be represented by the joint probability density function (pdf) of the measurement sequence, when the actual bearing sequence or TMA vector ($\underline{x}$) is known. Hence,

$$p_{\underline{B_m}/\underline{x}}(B_{m/x}) = (2\pi)^{-\frac{(N+1)}{2}} \prod_{k=0}^{N} \sigma_{B_k}^{-1} e^{-\left(\frac{1}{2} \sum_{k=0}^{N} \frac{(B_m(t_k) - B(t_k))^2}{\sigma_{B_k}^2}\right)} \tag{16}$$

where:

$$\underline{B}_m^T = \left[B_m(t_0), B_m(t_1), \ldots B_m(t_N) \right]$$

$B_m(t_k)$ - measured bearing at t_k

$B(t_k)$ - actual bearing at t_k

$\underline{x}$ - actual TMA vector at t_0

$\sigma^2_{B_k}$ - bearing error variance at time t_k

This model is somewhat simplistic since the bearing errors are all assumed to be independent from one sample to the next and unbiased. The assumption of independence is easily rationalized if the bearings are sampled at intervals larger than the tracker correlation times. The lack of bias does represent a departure from typical bearings obtained from existing sonar systems. The bias, if modeled, tends to bias the solutions and increase the total error. However, this study is sufficiently general in nature to preclude inclusion of specific sensor bias error models.

The external information on range and speed is not physically describable by Gaussian distributions but for lack of better information and to provide highly tractable solutions it is convenient to assign Gaussian distributions. Thus, the mean and variance are sufficient specifications for this assumption.

Define:

$$R^0 \equiv E\{R(t_0)\} \qquad \text{- a'priori range mean}$$

$$\sigma^2_{R_0} \equiv E\{(R(t_0) - R^0)^2\} \qquad \text{- a'priori range variance}$$

$$V_T^0 \equiv E\{V_T\} \qquad \text{- a'priori speed mean}$$

$$\sigma^2_V \equiv E\{(V_T - V_T^0)^2\} \qquad \text{- a'priori speed variance} \qquad (17)$$

where E { } denotes expectation over the ensemble of parameter values. The a'priori pdf for range is therefore:

$$p_R(\underline{x}) = \frac{1}{\sqrt{2\pi}\sigma_R} e^{-\frac{1}{2\sigma_R^2}(R(t_0)-R^0)^2} \tag{18}$$

The a'priori pdf for speed is:

$$p_V(\underline{x}) = \frac{1}{\sqrt{2\pi}\sigma_V} e^{-\frac{1}{2\sigma_V^2}(V_T-V_T^0)^2} \tag{19}$$

The a'posterior pdf for $\underline{x}$ is therefore:

$$p_{\underline{x}/\underline{B}_m}(\underline{x}/\underline{B}_m) = \frac{p_{\underline{B}_m/\underline{x}}(\underline{B}_m/\underline{x})\, p_{\underline{x}}(\underline{x})}{p_{\underline{B}_m}(\underline{B}_m)} \tag{20}$$

$$p_{\underline{x}}(\underline{x}) = p_R(\underline{x})p_V(\underline{x}) \quad \text{(a'priori pdf of } \underline{x}\text{)}$$

NOTE

$p_{\underline{B}_m}(\underline{B}_m)$ is not known but is independent of $\underline{x}$ and hence is a constant w.r.t. $\underline{x}$.

The MAP estimate of statistical information theory is the value of $\underline{x}$ which maximizes $p_{\underline{x}/\underline{B}_m}$. The MLE estimate maximizes $p_{\underline{B}_m/\underline{x}}$ and therefore excludes a'priori information. Since all pdf's are exponential, it is advantageous to work with the logarithm of the a'posterior pdf.

Let:

$$J^N \equiv -\ln\left[p_{\underline{x}/\underline{B}_m}(\underline{x}/\underline{B}_m)\right] \quad \text{(excluding constant terms)}$$

$$J^N = \frac{1}{2}\sum_{k=0}^{N}\frac{1}{\sigma^2_{B_k}(t_k)}\left[B_m(t_k)-B(t_k)\right]^2$$

$$+\frac{1}{2\sigma_R^2}(R(t_0)-R^0)^2+\frac{1}{2\sigma_V^2}(V_T-V_T^0)^2 \tag{21}$$

For an MLE algorithm the second and third terms in Equation 21 are dropped. Maximization of the a'posteriori pdf is equivalent to minimizing J. $B(t_k)$, $R(t_0)$ and V_T are nonlinear functions of $\underline{x}(t_0)$, so the solution is a nonlinear stochastic optimization problem for which a number of numerical approaches have been investigated by numerous researchers. The problems associated with the solution to this problem are well known. Until sufficient bearing change is induced by the own-ship motion, the function involved has a very shallow minima, and in fact prior to own-ship maneuvers it has no unique minima whatsoever. The measurement error sequence can induce multiple minima and in any event tends to obscure the true minimum. It was decided to use the Gauss-Newton method for this study. In essence this method involves a numerical iteration sequence which forces the gradient of the cost function to zero, thereby achieving a local minima of the function J^N. That is, $\hat{\underline{x}}$ is defined as the vector for which:

$$\nabla_{\underline{x}} J^N\Big|_{\underline{x}=\hat{\underline{x}}} = \underline{0} \tag{22}$$

$\nabla_x J$ is a column vector with components

$$\left(\frac{\partial J}{\partial x_1}, \frac{\partial J}{\partial x_2}, \frac{\partial J}{\partial x_3}, \frac{\partial J}{\partial x_4}\right)$$

Taking the gradient of Equation 21 w.r.t. $\underline{x}(t_0)$ for the MAP solution, results in:

$$\nabla_{\underline{x}} J^N = -\sum_{k=0}^{N} \frac{[B_m(t_k)-\hat{B}(t_k)]}{\sigma^2_{B_k}} \nabla_{\underline{x}} \hat{B}(t_k)$$

$$+ \frac{1}{\sigma^2_R} [\hat{R}(t_0)-R^0] \nabla_{\underline{x}} R(t_0)$$

$$+ \frac{1}{\sigma^2_V} [V_T-V_T^0] \nabla_{\underline{x}} V_T \qquad (23)$$

and for the MLE solution:

$$\nabla_{\underline{x}} J^N = -\sum_{k=0}^{N} \frac{[B_m(t_k)-\hat{B}(t_k)]}{\sigma^2_{B_k}} \nabla_{\underline{x}} \hat{B}(t_k) \qquad (24)$$

where,

$$\nabla_x \hat{B}(t_k) = \frac{1}{\hat{R}^2(t_k)} \begin{bmatrix} \hat{x}_2(t_k) - x_{os_2}(t_k) \\ -(\hat{x}_1(t_k) - x_{os_1}(t_k)) \\ (t_k - t_0)[\hat{x}_2(t_k) - x_{os_2}(t_k)] \\ -(t_k - t_0)[\hat{x}_1(t_k) - x_{os_1}(t_k)] \end{bmatrix} \tag{25}$$

$$\nabla_x \hat{R}(t_0) = \frac{1}{\hat{R}(t_0)} \begin{bmatrix} \hat{x}_1(t_0) - x_{os_1}(t_0) \\ \hat{x}_2(t_0) - x_{os_2}(t_0) \\ 0 \\ 0 \end{bmatrix} \tag{26}$$

$$\nabla_x \hat{V}_T = \begin{bmatrix} 0 \\ 0 \\ \sin \hat{C}_T \\ \cos \hat{C}_T \end{bmatrix} \tag{27}$$

For the simulations of this study $\sigma^2_{B_k}$ is constant over the duration of the problem and can be factored out of the summations. In practice, one can not set the gradients in Equations 23 and 24 to zero since the solution vector can not be explicitly obtained, because the resulting equations are highly nonlinear. The Gauss-Newton technique is an iteration procedure to converge to the solution vector for which the gradient is zero. The iteration algorithm can be derived heuristically by expanding the gradient in a multidimensional Taylor series about the previous iteration ($\underline{x}^l(t_0)$.

That is:

$$\nabla_x J^N \approx \nabla_{x^l} J^N + \nabla_{x^l}\nabla^T_{x^l} J^N(\hat{x}^{l+1} - \hat{x}^l) \tag{28}$$

where $\nabla_{x^l} J^N$ was defined in 23, 24, ∇^T denotes a gradient vector transpose and,

$$\nabla_{x^l}\nabla^T_{x^l} J^N = -\sigma^{-2}_{B_m} \sum_{k=0}^{N} [B_m(t_k) - \hat{B}(t_k)]\nabla_{x^l}\nabla^T_{x^l}\hat{B}(t_k)$$

$$+ \sigma^{-2}_{B_m} \sum_{k}^{N} \nabla_{x^l}\nabla^T_{x^l}\hat{B}(t_k)$$

$$+ \sigma^{-2}_{R} \nabla_{x^l}\hat{R}(t_0)\nabla^T_{x^l}\hat{R}(t_0)$$

$$+ \sigma^{-2}_{V} \nabla_{x^l} V_T \nabla^T_{x^l} V_T \tag{29}$$

The first term in Equation 29 contains the random measurement error sequence which prevents the matrix $\nabla_x\nabla^T_x J$ from being non-negative definite. Since this can preclude convergence it is useful to replace Equation 29 by its expectation (over the bearing error sequence). Assuming $\hat{B}(t_k)$ to be an unbaised estimate, the first term drops out.

Then;

$$\nabla_x J^N \approx \nabla_{x^1} J^N + E[\nabla_{x^1} \nabla_{x^1} J^N](\hat{x}^{1+1} - x^1) \tag{30}$$

With $E[\nabla_{x^1} \nabla_{x^1} J^N]$ given by the last three terms of Equation 29. Although Equation 30 is an approximation at the initial TMA time, the importance of the linearization error becomes negligible as the solution converges, i.e., as N becomes sufficiently large

The two terms in Equation 30 can be derived in explicit form by making use of the trigonometric relations given in Equations 5 through 10, the PK Equations 13 and 14, and properties of partial differentiation, resulting in (dropping the superscript 1 on $\hat{x}^1$):

$$\nabla_x J^N = \begin{bmatrix} \gamma_1 \\ \gamma_2 \\ \gamma_3 \\ \gamma_4 \end{bmatrix} \tag{31}$$

where,

$$\gamma_1 = -\sigma_{B_m}^{-2} \sum_{k=0}^{N} \frac{[B_m(t_k) - \hat{B}(t_k)][\hat{x}_2(t_k) - x_{os_2}(t_k)]}{\hat{R}^2(t_k)}$$

$$+ \frac{[\hat{R}(t_0) - R^0][\hat{x}_1(t_0) - x_{os_1}(t_0)]}{\sigma_R^2 \hat{R}(t_0)}$$

$$\gamma_2 = \sigma_{B_m}^{-2} \sum_{k=0}^{N} \frac{[B_m(t_k) - \hat{B}(t_k)][\hat{x}_1(t_k) - x_{os_1}(t_k)]}{\hat{R}^2(t_k)}$$

$$+ \frac{[\hat{R}(t_0) - R^0][\hat{x}_2(t_0) - x_{os_2}(t_0)]}{\sigma_R^2 \; \hat{R}(t_0)}$$

$$\gamma_3 = - \sigma_{B_m}^{-2} \sum_{k=0}^{N} \frac{(t_k - t_0)[B_m(t_k) - \hat{B}(t_k)][\hat{x}_2(t_k) - x_{os_2}(t_k)]}{\hat{R}^2(t_k)}$$

$$+ \frac{[\hat{V}_T - V_T^0][\hat{x}_1(t_0) - x_{os_1}(t_0)]}{\sigma_V^2 \; \hat{R}(t_0)}$$

$$\gamma_4 = \sigma_{B_m}^{-2} \sum_{k=0}^{N} \frac{(t_k - t_0)[B_m(t_k) - \hat{B}(t_k)][\hat{x}_1(t_k) - x_{os_1}(t_k)]}{\hat{R}^2(t_k)}$$

$$+ \frac{(\hat{V}_T - V_T^0)[\hat{x}_2(t_0) - x_{os_2}(t_0)]}{\sigma_V^2 \; \hat{R}(t_0)}$$

let:

$$E[\nabla_x] \nabla_x^T] \; J^N] \equiv \Psi = \Psi_b + \Psi_R + \Psi_v \tag{32a}$$

where the three terms representing bearing, a'priori range, a'priori speed respectively, are each a 4 x 4 matrix; then it is more convenient to define the components as,

$$\Psi_{B_{i,j}} = \sigma_{B_m}^{-2} \sum_{k=0}^{N} \frac{a_{i_k} \; a_{j_k}}{\hat{R}^3(t_k)} \tag{32b}$$

i = row

j = column

$$a_{1_k} = \hat{x}_2(t_k) - x_{os_2}(t_k)$$

$$a_{2_k} = -[\hat{x}_1(t_k) - x_{os_1}(t_k)]$$

$$a_{3_k} = (t_k - t_0)[\hat{x}_2(t_k) - x_{os_2}(t_k)]$$

$$a_{4_k} = -(t_k - t_0)[\hat{x}_1(t_k) - x_{os_1}(t_k)]$$

$$\Psi_{R_{i,j}} = \frac{b_i\, b_j}{\sigma_R^2} \tag{32c}$$

$$b_1 = \hat{x}_1(t_0) - x_{os_1}(t_0)$$

$$b_2 = \hat{x}_2(t_0) - x_{os_2}(t_0)$$

$$b_3 = b_4 = 0$$

$$\Psi_{V_{i,j}} = \frac{C_i\, C_j}{\sigma_V^2} \tag{32d}$$

$$C_1 = C_2 = 0$$

$$C_3 = \sin \hat{C}_T$$

$$C_4 = \cos \hat{C}_T$$

A.3 Solution Computation Methodology

To initiate computation of Equations 31 and 32 at the first TMA track time increment t_0, the initial $\hat{\underset{\sim}{x}}$ estimate is defined as,

$$\hat{x}_1(t_o) = x_{os_1}(t_0) + R^0 \sin B_m(t_0)$$

$$\hat{x}_2(t_0) = x_{os_2}(t_0) + R^0 \cos B_m(t_0)$$

$$\hat{x}_3(t_0) = \hat{x}_4(t_0) = 0 \qquad (33)$$

where the initial range estimate R^0 is utilized (in both MLE and MAP) in conjunction with the first measured bearing value, but the initial target speed estimate is not utilized, due to the fact that the target course is unknown, resulting in the 3rd and 4th components being 0.

With these initial conditions at t_0, computation of Equations 31 and 32 can progress up to t_k, the present TMA track time increments. Equation 30 is then formed into a nonhomogeneous linear equation set for simultaneous solution of the $\hat{x}^{l+1}$ components by Gauss Elimination as follows:

from 30, 31 and 32

$$\begin{bmatrix} \gamma_1^l \\ \gamma_2^l \\ \gamma_3^l \\ \gamma_4^l \end{bmatrix} + [\psi^l] \begin{bmatrix} \hat{x}_1^{l+1}(t_k) - \hat{x}_1^l(t_k) \\ \hat{x}_2^{l+1}(t_k) - \hat{x}_2^l(t_k) \\ \hat{x}_3^{l+1}(t_k) - \hat{x}_3^l(t_k) \\ \hat{x}_4^{l+1}(t_k) - \hat{x}_4^l(t_k) \end{bmatrix} = \begin{bmatrix} 0 \\ 0 \\ 0 \\ 0 \end{bmatrix} \qquad (34)$$

Now by multiplying Equation 33 out and rearranging terms gives,

$$\psi_{11}\hat{x}_1^{l+1}(t_k) \cdots \psi_{14}\hat{x}_4^{l+1}(t_k) = [\psi_{11}\hat{x}_1^{l}(t_k) + \cdots + \psi_{14}\hat{x}_4^{l}(t_k)] - \gamma_1$$

$$\cdot \quad \cdot\ \cdot \quad \cdot \quad = \quad \cdot \quad \cdot\ \cdot\ \cdot \quad \cdot \quad \cdot$$

$$\cdot \quad \cdot\ \cdot \quad \cdot \quad = \quad \cdot \quad \cdot\ \cdot\ \cdot \quad \cdot \quad \cdot$$

$$\psi_{41}\hat{x}_1^{l+1}(t_k) \qquad \psi_{44}\hat{x}_4^{l+1}(t_k) = [\psi_{41}\hat{x}_1^{l}(t_k) + \cdots + \psi_{44}\hat{x}_4^{l}(t_k)] - \gamma_4 \tag{35}$$

The Gauss Elimination method solves for the unknown $\hat{\underline{x}}^{l+1}(t_k)$ by forcing the 4 equation set of Equation 35 into a triangular form. This is accomplished primarily by repeated coefficient normalizations wherein rows are interchanged if the pivot coefficient is less than $1_x 10^{-6}$, to help prevent computer underflow/overflow (16 digit - double precision). Once the triangular form is achieved, i.e., left-hand side of 4th equation in Equation 35 has 1 term, 3rd equation - 2 terms, 2nd equation - 3 terms, 1st equation - 4 terms, then back substitution (from equation 4→3→2→1) is done to solve for all 4 components of $\hat{\underline{x}}^{l+1}(t_k)$.

A.3.1 Stopping Criteria

Because of the linearization approximation inherent in Equation 30, it is necessary to iterate the Gauss Elimination solution until the difference between the present iteration $\hat{\underline{x}}^{l+1}(t_k)$ and previous iteration $\hat{\underline{x}}^{l}(t_k)$ is "small" in some meaningful sense. The difference between successive iterations is measured by a weighted sum of the squares of the $\hat{\underline{x}}$ component differences. The two position components $(\hat{x}_1,\hat{x}_2)$ are weighted equally, as are the two velocity components $(\hat{x}_3,\hat{x}_4)$.

The test parameter takes the form,

$$\varepsilon = \frac{[\hat{x}_1^{l+1}(t_k) - \hat{x}_1^{l}(t_k)]^2 + [\hat{x}_2^{l+1}(t_k) - \hat{x}_2^{l}(t_k)]^2}{\sigma_1^2}$$

$$+ \frac{[\hat{x}_3^{l+1}(t_k) - \hat{x}_3^{l}(t_k)]^2 + [\hat{x}_4^{l+1}(t_k) - \hat{x}_4^{l}(t_k)]^2}{\sigma_2^2} \qquad (36)$$

The values of σ_1 and σ_2 are chosen to balance the differences between position errors and speed errors. One way to accomplish this is to choose a speed error which results in a PK position error of the order of the desired position error over an interval of time. For example a speed error of 0.5626 yd/sec (0.1 kts) yields a position error of 33.75 yds over a ten minute time interval. Based on this logic the following values were selected:

$$\sigma_1^2 = 3600 \text{ yds}^2$$

$$\sigma_2^2 = .01266 \text{ (yds/sec)}^2 \qquad (37)$$

The test criteria for ε is a value of one. Figure A.2 shows a typical interaction of term 1 versus term 2 of Equation 36, drawn from one of the cases run. It is seen that term 1 has the same overall relative importance as term 2, in determining ε.

A number of sample cases were run to establish the proper maximum allowable number of iterations for Gauss Elimination. If too few iterations are allowed, then convergence may never occur over the entire TMA track time. If too many iterations are allowed then the computer time burden can become unacceptable. It was determined that allowing 20 iterations is a good compromise. In some

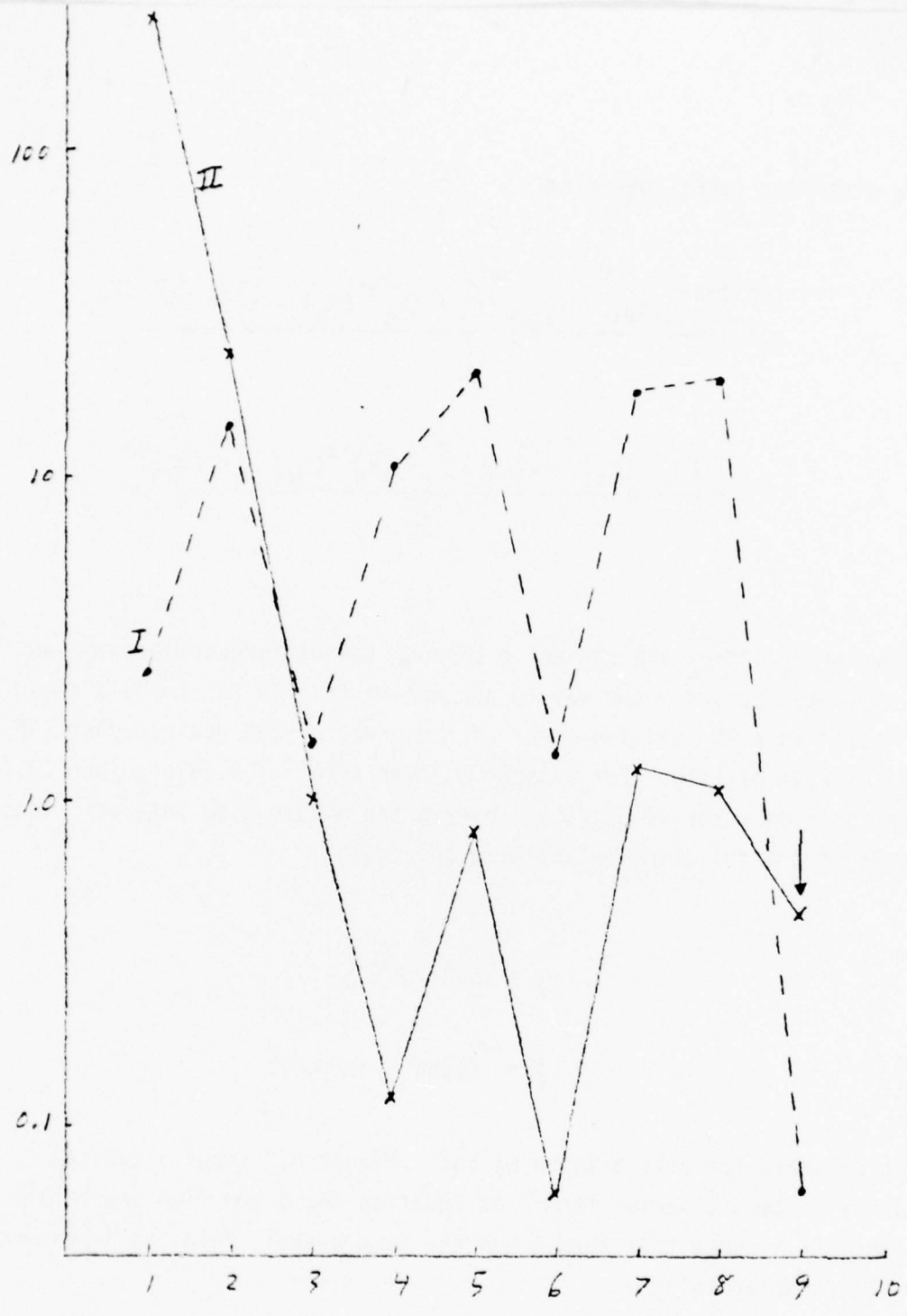

Figure A-2 Stopping Criteria on Gaussian Iterations for $\hat{x}$ Solution.

cases, a maximum of 10 iterations did not allow convergence, whereas, cases allowing 50 iterations usually would rapidly decrease (with time into TMA track) to a range around 20, without significant improvement in solution convergence time or accuracy. A maximum of 20 Gauss Elimination iterations were therefore allowed for each bearing update.

A.3.2 Step Size Limiting

When the difference between successive iterations is very large, the iterations oscillate wildly without converging. It is important therefore to limit the maximum step size to reduce the tendency to overshoot the minima. This is accomplished by weighting the iteration update by a factor which is unity or smaller. This has the effect of steering the solution to convergence more rapidly. The weighting factor used is $\sqrt{\frac{W}{\varepsilon}}$

where;

$$W = \frac{\sigma_R^2}{\sigma_1^2} + \frac{\sigma_V^2}{\sigma_2^2} \quad \text{, for MAP}$$

$$W = \frac{\sigma_R^2}{\sigma_1^2} \quad \text{, for MLE} \tag{38}$$

(σ_1^2, σ_2^2 defined in Equation 37, σ_R^2, σ_V^2 defined in Equation 17), then for $\varepsilon > W >> 1.0$,

$$\hat{\underline{x}}_{new}(t_k) = \hat{\underline{x}}^{l}(t_k) + \sqrt{\frac{W}{\varepsilon}}\ [\hat{\underline{x}}^{l+1}(t_k) - \hat{\underline{x}}^{l}(t_k)] \tag{39a}$$

for $1.0 < \varepsilon \leq W$,

$$\hat{\underline{x}}_{new}(t_k) = \hat{\underline{x}}^{l+1}(t_k) \tag{39b}$$

for $\varepsilon \leq 1.0$,

$$\hat{\underline{x}}^{l+1}(t_k) \text{ is the optimum solution} \tag{39c}$$

A series of 28 test cases were run which demonstrated that, on the average, there is a 23 percent reduction in the number of Gauss Elimination iterations needed for convergence when the weighting factor $\sqrt{\frac{W}{\varepsilon}}$ is used, as opposed to no weighting factor.

It is recognized that this step size limiting criteria is not optimum, but it was simple and did not impact run time nor impact software development. The best procedure would involve solving for the optimum step size at each iteration. In effect performing a one dimensional optimization for the step size limiting coefficient. It was decided not to pursue that approach in the interest of expediency.

For some time increments near the beginning of own-ship maneuver (first few legs), it often happens that no convergence results, even with 20 iterations and convergence steering weighting. In such a case the solution error at the 20th iteration can be quite large. To ensure that a "poor" early solution does not preclude eventual convergence, all unconverged iterations are discarded and the a'priori information given in Equation 33 is used to initialize computations for the next time increment t_{k+1}. This method was used in all runs although test cases demonstrated that the improvement is significant only where unconverged solutions are very poor.

The solution is solved sequentially in time, wherein the first solution is based on the first three bearings. Since each bearing measurement used, represents an average value of 20 one-second samples, the first three bearings cover the first minute of the TMA track. Each new solution is computed based on adding three bearing measurements to the previous data base. If the previous solution iterations converged in 20 or fewer iterations, then the solution from this previous data base is taken as the first iteration for the present data base. Thus, a new solution is generated at one-minute intervals to show solution convergence as a function of time.

A.4 Error Bounds on TMA Solutions

In an operational scenario the true target positior is of course unknown, and it is necessary for the TMA algorithm to indicate when convergence has been reached. The method used in the algorithm for each converged time increment is based on the Cramer-Rao bound for unbaised estimates.

The matrix;

$$E[\nabla_x \nabla_x^T J^N] \tag{40}$$

is Fisher's Information Matrix. The inverse matrix is a lower bound on the covariance matrix of the solution when evaluated at the true solution. Now from Equations 32 and 35 it is seen that $E[\nabla_x \nabla_x^T J^N]^{-1} = \psi^{-1}$ is just the inverse of the coefficient matrix for the simultaneous equation set Equation 35. The ψ^{-1}matrix can be calculated from the relation,

$$\psi^{-1} = \frac{\text{adjoint } \psi}{|\psi|} \tag{41}$$

where the adjoint ψ matrix is found from the transpose of the cofactors of ψ and $|\psi|$ is calculated by pivotal condensation. Submatrices of ψ^{-1} are next used to generate the orientation angles and eigenvalues defining the major and minor axis of an error bound ellipse for position and velocity errors.

Let;

$$\psi^{-1} = \begin{bmatrix} a_{11} & a_{12} & a_{13} & a_{14} \\ a_{21} & a_{22} & a_{23} & a_{24} \\ a_{31} & a_{32} & a_{33} & a_{34} \\ a_{41} & a_{42} & a_{43} & a_{44} \end{bmatrix} \tag{42}$$

then major, minor axes for velocity errors are the eigenvalues of the matrix:

$$\begin{bmatrix} \lambda - a_{33} & -a_{34} \\ -a_{43} & \lambda - a_{44} \end{bmatrix} \tag{43}$$

$$\text{ellipse orientation angle} = \frac{1}{2} \tan^{-1} \left[\frac{2a_{34}}{a_{44} - a_{33}} \right] \tag{44}$$

and the major, minor axes, orientation angle for the position errors are given by Equations 42, 43 and 44 after substituting row, column (1, 2) for row, column (3, 4).

Thus, for each time increment for which the $\underline{x}(t_k)$ solution converges, a lower bound on the range error variance and velocity error variance is obtained. Once these generally monotonically decreasing functions of time reach a predefined level, convergence can be said to be achieved. Note that in practice it is more convenient to work with the square root of the error variances, i.e., the standard deviations.

A.5 MAP and MLE Formulation for Line Array Sonars

The mathematical derivation is analogous to the horizontal bearing sonar case given in Section A.2, Equations 16 through 35, with the auxiliary derivations for weighting function, eigenvalues, etc., of Equations 36 through 44 being identical. The basic difference for the line array case is that a line array cannot discriminate between different depression/elevation (D/E) angles of arrival. It is therefore necessary to first estimate the D/E angle of arrival in order to obtain the horizontal plane bearing. In addition, the more useful measurement variable for the line array case is the cosine of the relative measured bearing rather than the measured true bearing, since the errors in the measurement are independent of relative bearing when the cosine is used.

The cosine of the measured relative bearing $B_r(t_k)$ is given by,

$$\cos B_r(t_k) = \cos [B_H(t_k) - C(t_k)] \cos D + G_k \sigma_B \tag{45}$$

where

$B_H(t_k)$ = horizontal true bearing

$C(t_k)$ = own ship true course

D = Depression/elevation angle of arrival

G_k = Gaussian distributed random number (unit variance, 0 mean)

σ_B = standard deviation for cosine bearing error

Equation 45 gives the method for generating cos $B_r(t_k)$ in the algorithm and this is equivalent to a noisy horizontal bearing $B_{H_m}(t_k)$ combined with an initial estimate of the depression/elevation angle D°.

That is,

$$\cos B_r(t_k) \equiv \cos [B_{H_m}(t_k) - C(t_k)] \cos D° \tag{46}$$

thus,

$$B_{H_m}(t_k) = \cos^{-1}\left[\frac{\cos B_r(t_0)}{\cos D°}\right] + C(t_0) \tag{47}$$

Where Equation 47 is used to define the initial $\hat{x}(t_0)$ condition given in Equation 33. But, the true quadrant range in which $B_{H_m}(t_k)$ lies is ambiguous* - it can either be in the $0 \rightarrow \pi$ range or $\pi \rightarrow 2\pi$ range. Therefore, two separate, simultaneous solutions should be run - one solution using $B_{H_m}(t_0)$ and one solution using $B_{H_m}(t_0) + \pi$ as an initial condition.

With the changes noted in the discussion connected with Equations 45, 46 and 47 the total conditional pdf analogous to Equation 20 is,

---

*The $\cos^{-1}$ range for the computer used is $0 \rightarrow \pi$ regardless of the true range of cos $B_r(t_k)$/cos D°.

$$p(B_{H_m}|x) = e^{-\frac{1}{2\sigma_B^2} \sum [\cos B_r(t_k) - \cos \hat{B}_r(t_k)]^2}$$

$$\cdot e^{-\frac{1}{2\sigma_R^2} [R(t_0) - R^0]^2} \; e^{-\frac{1}{2\sigma_V^2} [V_T - V_T^0]^2} \tag{48}$$

again setting $\nabla_x[-\ln p(B_{H_m}|x)\, p_R(x)\, p_V(x)] = 0 = \nabla_x J^N$ for the MAP solution and carrying through the differentiation results in,

$$\nabla_x J^N = \frac{\cos D^\circ}{\sigma_B^2} \sum_{k=0}^{N} \{\cos B_r(t_k) - \cos [\hat{B}_{H_m}(t_k) - C(t_k)] \cos D^\circ\}$$

$$\cdot \sin [\hat{B}_{H_m}(t_k) - C(t_k)] \quad \nabla_x \hat{B}_{H_m}(t_k)$$

$$+ \frac{(\hat{R}(t_0) - R^0)\, \nabla_x \hat{R}(t_0)}{\sigma_R^2} + \frac{(\hat{V}_T - V_T^0)\, \nabla_x \hat{V}_T}{\sigma_V^2} \tag{49}$$

where,

$$\nabla_x \cos \hat{B}_r(t_k) = \nabla_x[\cos [\hat{B}_{H_m}(t_k) - C(t_k)] \cos D^\circ]$$

$$= - \sin [\hat{B}_{H_m}(t_k) - C(t_k)] \cos D^\circ \nabla_x \hat{B}_{H_m}(t_k) \tag{50}$$

The same values for $\nabla_x \hat{B}_{H_m}(t_k)$, $\nabla_x \hat{R}(t_0)$, $\nabla_x \hat{V}_T$ as given in Equations 25, 26 and 27 again apply and letting

$$\tau_k = [\cos B_r(t_k) - \cos \hat{B}_r(t_k)] \sin [\hat{B}_{H_m}(t_k) - C(t_k)]$$

$$= [\cos B_r(t_k) - \cos [\hat{B}_{H_m}(t_k) - C(t_k)] \cos D^\circ] \sin [\hat{B}_{H_m}(t_k) - C(t_k)] \tag{51}$$

then

$$\nabla_x J^N = \begin{bmatrix} \gamma_1 \\ \gamma_2 \\ \gamma_3 \\ \gamma_4 \end{bmatrix}$$

where

$$\gamma_1 = \frac{\cos D^\circ}{\sigma_B^2} \sum_{k=0}^{N} \frac{\tau_k(\hat{x}_2(t_k) - x_{os_2}(t_k))}{\hat{R}^2(t_k)} + \frac{(\hat{R}(t_0) - R^0)[\hat{x}_1(t_0) - x_{os_1}(t_0)]}{\sigma_R^2 \hat{R}(t_0)}$$

$$\gamma_2 = -\frac{\cos D^\circ}{\sigma_B^2} \sum_{k=0}^{N} \frac{\tau_k[x_1(t_k) - x_{os_1}(t_k)]}{\hat{R}^2(t_k)} + \frac{[\hat{R}(t_0) - R^0][\hat{x}_2(t_k) - x_{os_2}(t_k)]}{\sigma_R^2 \hat{R}(t_0)}$$

$$\gamma_3 = \frac{\cos D^\circ}{\sigma_B^2} \sum_{k=0}^{N} \frac{\tau_k(t_k - t_0)[\hat{x}_2(t_k) - x_{os_2}(t_k)]}{\hat{R}^2(t_k)} + \frac{(\hat{V}_T - V^0) \cos \hat{C}_T}{\sigma_V^2}$$

$$\gamma_4 = -\frac{\cos D^\circ}{\sigma_B^2} \sum_{k=0}^{N} \frac{\tau_k(t_k - t_0)[\hat{x}_1(t_k) - x_{os_1}(t_k)]}{\hat{R}^2(t_k)} + \frac{(\hat{V}_T - V_T^0) \cos \hat{C}_T}{\sigma_V^2} \tag{52}$$

Following the procedure discussed surrounding Equations 29 and 30, i.e., assuming cos $\hat{B}_r(t_k)$ to be an unbiased estimate and taking the expected value of $\nabla_x \nabla_x^T J^N$, results in $E[\nabla_x \nabla_x^T J^N] = \psi_B + \psi_R + \psi_V$ for the line array case, which differs from that for the horizontal bearing case only by the factor $[\sin^2[B_{H_m}(t_k) - C(t_k)] \cos D^\circ]^2$ in ψ_B.

Hence,

$$\psi_B = \sum_{k=0}^{N} \frac{\{\sin[B_{H_m}(t_k) - C(t_k)] \cos D^\circ\}^2 a_{i_k} a_{j_k}}{\hat{R}^2(t_k)\sigma_B^2}$$

where a_{i_k}, a_{j_k} are defined in Equation 32b and ψ_R, ψ_V remain identical to Equations 32c and 32d.

APPENDIX B

Description of the MAP/MLE TMA Computer Simulation Program

The TMA simulation program was written in FORTRAN V and executed on a Data General Eclipse M600 minicomputer. This 16 bit computer uses double words for floating point arithmetic (24 bit mantissa) which provides sufficient dynamic range for the required computations. This appendix provides the basic description of the computer program. The detailed equations and theoretical background is provided in Appendix A.

The program flow chart in Figure B-1 illustrates the sequence of calculations. The program has three basic sections which calculate simulated inputs, update the solution, and assemble solution statistics. The program loops through the calculations for a specified number of Monte Carlo repetitions to allow calculation of the statistical properties of the TMA solution errors.

Blocks one through six in Figure B-1 provide the simulated inputs to the TMA calculations. The inputs are the own-ship maneuver plan, target course, speed, initial true bearing (horizontal plane) and range. The maneuver plan consists of a set of TMA leg times with a relative bearing at the start of each leg. For this study five-minute legs were used with a conventional 60° lead/lag tactic. Maneuvers were accomplished at a constant turning rate of two degrees per second. The motion simulator calculates own-ship course and position on a North/East coordinate frame based on this maneuver plan at one second intervals. Target position is also calculated and combined with own-ship position to generate a sequence of (horizontal) true bearings and ranges every second of problem time. The bearings, own-ship course and position values are averaged over 20-second intervals. The averaged bearings are corrupted by Gaussian noise to simulate measured bearings. For simulating line array bearings the cosine of the conical angle is computed before the measurement noise is added. The cosine of the conical angle is obtained by multiplying the cosine of the horizontal plane relative bearing by the cosine of the (actual) D/E angle. The cosine of the line array angle is used because

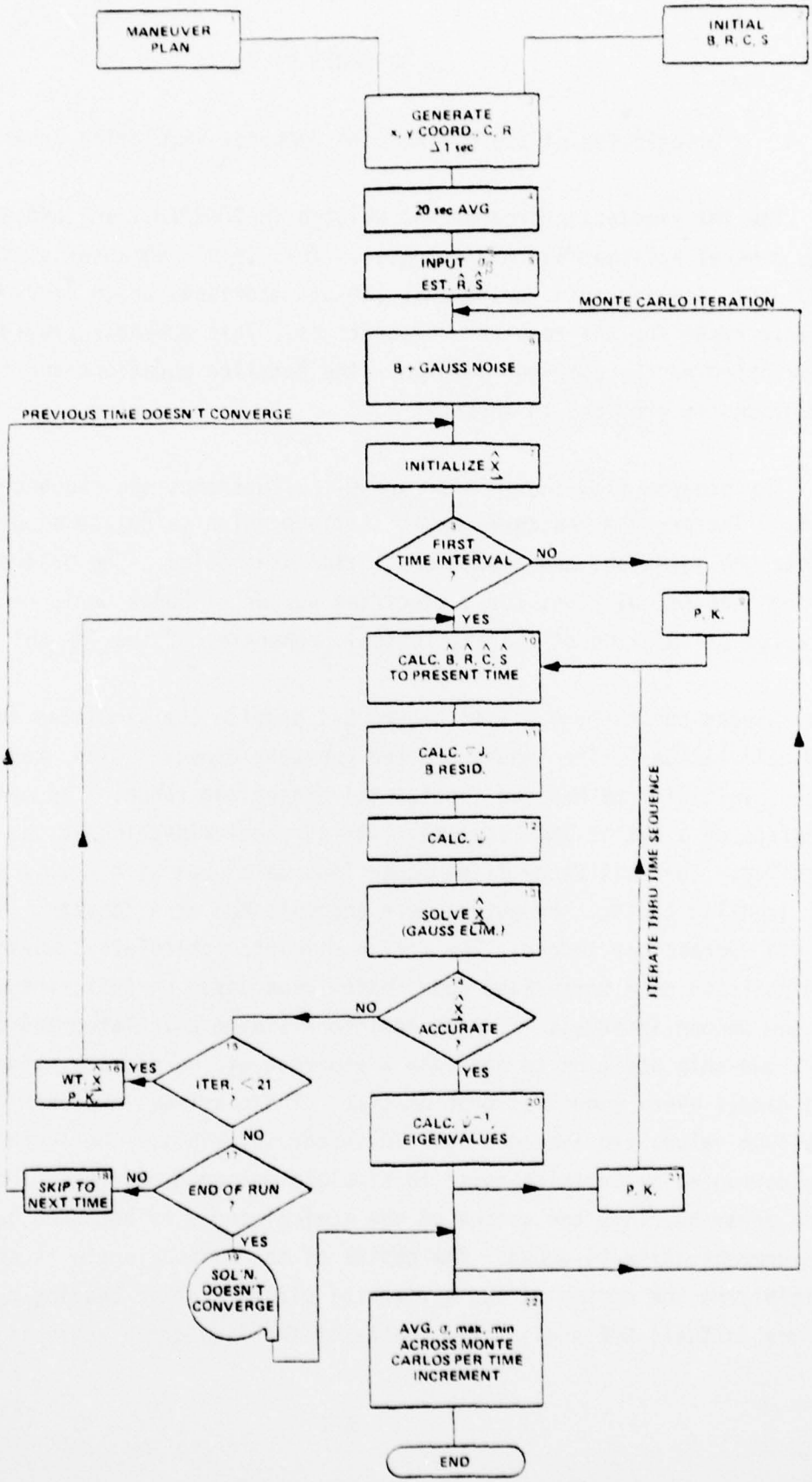

Figure B-1 MLE/TMA and MAP/TMA Algorithm Flow Chart

the measurement error for that quantity is independent of the angle. The Gaussian random numbers are generated by combining twelve uniformly distributed random numbers and normalizing the result to provide zero mean, unit variance Gaussian numbers. These are scaled by an input bearing error standard deviation to generate the measurement error. For each Monte Carlo iteration the sequence of measurement errors are independent of the sequence for every other Monte Carlo iteration. The measured bearings (or cosine line array measurements) are passed along with own-ship position coordinates to the TMA solution calculations. Target course, speed, range and bearing are passed to the statistical error routines for evaluation of solution errors.

The solution computation involves blocks 7 through 19 in Figure B-1. The program allows use of a'priori information in a MAP estimate or allows computation of a conventional MLE estimate which uses a'priori information only in initialization. The solutions are updated at every third bearing measurement (one minute of problem time) and calculations are made for a maximum of 40 minutes of problem time. The first measurement is used to initialize the first solution by establishing an initial line of sight. The target is placed on the line-of-sight at the a'priori range value with a speed of zero. An initial speed estimate of zero is required because no a'priori course estimate is available. For line array angle measurements an a'priori decision must be made whether the target lies on the port or starboard side of the array. Thus, two solutions must be executed if that information is not available a'priori. In addition, an a'priori estimate of the D/E angle for the assumed path is used to relate line array angle to horizontal plane bearings regardless of the input source. Blocks 7 through 10 indicate the initialization procedure and the calculations of bearing and range at every time a measurement is available. The bearings and range at any time are obtained by position keeping (PK) the solution at t_0 to the problem times, and combining the target positions with stored own-ship positions at these times. The procedure for obtaining a solution is an iterative one. For a given set of measurements the solution at t_0 is given by initial conditions if no previous solution is available. Otherwise, the solution obtained from the previous measurements is PK'd to time zero and used to replace normal initialization. In any event, the initial solution is used to calculate the

gradient matrix ($\nabla_x J$) and the average Hessian matrix (ψ). From these matrices the next iteration of the solution is computed by using Gauss Elimination methods to solve the approximation for the true gradient matrix. If the calculated iteration satisfies a stopping criteria relative to the last iteration, then this solution is taken as the optimal solution for that set of measurements. Normally, a number of iterations are required. If the stopping criteria is not met, the calculated solution is corrected by a variable step size algorithm to improve convergence properties and passed back to block 10 for calculation of a new iteration. If the stopping criteria is not met within 21 iterations the procedure is stopped, the solution is not used in the statistical averages, and the next solution (based on three more measurements) will use the initial estimate to start its iterative cycle. The computation of $\nabla_x J$ and ψ vary according to a flag to provide either a MAP or MLE solution as selected by the user.

Solutions at each time at which the Gauss Elimination iterations converge are stored for calculation of error statistics. The statistical error calculation involves averages taken over the independent Monte Carlo repetitions at one-minute problem time intervals. In addition to calculating solution errors the program calculates a set of error bounds obtained from the inverse of the ψ matrix. The inverse of the Ψ matrix is an approximation to Fisher's Information Matrix from the Cramer-Rao bound. The matrix (ψ^{-1}) is partitioned into two by two submatrices and the eigenvalues of the diagonal submatrices computed along with the angle of the eigenvectors. These eigenvalues can be used to define the error bound ellipses from the Cramer-Rao bound. The statistical algorithms compute mean, standard deviation and min max values over the Monte Carlo iterations for the following quantities.

- Range, course, speed and bearing errors, sum squared bearing residuals, eigenvalues and eigenvector angles.

In addition, the following information is printed:

- Input data, solution history for first Monte Carlo iteration, number of converged Monte Carlo iterations at each solution time, own-ship position track and true range time history.

Figure B-2 shows an example printout of a typical horizontal bearing run with the MAP estimator. In this case the true initial range via direct path is 20,000 yds and the range estimate (direct path) is 15,000 yds with a range σ = 7500 yds. The problem converges to a range solution at 8 minutes. ("RANGE SIG" drops below 1000 yds.)

US MANEUVER PLAN

TIME(MIN)	REL BEAR	CRS CHG RATE	SPEED	SPD CHG RATE	FLAG
.50000E 01	-.60000E 02	.20000E 01	.10000E 02	.00000E 00	.0
.10000E 02	.60000E 02	.20000E 01	.10000E 02	.00000E 00	.0
.15000E 02	-.60000E 02	.20000E 01	.10000E 02	.00000E 00	.0
.20000E 02	.60000E 02	.20000E 01	.10000E 02	.00000E 00	.0
.25000E 02	-.60000E 02	.20000E 01	.10000E 02	.00000E 00	.0
.30000E 02	.60000E 02	.20000E 01	.10000E 02	.00000E 00	.0
.35000E 02	-.60000E 02	.20000E 01	.10000E 02	.00000E 00	.0
.40000E 02	.60000E 02	.20000E 01	.10000E 02	.00000E 00	.0
.45000E 02	-.60000E 02	.20000E 01	.10000E 02	.00000E 00	.0
.50000E 02	.60000E 02	.20000E 01	.10000E 02	.00000E 00	.0

```
US CRS=    .000     OS SPD=10.0     TARG CRS= 256.000   TARG SPD=10.0
  INIT HORZ RGE=  .20000000E 05    INIT BEAR=  .56000000E 02     BEAR SIG=  .20000E 00
  GAUSS_TEST_EPSI, VAR1, VAR2:      .10000E 01     .36000E 04     .12660E-01


SEED=3311.00(   2)  X VECTOR DIMEN= 4  AVGING TIME= 20  CALC X TIME INC=  60
NUMBER OF CALC X TIME INC=   15  MOSS TIME INC=  1

INITIAL INFO: RANGE=  .15000E 05  RANGE SIG=  .75000E 04  SPEED=  .00000E 00  SPEED SIG=  .15000E 02

                    30  MONTE CARLO ITERATIONS               INITIAL RANGE,SPEED (0=A PRIORI, 1=GUESS):  0
                     3 LEGS,  15.00 MINUTE TOTAL TRACK TIME                     0=NO INIT X, 1=INIT X:  1
```

FIRST MONTE CARLO ITER:

TIME	TRUE RANGE	RANGE ERR	TRUE BEAR	BEAR ERR	BEAR RESID	SPEED ERR	COURSE ERR	ITER
5.00	.17565E 05	-.21722E 04	.58602E 02	-.72127E-01	.70774E 00	-.14067E 01	.13124E 03	11
7.00	.16476E 05	-.76453E 03	.57194E 02	-.13010E 00	.68168E 00	-.60750E 01	.41545E 02	16
8.00	.16000E 05	.10087E 04	.55742E 02	.25798E-01	.73448E 00	-.44084E 01	.12512E 03	6
9.00	.15535E 05	.12538E 04	.54202E 02	.16177E 00	.71274E 00	-.56427E 01	.11243E 03	6
10.00	.15081E 05	.80050E 03	.52568E 02	.19180E 00	.69962E 00	-.62494E 01	.40798E 02	6
11.00	.14515E 05	.16182E 03	.51578E 02	.10244E 00	.67881E 00	-.21514E 01	.48490E 01	5
12.00	.14021E 05	-.28498E 03	.52141E 02	.63179E-03	.66631E 00	.12190E 01	-.27036E 01	5
13.00	.13542E 05	-.43173E 03	.52801E 02	-.12940E-01	.69079E 00	.17420E 01	-.34406E 01	3
14.00	.13066E 05	-.53389E 03	.53510E 02	-.49721E-03	.70949E 00	.21946E 01	-.40264E 01	5
15.00	.12592E 05	-.75263E 03	.54272E 02	.47333E-01	.70801E 00	.26644E 01	-.47205E 01	3

10.000	256.000	21
TRUE SPEED	TRUE COURSE	MAX ITER

TIME	CONVERGED MONCAR ITER
1.00	1.
2.00	1.
3.00	2.
4.00	4.
5.00	8.
6.00	18.
7.00	24.
8.00	27.
9.00	29.
10.00	30.
11.00	30.
12.00	30.

Figure B-2 Typical Computer Run, MAP/TMA, Horizontal Bearing. (Continued)

```
 13.00       30.
 14.00       30.
 15.00       30.
TOTAL ITER= 294.
```

TIME	RANGE ERR	RANGE SIG	RANGE MAX	RANGE MIN	BEAM ERR	BEAM SIG	BEAM MAX	BEAM MIN
1.	-.466246E 04	.000000E 00	-.466246E 04	-.466246E 04	.194186E 00	.000000E 00	.194186E 00	.194186E 00
1.			-.466246E 04	-.466246E 04				
2.	-.398426E 04	.000000E 00	-.398426E 04	-.398426E 04	.277656E 00	.000000E 00	.277656E 00	.277656E 00
2.			-.398426E 04	-.398426E 04				
3.	-.335886E 04	.136126E 03	-.345506E 04	-.326266E 04	.125156E-01	.138406E 00	.110386E 00	-.853506E-01
3.			-.322276E 04	-.349496E 04				
4.	-.391466E 04	.178716E 04	-.655806E 04	-.257836E 04	.722516E-01	.534476E-01	.146096E 00	.221506E-01
4.			-.212756E 04	-.570176E 04				
5.	-.304196E 04	.170966E 04	-.719936E 04	-.215566E 04	-.360966E-01	.431696E-01	.422936E-01	-.761166E-01
5.			-.133226E 04	-.475146E 04				
6.	-.103726E 03	.375106E 04	.627066E 04	-.579876E 04	-.768526E-01	.139386E 00	.155386E 00	-.322026E 00
6.			.364736E 04	-.585476E 04				
7.	.388256E 03	.127106E 04	.276596E 04	-.266286E 04	-.307656E-01	.107046E 00	.252276E 00	-.231736E 00
7.			.165946E 04	-.982756E 03				
8.	.561016E 03	.828136E 03	.255206E 04	-.911136E 03	.742246E-02	.115846E 00	.253996E 00	-.202206E 00
8.			.138916E 04	-.267126E 03				
9.	.665566E 03	.648176E 03	.190446E 04	-.421916E 03	.568696E-01	.930106E-01	.231716E 00	-.907736E-01
9.			.151376E 04	.173906E 02				
10.	.365876E 03	.592926E 03	.124556E 04	-.659426E 03	.506696E-01	.104126E 00	.207046E 00	-.176546E 00
10.			.956796E 03	-.227056E 03				
11.	.212116E 03	.497896E 03	.119446E 04	-.799146E 03	.339886E-01	.101076E 00	.222246E 00	-.208296E 00
11.			.710006E 03	-.285746E 03				
12.	.162086E 03	.576406E 03	.133346E 04	-.114026E 04	.117146E-01	.776576E-01	.149186E 00	-.140516E 00
12.			.738486E 03	-.414326E 03				
13.	.120246E 03	.683526E 03	.141186E 04	-.154276E 04	-.150396E-01	.592696E-01	.126496E 00	-.122696E 00
13.			.803816E 03	-.561236E 03				
14.	.142716E 03	.806776E 03	.167216E 04	-.188706E 04	-.228406E-01	.467196E-01	.581086E-01	-.111776E 00
14.			.989486E 03	-.664066E 03				
15.	.161416E 03	.846546E 03	.172066E 04	-.175536E 04	-.222196E-01	.601246E-01	.111036E 00	-.155046E 00
15.			.100786E 04	-.684936E 03				

TIME	SPEED ERR	SPEED SIG	SPEED MAX	SPEED MIN	COURSE ERR	COURSE SIG	COURSE MAX	COURSE MIN
1.	-.954256E 01	.000006E 00	-.954256E 01	-.954256E 01	-.164726E 03	.000006E 00	-.164726E 03	-.164726E 03
2.	-.750886E 01	.000006E 00	-.750886E 01	-.750886E 01	.102516E 03	.000006E 00	.102516E 03	.102516E 03
3.	-.525836E 01	.708816E 00	-.573956E 01	-.273716E 01	.123296E 03	.852526E 00	.123756E 03	.122856E 03
4.	-.207716E 01	.179716E 01	-.412036E 01	-.203696E 00	.976776E 02	.563016E 02	.139086E 03	.135776E 02
5.	-.807516E 00	.297036E 01	.413286E 01	-.479496E 01	.116076E 03	.437946E 02	.146256E 03	.108716E 02
6.	-.171036E 01	.348906E 01	.371956E 01	-.644826E 01	.578056E 02	.612586E 02	.150356E 03	-.512086E 01
7.	-.247566E 01	.529406E 01	.794786E 01	-.642896E 01	.646896E 02	.605286E 02	.144886E 03	-.725526E 01
8.	-.333426E 01	.299016E 01	.206256E 01	-.683336E 01	.531936E 02	.521806E 02	.141876E 03	-.322966E 01
9.	-.352036E 01	.298166E 01	.579796E 01	-.651826E 01	.852896E 02	.476246E 02	.136476E 03	-.777416E 01
10.	-.225186E 01	.581296E 01	.824136E 01	-.684076E 01	.225946E 02	.335636E 02	.118536E 03	-.933476E 01
11.	-.141996E 01	.524046E 01	.480046E 01	-.647116E 01	.104366E 02	.184006E 02	.650136E 02	-.726616E 01
12.	-.898826E 00	.327616E 01	.615046E 01	-.577416E 01	.835296E 01	.137256E 02	.581526E 02	-.830726E 01
13.	-.351066E 00	.329186E 01	.754586E 01	-.594676E 01	.445426E 01	.108416E 02	.441716E 02	-.905226E 01
14.	-.311526E 00	.338146E 01	.797196E 01	-.573506E 01	.442596E 01	.106486E 02	.376216E 02	-.917466E 01
15.	-.387046E 00	.339306E 01	.807156E 01	-.592826E 01	.466866E 01	.109156E 02	.408196E 02	-.933606E 01

TIME	RESID AVG	RESID SIG	RESID MAX	RESID MIN	ITER AVG	ITER SIG	ITER MAX	ITER MIN
1.	.625596E 00	.000006E 00	.625596E 00	.625596E 00	.150006E 01	.000006E 00	.150406E 01	.150406E 01
2.	.698046E 00	.000006E 00	.698046E 00	.698046E 00	.150006E 02	.000006E 00	.160076E 02	.160076E 02
3.	.113986E 01	.567956E 00	.154116E 01	.734066E 00	.135006E 02	.494976E 01	.170076E 02	.100066E 02
4.	.740516E 00	.117086E 00	.915076E 00	.566276E 00	.125006E 02	.567866E 01	.150156E 02	.700606E 01
5.	.455896E 00	.089146E 00	.143156E 01	.594166E 00	.125006E 02	.494576E 01	.140216E 02	.900206E 01

Figure B-2 Typical Computer Run, MAP/TMA, Horizontal Bearing. (Continued)

6.	.84725E 00	.33066E 00	.14657E 01	.23687E 00	.11611E 02	.49365E 01	.20011E 02	.40170E 01
7.	.75790E 00	.27345E 00	.13143E 01	.34474E 00	.68333E 01	.33319E 01	.16001E 02	.40060E 01
8.	.79460E 00	.23431E 00	.13550E 01	.42692E 00	.80370E 01	.41831E 01	.18016E 02	.30100E 01
9.	.78175E 00	.22080E 00	.12693E 01	.39754E 00	.73793E 01	.35498E 01	.14023E 02	.30160E 01
10.	.78541E 00	.18876E 00	.11563E 01	.50688E 00	.62333E 01	.23880E 01	.12006E 02	.10030E 01
11.	.79222E 00	.17552E 00	.12653E 01	.53456E 00	.46333E 01	.16833E 01	.90060E 01	.20050E 01
12.	.78404E 00	.17492E 00	.11702E 01	.51094E 00	.39667E 01	.14967E 01	.80240E 01	.10210E 01
13.	.80367E 00	.16649E 00	.11800E 01	.47781E 00	.35333E 01	.11059E 01	.50160E 01	.10090E 01
14.	.79742E 00	.16201E 00	.11550E 01	.47543E 00	.31000E 01	.15166E 01	.70070E 01	.10050E 01
15.	.80783E 00	.17243E 00	.11612E 01	.51030E 00	.27000E 01	.13433E 01	.70260E 01	.10040E 01

MAJOR AXES-ERROR BOUND ELIPSES

TIME	SPEED AVG	SPEED SIG	SPEED MAX	SPEED MIN	X,Y AVG	X,Y SIG	X,Y MAX	X,Y MIN
1.	.19945E 02	.00000E 00	.19945E 02	.19945E 02	.74557E 04	.00000E 00	.74557E 04	.74557E 04
2.	.30100E 02	.00000E 00	.30100E 02	.30100E 02	.74734E 04	.00000E 00	.74734E 04	.74734E 04
3.	.18979E 02	.20729E 00	.19125E 02	.18834E 02	.75069E 04	.13856E 02	.75153E 04	.74905E 04
4.	.17060E 02	.21087E 01	.20153E 02	.15580E 02	.75713E 04	.16081E 03	.78111E 04	.74705E 04
5.	.13981E 02	.12680E 01	.16400E 02	.12442E 02	.74376E 04	.25197E 03	.76024E 04	.69111E 04
6.	.13601E 02	.16423E 01	.16232E 02	.10792E 02	.46697E 04	.10630E 04	.62224E 04	.27691E 04
7.	.12652E 02	.49933E 00	.15085E 02	.11048E 02	.20589E 04	.11249E 03	.22650E 04	.18365E 04
8.	.11569E 02	.10966E 01	.13994E 02	.10181E 02	.20564E 04	.16677E 03	.24126E 04	.18531E 04
9.	.91055E 01	.52168E 00	.10144E 02	.82111E 01	.19105E 04	.11415E 03	.21139E 04	.17044E 04
10.	.65455E 01	.27480E 00	.70329E 01	.59990E 01	.16201E 04	.75120E 02	.17769E 04	.14655E 04
11.	.47331E 01	.17433E 00	.50405E 01	.43567E 01	.13373E 04	.59959E 02	.14609E 04	.12142E 04
12.	.39421E 01	.12033E 00	.41596E 01	.37179E 01	.11728E 04	.44808E 02	.12503E 04	.10991E 04
13.	.35652E 01	.93074E-01	.37811E 01	.33858E 01	.10633E 04	.33202E 02	.11411E 04	.10055E 04
14.	.34567E 01	.84542E-01	.36330E 01	.32956E 01	.10064E 04	.28420E 02	.10688E 04	.95225E 03
15.	.34452E 01	.82629E-01	.36218E 01	.32900E 01	.99393E 03	.25670E 02	.10526E 04	.94213E 03

MINOR AXES-ERROR BOUND ELIPSES

TIME	SPEED AVG	SPEED SIG	SPEED MAX	SPEED MIN	X,Y AVG	X,Y SIG	X,Y MAX	X,Y MIN
1.	.52435E 01	.00000E 00	.52435E 01	.52435E 01	.48000E 02	.00000E 00	.48000E 02	.48000E 02
2.	.32161E 01	.00000E 00	.32161E 01	.32161E 01	.39395E 02	.00000E 00	.39395E 02	.39395E 02
3.	.21689E 01	.24261E 00	.23404E 01	.19973E 01	.33585E 02	.17116E 00	.33705E 02	.33466E 02
4.	.21241E 01	.11779E 00	.22567E 01	.20049E 01	.29803E 02	.22444E 01	.31496E 02	.26533E 02
5.	.21099E 01	.12659E 00	.22574E 01	.18301E 01	.29219E 02	.22067E 01	.32249E 02	.25612E 02
6.	.12242E 01	.30180E 00	.16350E 01	.68164E 00	.34475E 02	.47010E 01	.43081E 02	.26401E 02
7.	.30777E 00	.34138E-01	.40103E 00	.24548E 00	.27262E 02	.15776E 01	.30479E 02	.25100E 02
8.	.16521E 00	.78993E-02	.18482E 00	.15100E 00	.25626E 02	.10537E 01	.24103E 02	.23281E 02
9.	.13878E 00	.56438E-02	.15196E 00	.13045E 00	.25581E 02	.13420E 01	.24052E 02	.23108E 02
10.	.13700E 00	.64026E-02	.15005E 00	.12665E 00	.25963E 02	.13284E 01	.24120E 02	.23516E 02
11.	.13774E 00	.60502E-02	.15036E 00	.12721E 00	.26040E 02	.11415E 01	.28513E 02	.24000E 02
12.	.13572E 00	.53770E-02	.14584E 00	.12937E 00	.26156E 02	.10566E 01	.28625E 02	.24413E 02
13.	.12723E 00	.44655E-02	.13501E 00	.11993E 00	.25796E 02	.97220E 00	.27758E 02	.23906E 02
14.	.11033E 00	.33076E-02	.11663E 00	.10389E 00	.24235E 02	.81589E 00	.25988E 02	.22851E 02
15.	.89629E-01	.28163E-02	.94406E-01	.82665E-01	.21633E 02	.64858E 00	.23087E 02	.20454E 02

ANGLE- ERROR BOUND ELIPSES RMS VALUES

TIME	SPEED AVG	SPEED SIG	SPEED MAX	SPEED MIN	RANGE	BEAR	SPEED	COURSE
1.	.52913E 02	.00000E 00	.52913E 02	.52913E 02	.46624E 04	.19418E 00	.95425E 01	.16472E 03
2.	.58275E 02	.00000E 00	.58275E 02	.58275E 02	.39042E 04	.27765E 00	.75088E 01	.10251E 03
3.	.58045E 02	.27951E 00	.58241E 02	.57849E 02	.33618E 04	.13897E 00	.33150E 01	.12329E 03
4.	.58221E 02	.91856E 00	.58790E 02	.56849E 02	.43033E 04	.89870E-01	.27466E 01	.11222E 03
5.	.58878E 02	.15326E 01	.60101E 02	.55103E 02	.34893E 04	.56273E-01	.30318E 01	.12405E 03
6.	.58840E 02	.58265E 00	.60048E 02	.57050E 02	.37520E 04	.15717E 00	.38057E 01	.84211E 02
7.	.57171E 02	.12769E 00	.57425E 02	.57002E 02	.13240E 04	.11138E 00	.41245E 01	.88590E 02
8.	.56589E 02	.89337E-01	.56717E 02	.56516E 02	.10003E 04	.11011E 00	.44706E 01	.74513E 02
9.	.56279E 02	.94491E-01	.56405E 02	.56176E 02	.92403E 03	.10998E 00	.46003E 01	.65717E 02
10.	.56118E 02	.92598E-01	.56322E 02	.55974E 02	.84672E 03	.11580E 00	.44282E 01	.50460E 02
11.	.56049E 02	.92888E-01	.56247E 02	.55073E 02	.54118E 03	.10663E 00	.35378E 01	.21157E 02

Figure B-2 Typical Computer Run, MAP/TMA, Horizontal Bearing. (Continued)

12.	.55846E 02	.65653E-01	.56037E 02	.55694E 02	.59876E 03	.78536E-01	.33961E 01	.13336E 02
13.	.55523E 02	.80408E-01	.55569E 02	.55395E 02	.69402E 03	.61148E-01	.33106E 01	.11722E 02
14.	.55272E 02	.65653E-01	.55361E 02	.55178E 02	.81930E 03	.51916E-01	.33967E 01	.11531E 02
15.	.55278E 02	.65653E-01	.55376E 02	.55151E 02	.86159E 03	.66098E-01	.34150E 01	.11861E 02

(INPUT/OUTPUT UNITS: YDS, SEC, DEGREES, KNOTS)

TOTAL GAUSS ITER= 5055

TIME	DELTA TRUE RANGE	US X,Y COORD.	
1.	337.	0.	284.
2.	842.	0.	622.
3.	1345.	0.	960.
4.	1846.	0.	1298.
5.	2346.	0.	1636.
6.	2940.	189.	1848.
7.	3435.	489.	1696.
8.	3911.	785.	1534.
9.	4377.	1082.	1372.
10.	4830.	1378.	1210.
11.	5396.	1654.	1274.
12.	5891.	1629.	1607.
13.	6369.	1584.	1942.
14.	6845.	1538.	2276.
15.	7319.	1493.	2611.

Figure B-2 Typical Computer Run, MAP/TMA, Horizontal Bearing. (Concluded)

Bibliography

(Gauss Elimination)
B. J. Ley, Computer Aided Analysis and Design for Electrical Engineers, Holt Rinehart and Winston, New York, 1970.

(Matrix Operations, Eigenvalues)
P. M. DeRusso, R. J. Roy, C. M. Close, State Variables for Engineers, Wiley, New York, 1965.

(MAP, MLE, Cramer-Rao Bounds)
H. L. VanTrees, Detection, Estimation and Modulation Theory, Part I, Wiley, 1968.

Distribution List for
"Target Tracking with Multiple Data Sources"

Name	Number of Copies
Defense Documentation Center Cameron Station Alexandria, VA 22314	12
Office of Naval Research Code 431 Arlington, VA 22217	2
Dr. Byron D. Tapley The University of Texas at Austin Department of Aerospace Engineering and Engineering Mechanics Austin, TX 78712	1
Dr. Fred W. Weidmann Tracor, Inc. Tracor Sciences & Systems 6500 Tracor Lane Austin, TX 78721	1
Office of Naval Research Branch Office Building 114 Section D 666 Summer Street Boston, MA 02210	1
Dr. Harold A. Titus Naval Postgraduate School Department of Electrical Engineering Code 62Ts Monterey, CA 93940	1
Dr. C. Carter Naval Underwater Systems Center New London Laboratory Code 313 New London, CT 06320	3
Naval Underwater Systems Center Code 352 Newport, RI 02840	3
Dr. J. Anton Systems Control, Inc. 1801 Page Mill Road Palo Alto, CA 94304	1

Name	Number of Copies
Dr. Thomas O. Mottl The Analytic Sciences Corporation Six Jacob Way Reading, MA 01867	1
Naval Ocean Systems Center Code 6212 San Diego, CA 92152	1
Naval Surface Weapons Center White Oak Laboratory Code U-20 Silver Spring, MD 20910	2
Dr. Yaakov Bar-Shalom The University of Connecticut Department of Electrical Engineering and Computer Science Box U-157 Storrs, CT 06268	1
Mr. Conrad Naval Intelligence Support Center Code 20 Suitland, MD 20390	1
Dr. V. T. Gabriel General Electric Company Sonar Systems Engineering Farrell Road Plant Building 1, Room D6 Syracuse, NY 13201	1
Naval Research Laboratory Washington, DC 20375	
Code 2627	6
Code 5308	1
Code 7932	1
Naval Sea Systems Command Washington, DC 20360	
Code 63R-1	1
Code 63R-16	1
Administrative Contracting Officer Defense Contract Administration Services Management Area - Hartford 96 Murphy Road Hartford, CT 06114	1